Graduate School Form 30
Updated 1/15/2015

PURDUE UNIVERSITY
GRADUATE SCHOOL
Thesis/Dissertation Acceptance

This is to certify that the thesis/dissertation prepared

By Feifei Jiang

Entitled

UNDERSTANDING MECHANICAL ENVIRONMENT CHANGES AND BIOLOGICAL RESPONSES TO CANINE RETRACTION USING T-LOOP

For the degree of Doctor of Philosophy

Is approved by the final examining committee:

Jie Chen Chair	Eric Nauman
Anil Bajaj Co-chair	
Hazim El-Mounayri	
Thomas Katona	

To the best of my knowledge and as understood by the student in the Thesis/Dissertation Agreement, Publication Delay, and Certification Disclaimer (Graduate School Form 32), this thesis/dissertation adheres to the provisions of Purdue University's "Policy of Integrity in Research" and the use of copyright material.

Approved by Major Professor(s): Jie Chen

Approved by: Ganesh Subbarayan 4/24/2015

Head of the Departmental Graduate Program Date

UNDERSTANDING MECHANICAL ENVIRONMENT CHANGES AND BIOLOGICAL RESPONSES TO CANINE RETRACTION USING T-LOOP

A Dissertation

Submitted to the Faculty

of

Purdue University

by

Feifei Jiang

In Partial Fulfillment of the

Requirements for the Degree

of

Doctor of Philosophy

May 2015

Purdue University

West Lafayette, Indiana

ACKNOWLEDGEMENTS

I would like to express the deepest appreciation to my mentor, Dr. Chen, who has extraordinarily supported me in this dissertation process.

I would like to thank my advisor and committee members Dr. Bajaj, Dr. Katona, Dr. El-Mounayri, and Dr. Nauman, for their expert advice throughout the project.

I would like to thank Dr. Eckert for his help in statistical analysis.

In addition, a thank you to my parents, who always support me in my life.

TABLE OF CONTENTS

Page

Page

LIST OF TABLES

Table Page

LIST OF FIGURES

Figure Page

Figure Page

ABSTRACT

Jiang, Feifei. Ph.D., Purdue University, May 2015. Understanding Mechanical Environment Changes and Biological Responses to Canine Retraction Using T-loop. Major Professors: Jie Chen, School of Engineering and Technology, Anil Bajaj, School of Mechanical Engineering.

Predictability of tooth displacement in response to specific orthodontic load system directly links to the quality and effectiveness of the treatment. The key questions are how the tooth's environment changes in response to the orthodontic load and how the biological tissues respond clinically. The objectives of this study are to determine the mechanical environment (ME) changes and to quantify the biological tissues' response. Eighteen (18) patients who needed maxillary bilateral canine retractions were involved in the study. A method was developed to quantify the 3D load systems on the canine, which allowed the treatment strategies to be customized in terms of orthodontic loading systems to meet either translation (TR) or controlled tipping (CT) requirement. Dental casts were made before and after each treatment interval, and the Cone Beam Computed Tomography (CBCT) scans were taken prior to and following the entire treatment for control of treatment strategy and post treatment evaluations. Finite element method (FEM) was applied to calculate the location of center of resistance (CRes) for tooth movement control. The location and variation of CRes were recorded and compared with previous studies. A quick CRes assessment method that locates CRes by calculating the centroid of the contact surface (CCS) and the centroid of the projection of root surface (CPCS) in certain direction was also tested and compared with the results from FEM. Customized T-loop spring, a kind of orthodontic appliance, was designed, fabricated, and calibrated on a load measuring system to ensure that the load met the clinician's

prescription. The treatment outcomes in terms of tooth displacement and root resorption characterized by the changes of tooth length and volume as well as the bone mineral density (BMD) represented by the Hounsfield units (HU) change were recorded and analyzed. The ME in terms of stress were also calculated by using FEM. Paired t-test and mixed model ANOVA methods were used to analyze the relationships between the mechanical inputs (quantified and customized load, and corresponding stress) and clinical outcomes (root resorption and BMD change). It was found that the overall root resorption is not significant for canine retraction, but apical root resorption does occur, meaning that orthodontic load is not a sufficient factor. Also, it was observed that HU distribution changed significantly in both root and alveolar bone. The maximum reduction was on the coronal level in the direction perpendicular to the direction of movement in root, and in the direction of the tooth movement at the coronal level in bone. In addition, it was determined that the locations of the CRes in the MD and BL directions were significantly different. The locations of the CRes of a human canine in MD and BL directions can be estimated by finding the CPCSs in the two directions. Finally, it was shown that the stress invariants can be used to characterize how the osteocytes feel when ME changes. The stress invariants in the alveolar bone are not significantly affected by different M/F. The higher bone modeling/remodeling activities along the direction of tooth movement may be related to the initial volumetric increase and decrease in the alveolar bone.

CHAPTER 1. INTRODUCTION

1.1 General Background

Orthodontists move patients' teeth to certain locations by using mechanical force. The orthodontic load is three-dimensional (3D) and includes all six force and moment components. Different combinations of force and moment lead to different tooth movement patterns, translation, tipping, or combinations. The current orthodontic treatment is more experience based rather than evidence based. Biomechanics theory was used to predict clinical outcomes. However, more quantitative clinical validations are lacking. The relationship between the mechanical environment (ME) change and biological response is still not clear clinically. The objective of this study is to better understand this relationship by quantitatively analyzing the tooth response to well-controlled force systems in maxillary canine retraction, a common clinical treatment.

1.2 Tooth Movement and Canine Retraction

Orthodontic tooth movement is in response to orthodontic load applied by appliances. The process is both pathologic and physiologic [1]. Figure 1.1 shows the anatomic structure of a tooth as well as its surrounding tissues. Crown, root, and alveolar bone are hard tissue, and periodontal ligament (PDL) is soft tissue. While applying a load on the tooth, the PDL is compressed on one side and stretched on the other side. The change of ME in terms of stress and strain triggers the biological reaction. On the compression side, osteoclasts are recruited and absorb the bone [2, 3]. The process is called remodeling. On the tension side, osteoblasts are recruited, and new bone is deposited [2]. This process is called modeling. It is the modeling and remodeling process that results in tooth translocation.

A mechanical stimulus is one of the determination factors to the number and activity of osteoclasts and osteoblasts, and other factors, such as hormones and cytokines, are also influential and patient dependent [4-6]. The osteocyte is commonly believed to be a source of soluble factors targeting cells on bone surface and distant organs [7]. It is embedded within the calcified bone matrix, and likely to be responsible for sensing the mechanical stimuli and regulating bone formation and resorption [8]. Mechanically activated osteocytes have the function to modulate the recruitment, differentiation, and activity of osteoblasts and osteoclasts [6, 9-11].

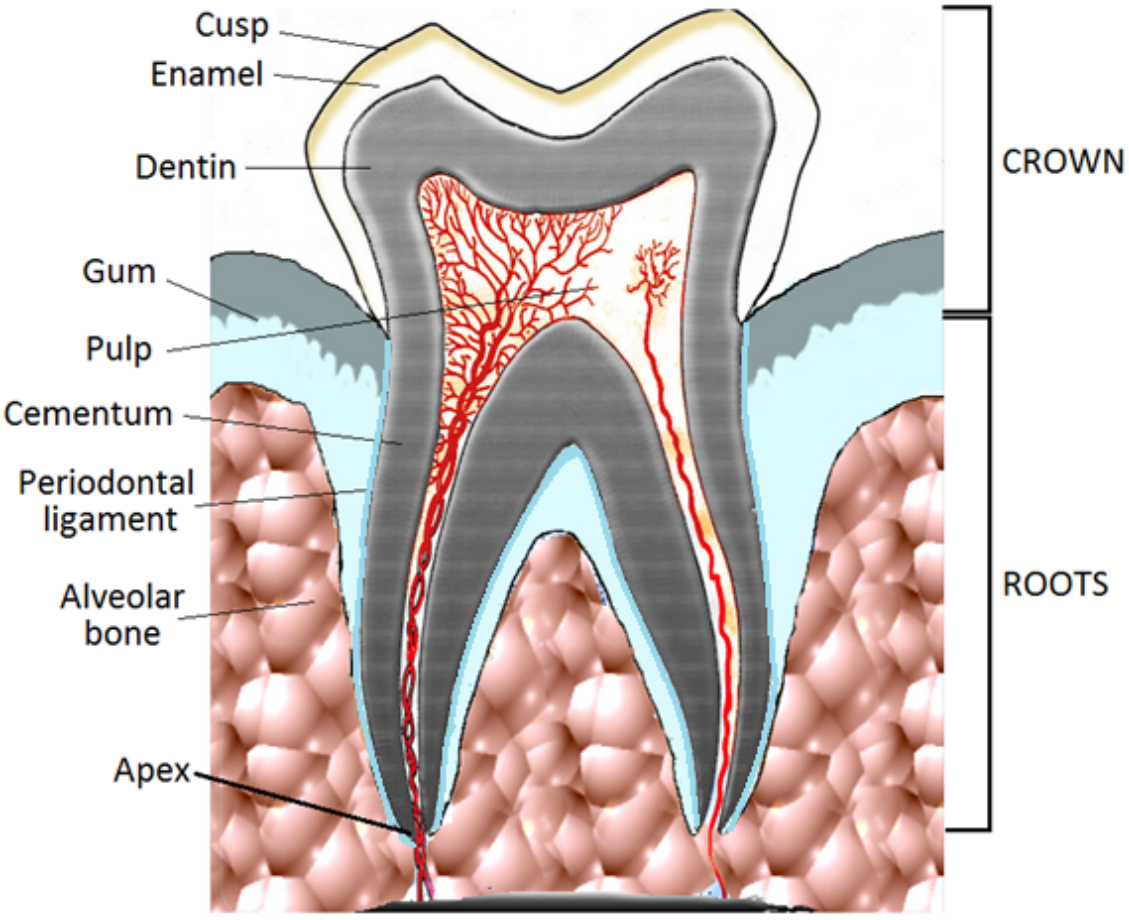

Figure 1.1: Basic tooth structure.

The questions remain as how the cells are triggered; whether the mechanotransduction process is initiated in bone or PDL; and whether the resulting bone modeling/remodeling characterized by the BMD changes are predominantly determined by the initial stress changes. The answers to the questions help understand the root-cause of the tooth movement and require study of ME changes due to orthodontic treatment.

While orthodontists try to control the tooth movement and root resorption, it will be beneficial to understand how biological tissues respond to the ME changes. Heavy force cause more root resorption [12-15]. Compressive stress in PDL is reported to be related to the root resorption in an animal study [16]. Clinical studies had shown the potential correlation between movement direction and BMD loss [17]. However, to understand the root cause, it is important to understand how the cells sense the ME changes in different tissues.

Figure 1.2 shows the dental arch and the names of the teeth. The direction away from the midline is called distal, which is also the direction that canine is retract to; toward to midline is called mesial; toward to facial is called buccal; toward to the tongue is called lingual; toward to crown is called occlusal; toward to root is called apical.

Canine retraction is a treatment that moves the canine to the extracted first premolar site. During the treatment, the molars and second premolar are bonded together and serve as the anchorage. A spring connects the canine to the anchorage, and retracts the canine to close the vacant 1st premolar space. The incisors are not directly involved. (See Figure 1.3)

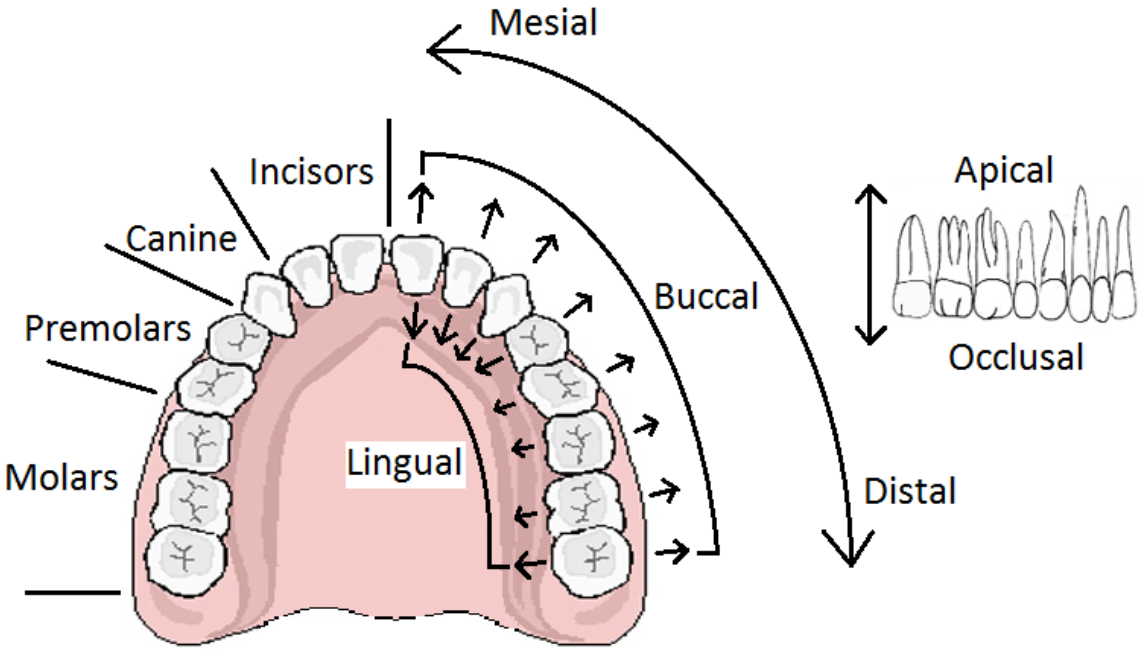

Figure 1.2: Diagram of dental arch.

Figure 1.3: Canine retraction treatment.

While retracting the canine, two strategies are commonly applied: (See Figure 1.4)

1. One step translation (TR): the tooth is directly translated to the target position.
2. Two-step controlled tipping (CT): the crown of tooth is tipped to the target position without back tipping at the root apex, then the root was corrected.

The clinical responses to the strategies in terms of treatment time and side effects, such as the root resorption, have not been reported.

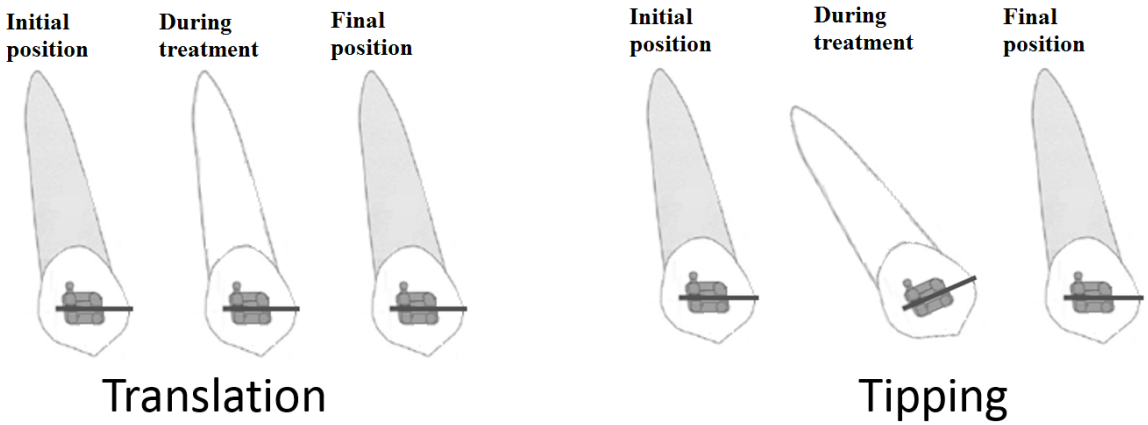

TR: the position of the tooth is always straight during the treatment as the tooth is translated. CT: the crown is tipped first, then the root is corrected.

Figure 1.4: Treatment strategies of TR and CT.

1.3 Concept of Center of Resistance and Moment-to-Force Ratio

Tooth movement is 3D and consists of both translation and rotation. Center of resistance (CRes) is a concept to relate expected tooth movement with the orthodontic load system. The orthodontic load system is applied to a tooth through dental appliances, such as brackets, archwires, and various kinds of springs. The activation of the spring results in a 3D load system on the tooth. The load system consists of three moment and three force components. The moment tends to rotate and tip the tooth while the force tends to translate it. Moment-to-force ratio (M/F) can be adjusted in appliance design to

control the displacement pattern, thus is a commonly used parameter in orthodontic appliance design. To determine the desired M/F, the concept of CRes was brought up. The location of CRes has been considered as an important reference point [18]. The CRes in tooth movement is equivalent to the concept of mass center of a free body [19]. It is a conceptual point at where to apply a pure force to translate or a pure moment to rotate the tooth about it initially [20]. (Figure 1.5) The location of CRes is inside the root for single root tooth. However, the force can only be applied at the bracket, which causes the tooth to tip. To translate the tooth, an anti-tipping moment on bracket is also required to cancel the tipping moment. Translation is expected when M/F is equal to the distance between CRes and the bracket. Some clinical cases require both translation and tipping, causing the entire tooth to move in one direction, called controlled tipping. In case a controlled tipping is required, the level of tipping can be controlled by adjusting the M/F.

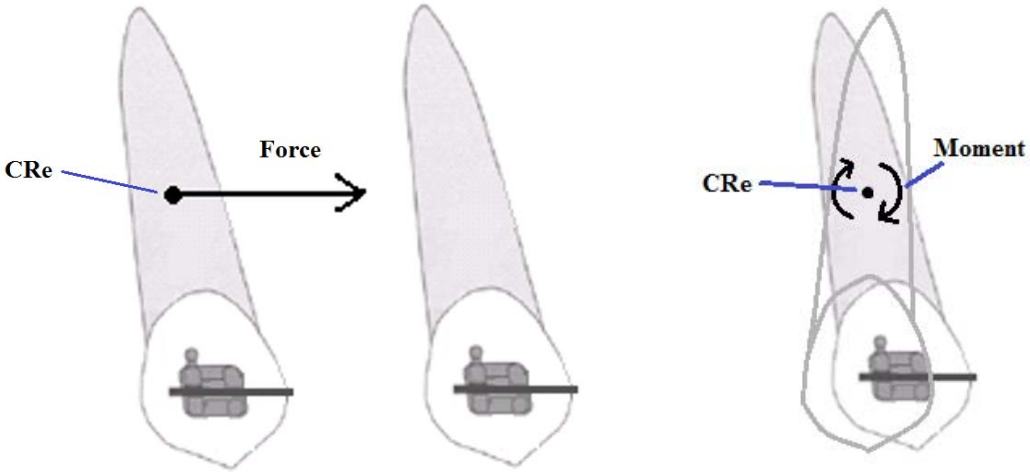

Definition 1 Definition 2

Definition 1: while applying a pure force on the CRes, the tooth translate with no tipping.
Definition 2: while applying a pure moment, the tooth rotate around the CRes.

Figure 1.5: Concept of CRes.

Pre-designed M/F is usually needed in treatment planning, which requires approximate location of CRes. Previous literatures had reported the locations of CRes,

which are primarily at 1/2 to 2/3 of root length measured from the apex [21-23]. These results were primarily from animal studies.

Recent studies also reported that the location of CRes depends on the direction [18, 24, 25]. The location of CRes is commonly described on the tooth's long axis. The CRes in the mesial-distal (MD) and buccal-lingual (BL) directions do not intersect in 3D, which means that there is no 3D CRes on the long axis of the tooth. Furthermore, the variation of CRes corresponding to different directions and within each direction need to be quantified for better understanding of variations among the clinical treatment outcomes.

Finite element (FE) method was commonly used to analyze the locations of CRes in previous studies [18, 26-30] because of its unique ability to deal with completed bio-structures in the clinic [31-33]. However, FE method requires special training and is time consuming, which is not practical to be used in the clinics. Other alternative methods are needed.

Individualized medical treatment requires patient specific information. For better treatment planning and clinical research, a quick assessment method is needed to determine the patient specific CRes. Geiger, M E et.al [34] had tested if the centroid of root projection in BL direction is close to the CRes calculated using FE method on three human incisors. However, the conclusion is uncertain due to the small sample size, which did not show the variation and did not fully support the usage of the method in the clinic. Furthermore, the method has not been used for determining CRes in the MD direction. A further investigation is needed to assess the method.

The location of CRes depends on the geometry and boundary condition of root and supports from the periodontal ligament (PDL) and bone. The tooth displacement depends on the 3D contact surface. Thus, the location of CRes might be a function of the

contact surface. Based on the mass center concept, we hypothesized that the centroid of the contact surface (CCS) between root and PDL can be used as the location of CRes. To ease the computation, we further hypothesized that the CRes can be estimated based on the centroid of projection of the contact surface (CPCS) in the corresponding direction.

1.4 Segmental T-loop

Segmental T-loop, a specially designed spring, had been used in maxillary canine retraction treatments. It can be customized to provide different M/F and provides 3D force and moment components as prescribed by the clinicians. The T-loop connects the canine and anchorage through the brackets. Once activated, it generates the load systems on both canine and anchorage. The load system and its share on both sides can be controlled by multiple factors including, level of activation, shape of the loop, interbracket distance (IBD), material, size, and gable angles that are added to control the moment components in 3D [35-39]. (See Figure 1.6) The size of the loops is restricted by the available space in the mouth. Titanium molybdenum alloy is a commonly used material. T-loop is the shape widely used commercially. The gable angles, θ, are used to adjust M/F. As shown in Figure 1.7, 1st order (out of plane) gable bend is to bend the legs of the loop to lingual direction, increasing the anti-rotation moment in this study. The 2nd order (in-plane) gable bend is to bend the legs of the loop to apical direction, increasing the anti-tipping moment in this study. 1st and 2nd order gable bends control the 3D tooth rotation and tipping.

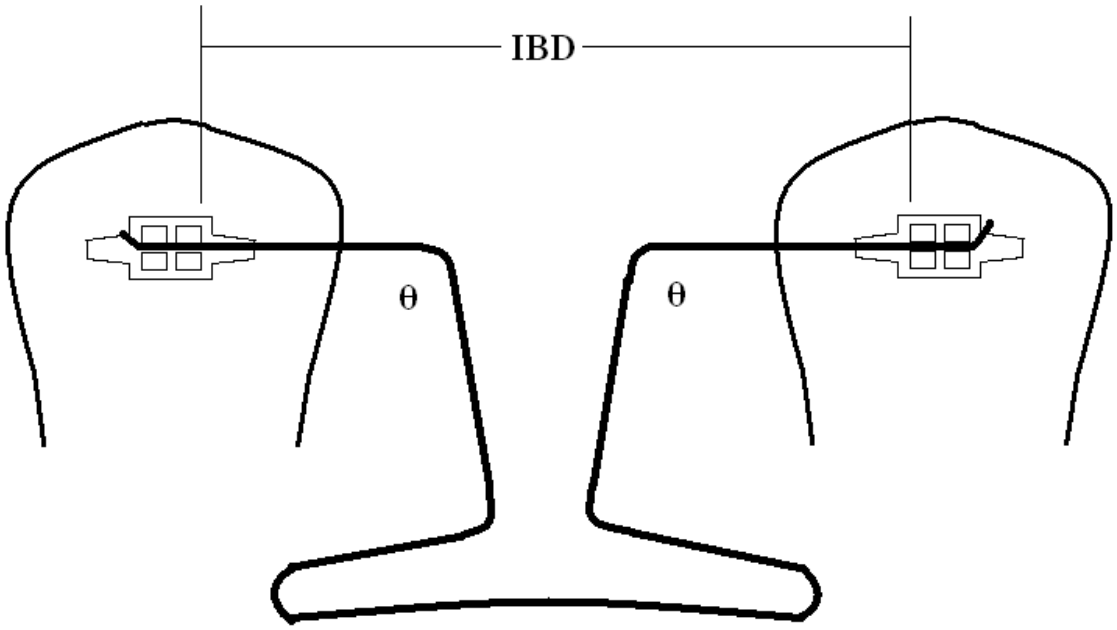

The original length of the loop has to be smaller than the IBD to provide retracting force. θ is the gable bend angle to control the M/F ratio

Figure 1.6: Activated segmental T-loop.

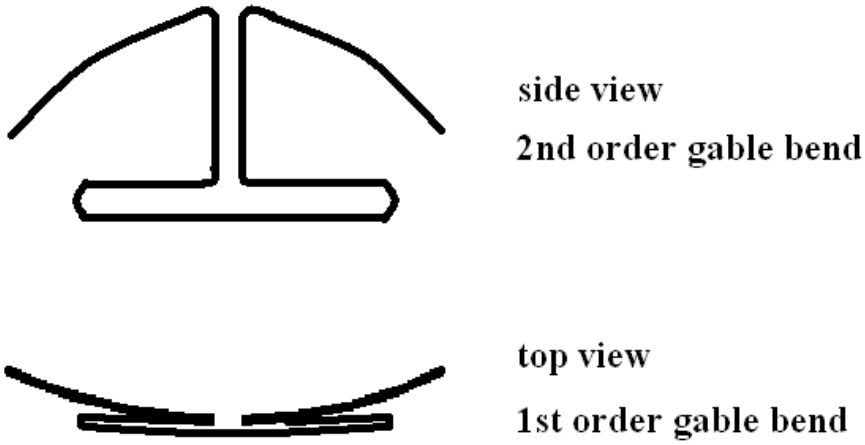

The 1st order gable bend is in the original geometry plane, and the 2nd order gable bend is out of the original geometry plane.

Figure 1.7: 1st and 2nd order gable bends of segmental T-loop.

1.5 Quantification of the Load System

It is important to quantify the orthodontic load system in order to control the tooth displacement and study the effects of the load on the clinical outcomes. The 3D load system used in canine retractions had not been quantified clinically. T-loops with different M/F ratio result in different movement patterns. The load of clinically used loops is controlled by adjusting the level of activation, shape of the loop, material, size, and gable angles [35-39]. The orthodontic loads of commercial archwires or customized segmental loops are normally estimated based on experiments on laboratory settings with archwires being tested on dental casts with ideal denture [40-42] or simulated with numerical method [27-29, 43, 44]. The test is not customized for individual patient, thus the results are not validated. It is also uncertain that customization is needed because the variation of the load on different patients has not been studied. It is difficult to measure the actual 3D load on patients' teeth clinically, thus alternative methods are needed. Some in-vitro methods have been developed to measure the load system in simulated clinical conditions [41, 45-48].

These methods simulated clinical cases with compatible boundary conditions for testing the appliances, which should provide more reliable results.

1.6 ME Change in Terms of Stress/Strain and Initial Displacement

1.6.1 Initial Displacement and Stress

A tooth can be moved by applying an orthodontic load system to it. The load results in ME change, which affects differentiations of different cells, such as osteoblasts and osteoclasts. Osteoblasts deposit new bone and osteoclasts remove existing bone. A tooth can move by absorption of the bone in the direction of movement and deposition of new bone behind. The biological changes are referred to as bone modeling and

remodeling. It is important to study how the mechanical load triggers the modeling and remodeling process. However, this dynamic process has not been fully investigated clinically. The tooth movement is triggered by orthodontic force, mediated by the surrounding tissues' reactions, and dynamically controlled by constant modeling and remodeling in the alveolar bone. These events occur at different time points [2, 3]. The orthodontic force causes an initial tooth displacement and change of ME. Then, the tooth moves further as the bone models and remodels [1]. The orthodontic load changes as the tooth moves resulting in new ME changes. Consequently, the tooth moves to a new location. Predicting the final clinical outcomes in terms of tooth displacement using the treatment strategy is challenging because of the multiple factors involved.

Previous research on the ME has been based on the initial response in the tooth, PDL, and alveolar bone [30]. Finite element method (FEM) is the tool, which requires geometrical information. CT images are commonly used, which is normally taken before the treatment. Therefore, only the initial tooth displacement and stress/strain change can be calculated. Similarly, CRes was also determined based on the initial condition in the previous literatures [18, 22, 23].

It is commonly believed that the tooth moves in the direction of force. However, the orthodontic force dictates an initial tooth displacement, which is also affected by the structure of the alveolar bone. The final detectable displacement will occur months later. It is imperative to validate whether the final displacement is correlated to the initial one.

1.6.2 Methods Used

FEM had been used to analyze initial displacement, stress, and the locations of CRes in previous studies [18, 26-30] because these parameters can hardly be determined experimentally in clinical studies. The method has been proven to be useful to non-destructively analyze ME in orthodontics [49-51]. FEM requires geometry and material properties to do the calculation. Geometry can be reconstructed from 3D cone-beam

computed tomography (CBCT) scan, and material properties had been estimated in previous literatures [17, 52].

1.7 Bone Modeling and Remodeling Related Bone Mineral Density Change

During the tooth movement, the surrounding alveolar bone models and remodels, leading to bone mineral density (BMD) changes, typically BMD reduction [26]. The modeling and remodeling have their own cycles, which consist of replacing the old bone with new one. Both bone resorption and initial stage of new bone formation result in lower BMD. The new bone is mineralized resulting in BMD increase as it becomes mutual. The ability to monitor the BMD change helps to understand the cycles.

While the ME change triggers the tooth movement, it is expected that the tooth moves in the direction of applied force because of the resulting higher stress. The higher stress results in bone modeling and remodeling causing more BMD reduction. While biological responses have been widely investigated in animal experiments [2, 49-52], direct evidence of bone modeling and remodeling during orthodontic tooth movement is still lacking due to limitations of clinical studies. Reduction in BMD with decreased alveolar bone fraction had been noted in both animal and human studies [17, 49, 53]. Chang et al. [17] demonstrated that maximum BMD reduction occurs along the direction of the tooth movement, and Hsu et al. [53] showed that BMD changes along the tooth long axes. However, in these clinical studies, the tooth displacement in terms of magnitude and direction was not well defined and the BMD was checked only in scattered areas. Furthermore, the mineral density change in the root has not been reported previously. Revealing the relationship between BMD change, movement direction, and stress will help to understand the modeling process and to make better treatment plan.

1.8 Root Resorption is a Severe Side-effect and Need to be Quantified

During an orthodontic treatment, a side effect, root resorption, may occur. It is characterized by root shortening or shrinking [54]. Root length change had been widely reported in clinical studies [54, 55]. However, the root length is normally measured with 2D images in clinical study [54, 55], which may cause large error due to difficulty to align the images taken at different time points.

Several contributing factors to root resorption, like treatment type, duration, and level of force, had been tested. Dentists believe that the elevated stress causes more root resorption [54, 55]. However, this theory was not fully validated clinically. The major obstacles had been the ability to control the orthodontic loading and to reliably assess the root resorption. Whether the root resorption is proportional to the stress has not been proved. It is imperative to develop reliable methods to measure the root length/volume in vivo, to quantify the root changes, and also determine the relationship between stress and root length/volume change.

1.9 Quantification of ME, BMD Change, and Root Resorption Using CBCT

1.9.1 CBCT Based Morphological Analysis and FEA Method

Recently developed CBCT technology can be used for acquiring 3D radiographs for dental uses [56]. CBCT generate lower doses of radiation than medical CT [56], which allows us to assess bone densities during orthodontic treatment. It also allows longitudinal analysis, by taking sequence of images to record changes during treatment. Hounsfield units (HU) has been used to represent BMD to evaluate bone remodeling on CBCT images [57]. Studies suggested that HU is reliable to represent BMD on CBCT images [17, 53, 58-60]. With serial data acquisition in longitudinal studies, HU acquired

from CBCT has been shown highly correlation with medical CT. The parameter has been used to predict BMD and to quantify relative changes in bone [57, 61-64].

By using 3D images from CBCT, the clinically significant morphological change can be determined. Tooth length and volume can be measured in 3D, and BMD change can be represented by HU change. The ability of building FE model based on CT scans had also been validated in previous studies [30, 65-67]. The ME, like stress/strain, can be calculated. The challenge is how to effectively control the orthodontic load and test the relationships under patient variations. The solutions are to use reliable force measuring system to experimentally measure the load and applying proper statistical analysis to test inter-patient variation.

1.9.2 CBCT Limitations

There are limitations of the CBCT technology, which may affect the accuracy of the results. Unlike medical CT, assigned HU to voxels in CBCT images are relative HU, which is affected by the surrounding tissues [61, 68] and cannot be directly used to calculate BMD values [57, 69]. In addition, HU scale varies from different CBCT machines, which makes HU values incomparable [64]. The quality of the image is affected if the patient moves during the scanning, which reduce the reliability of the image, called “motion blur”. Furthermore, the resolution of CBCT is relatively low compared with medical CT. Minor tissue geometrical changes may not be detectable. The effects of these limitations need to be assessed before using the technology.

Researches have been done to provide partial answers. Some studies suggested that to observe changes during orthodontic treatment, it is necessary to take CBCT scans using the same machine with identical scanning settings to reduce error [17, 53]. Thus, the longitudinal analysis is applicable because the relative change can be reliably determined. The consistency need to be pre-validated. Furthermore, the effects of

resolution on the precision of the technology need to be evaluated. Due to the relative low resolution, minor tooth length and volume change may not be identifiable using CBCT.

1.10 Motivation

As mentioned above, in previous clinical studies, the force was not quantified and well controlled. The tooth movement mechanism was not clear and required clinical validation. The location of CRes, which is the key concept of the tooth movement control, has unknown variation, and the calculation was time consuming. The correlation between mechanical environment change and biological response was not clinically studied. A clinical study with customized and quantified load, quantified outcomes, and moderate sample size is required to validate and understand the tooth movement mechanism.

1.11 Objectives

The goal of this study is to establish the relationship between the treatment strategies to the clinical outcomes. The hypotheses are:

1. TR cause more root resorption and BMD reduction;
2. The portion of root and bone in the tooth movement direction has more BMD reduction;
3. The centroid of the projection of root surface is close to CRes;
4. The stress distribution is correlated with BMD change.

The objectives (OBJ) of this project are to validate the hypotheses by:

1. Developing a method to quantify the 3D load systems on the canine;
2. Determining the root resorption due to canine retraction using two treatment strategies;
3. Determining the BMD change distribution at the root surface and surrounding alveolar bone represented by HU;

4. Determining the relationship between BMD change and movement direction;
5. Determining the location, variation of CRes between patients;
6. Establishing a reliable and quick assessment method of CRes determination;
7. Determining stress in root, PDL, and bone, and test the relationship between stress and BMD change to understand the biological response to ME change.

CHAPTER 2. MATERIALS AND METHODS

2.1 Overview

To achieve the objectives of this study, a clinical study was conducted. Eighteen patients who needed maxillary canine retraction were recruited. The patients were treated at the orthodontic clinic of Indiana University School of Dentistry. The treatments were conducted by dental school faculty assisted by the orthodontics residents. The responsibilities of our engineering team were to design the T-loops that provide well-controlled orthodontic loads for translating or tipping the canine, to quantify clinical outcomes including tooth displacement, BMD changes in the tissues, root resorption, and ME changes. I was in charge of these tasks except the clinical tooth displacement analyses.

The treatment included the following steps:

1. A pre-treatment CBCT scan was taken for the patient who needed maxillary canine retraction on the first appointment. CRes of the patient's canines were calculated using FEM based on the CBCT scan. Customized M/F ratios for TR and CT were determined.
2. A dental cast of the patient was made, which copied the dental geometry.
3. The dental cast was attached to an orthodontic force measuring device, with the canines being separated from the cast and fixed to the loadcells that can simultaneously measure the three moment and three force components. Two T-loops, one for TR and one for CT, were made and tested on the force measuring device to gain designed M/F ratios.
4. The T-loops were delivered to the clinicians and for the canine retraction treatment.

5. Steps 2 to 4 would be repeated if a treatment milestone was reached and the treatment would continue. If the spaces were closed, a post-treatment CBCT scan was taken, and the treatment was finished.

Tooth length, volume, and mineral density change would be determined by comparing the pre- and post-treatment scans. The ME changes were calculated with FEM. The results were compared and analyzed to determine the relationship between the ME change and biological response. The experiment design is shown in Figure 2.1. The process done by clinics is marked green, and the results are marked red. The details are shown in the following sections.

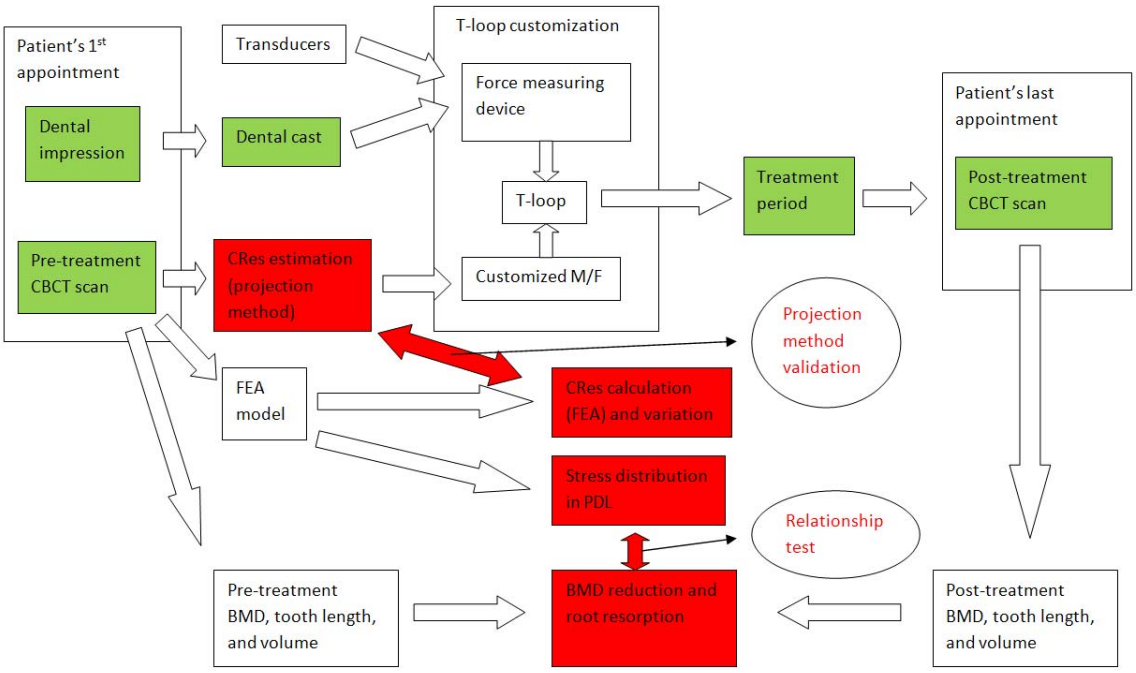

The steps marked green was done by clinics, and red were the results.

Figure 2.1: Experiment design showing the entire process of the treatment.

2.2 Materials

After receiving Institutional Review Board approval, eighteen patients (7 males and 11 females) were recruited in this prospective study. Informed consents were presented to and signed by the patients. The inclusion criterion was necessity of extraction of both maxillary 1st premolars and maxillary canine retraction for orthodontic treatment. The average age of patients was 19 years old. The age ranged from 12 to 47 years old with the standard deviation 9. One of the patient was 47 years old, one was 35 years old, and the other fourteen patients were between 12 to 22 years old. Prior to the study, the right and left 1st premolars were extracted and the upper dental arch was leveled and aligned with 0.019×0.025-inch Stainless Steel archwire engaged in the .022×.028-inch slot brackets. The maxillary second molars were included in the archwire and the maxillary 2nd premolar, 1st molar, and 2nd molar were co-ligated with a .010 stainless steel wire on each side, which served as the anchorage. The bilateral first molars were connected with a transpalatal arch for anchorage reinforcement. Segmental T-loops designed for the desired M/F were attached to the corresponding first molar and the canine by the clinicians. The loops were activated based on the calibration results. The treatment period varied depending on the size of initial space, appointment, and inter-patient variations. The average was 4.9 months. The canines displaced 2.1±1.5 mm. The canine displacement and its direction at the end of the canine retraction were obtained [70].

For each patient, segmental T-loops (See Figure 2.12 in section 2.7) were randomly assigned to the right and left canines to implement either translation (TR) or controlled tipping (CT). The T-loop delivered approximately 125 cN of closing force with predesigned moment-to-force ratio (M/F) to provide TR or CT load [71]. The load system delivered was quantified by the orthodontic force tester. (See section 2.5 of T-loop design and load measuring system) The CT load has relatively lower M/F than TR. Consequently, the stress on PDL would be different between two sides, which could lead to different outcomes.

The treatment was completed through several milestones. A milestone was defined as the time when one of the canines moved more than 1 mm. The time period between the milestones was considered as the treatment period. (See steps 2 to 4 in the overview) Dental casts were built before and after each treatment time as the dental records. The cast was made with polymer (DENTSPLY Repair Material, DENTSPLY International Inc., PA) using the dental impressions obtained in the clinic. Two sets of casts were made, one was for load testing and the other was for tooth displacement analysis, which was reported in a separate study [70]. The clinical part was supervised by Dr. Sean Liu of Department of Orthodontics and Oral Facial Genetics in the School of Dentistry at Indiana University.

The maxillary CBCT scans were performed on the same i-CAT Imaging System (Imaging Sciences i-CAT) of the Indiana University School of Dentistry. The voxel size was 0.25 mm and the scan time was 26.9 seconds. The scans of each patient were taken before and right after the canine retraction. The same setting was used for all the scans.

2.3 3D Feature Construction and Segmentation

Both CBCT images were imported into MIMICS 13.0 (Materialise, Belgium) to construct the 3D root and alveolar bone. The occlusal plane was aligned with the horizontal plane. The feature was constructed by 0.25 mm voxel size. Each voxel had a HU value. (See Figure 2.2)

The canine was then segmented semi-automatically by using the threshold function. Part of the root might need to be manually cleared. The scan would be dropped if severe motion blur was detected. The neighbor alveolar bone was also segmented similarly for further finite element modeling. Figure 2.3 shows the normal scan segmentation and motion blur.

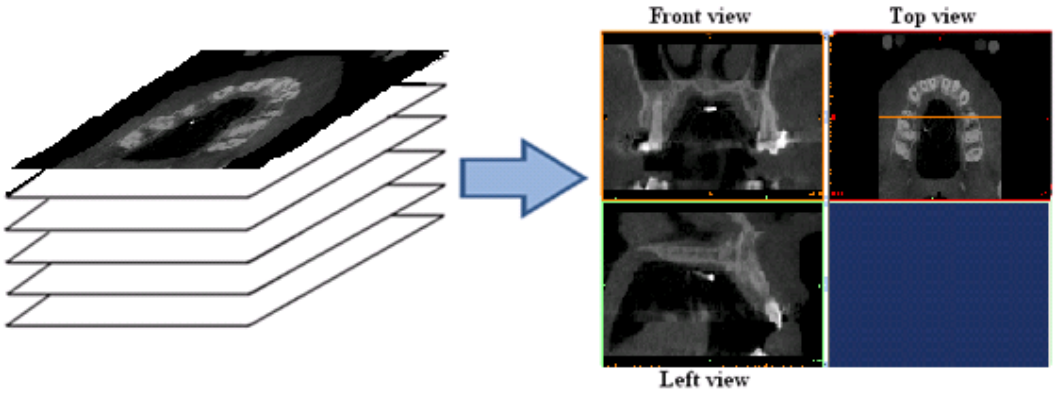

The 3D feature was generated by piling the CBCT images in MIMICS, composing with cubic voxels in 0.25 mm size.

Figure 2.2: 3D feature generation.

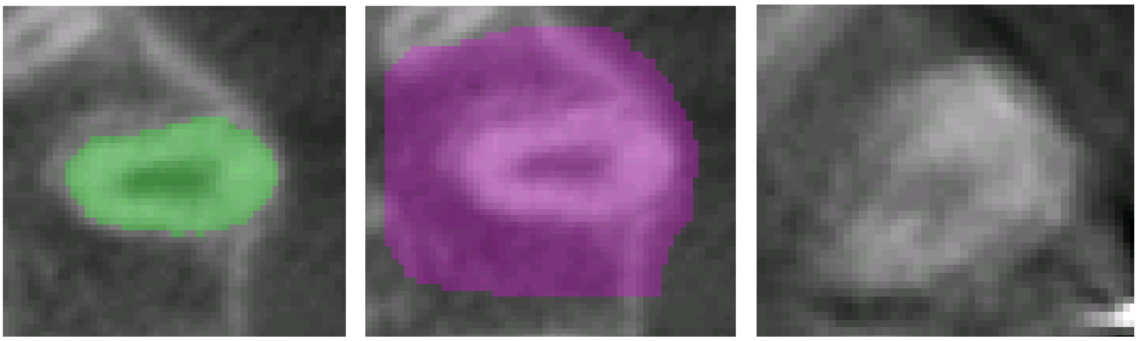

(a) Canine segmentation (b) Neighbor alveolar bone (c) Motion blur

(a) The root was segmented first as it had the highest HU. (b) Sufficient neighbor alveolar bone was also segmented for further modeling. (c) The low quality scans due to severe motion blur were dropped as the boundary was unclear.

Figure 2.3: Segmentation in MIMICS.

2.4 CRes and ME Determination

2.4.1 FEM

The FE model consists of the tooth, the PDL, and the alveolar bone. The schematics of the model is shown in Figure 2.4. Alveolar bone consists of the cancellous bone and a thin layer of cortical bone [72]. The crown, root, and cortical bone are dense material. The cancellous bone has relatively lower density, and PDL is soft tissue. PDL had been demonstrated as a fiber-reinforced structure in histologic studies [73-75]. Principal fibers resist tensile forces only.

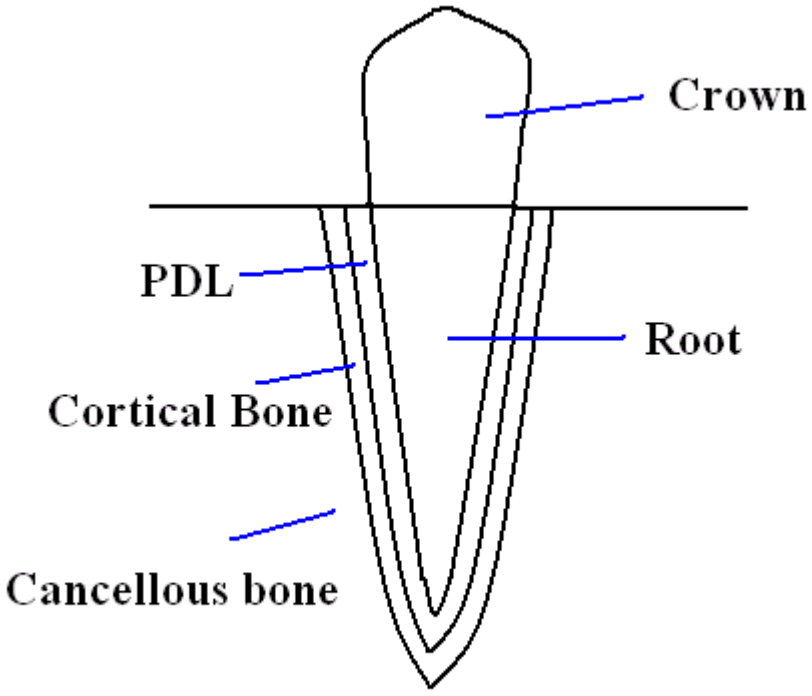

Figure 2.4: Schematic diagram of the finite element model.

After segmentation, the polylines of the canine and surrounding alveolar bone were exported to Pro-E to rebuild the geometry. The thickness of human PDL was around 0.1 to 0.3 mm (0.2 mm in average) [76]. Because of the CBCT resolution, the PDL layer was not clearly shown thus can only be estimated. In this study, the root was identified first. The PDL and cortical bone were grown from the surface of the root. The thickness of the PDL and cortical bone was 0.2 mm based on the literature [33]. The Pro-E file was then exported to ANSYS (Ansys Inc., Canonsburg, PE), FE analysis software. A bracket, on which the force and moment would be applied, was built and attached to the crown. The volumes were meshed with equal element edge length. 10 nodes element Solid187 had been used for its suitability to modeling irregular mesh. (See Figure 2.5) It was a tetrahedral element with mid-node on the edges.

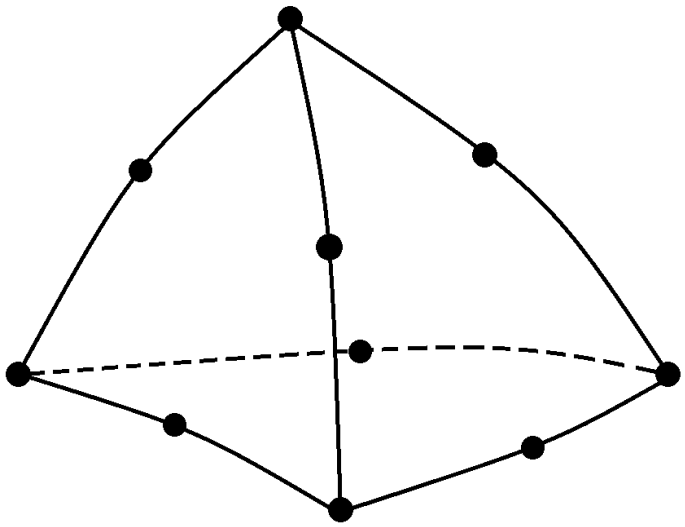

Figure 2.5: Diagram of 10 nodes tetrahedral element (Solid187).

As PDL was fiber-reinforced matrix and the fibers may affect the stress, horizontal two nodes link elements were created to connect the nodes on the root surface and cortical bone surface to simulate the fibers in PDL [33, 77]. The fibers were evenly distributed, and positioned 20 to 30 degrees to horizontal plane. Figure 2.6 shows the

structure of the FEA model. For boundary conditions, the bottom and MD sides of the bone were fixed.

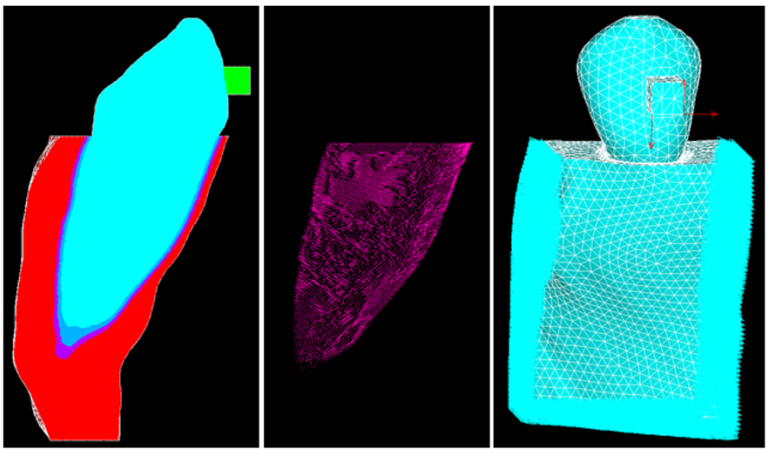

(a) FE model: Root – cyan; PDL – blue; Cortical bone – purple; Alveolar bone – red; Bracket – green (b) Fibers in PDL (c) Load and boundary conditions: the force and moment were applied on bracket; bottom, mesial, and distal sides of the bone were fixed.

Figure 2.6: Structure of the FEA model.

2.4.2 Convergence Test

As element size might affect the accuracy, a convergence test was made to determine it. While the tooth had irregular geometry, coarse mesh might not be able to represent the geometry well, which leads to error. The convergence test was conducted by incrementally increasing the element size and evaluating the resulting stresses. The tooth structure was meshed five times with the maximum element size varied from 1.0 to 0.2 mm. With the same loading condition, the maximum von-Mises stresses at several locations were recorded to check the convergence. The maximum element size needed for achieving consistent results were chosen for this study. The result is shown in section 3.5.

After the convergence test, the final finite element model was created, which included approximately 200,000 nodes and 150,000 elements for each tooth, including 7000 fibers. The material properties were assigned based on the literatures. Table 2.1 summarizes the material properties used in the study.

Table 2.1: Material properties assignment.

	Young's modulus	Poisson's ratio	Reference
Root	18 GPa	0.3	[31]
Cortical bone	13 GPa	0.3	[32]
Cancellous bone	1 GPa	0.3	[32]
PDL	0.5 MPa	0.45	[33]
Fibers in PDL	10 MPa	0.35	[33]
Bracket	200GPa	0.3	

2.4.3 CRes Location

To calculate the location of CRes by using FEM, a pure moment was applied on the crown in MD and BL directions respectively. The rotation center was considered as the CRes. Theoretically, the moment can be applied at any location. In a pilot study, the effect of applying the moment at different locations were tested. Applying the moment on root may cause only 0.5% difference in CRes location calculation. Applying the moment on the crown was preferred as the orthodontic load was applied on the crown and the difference was small.

2.4.4 Stress Calculation

To calculate the stress distribution in root, PDL, and surrounding alveolar bone, the load measured by the load measuring system was applied on the bracket. The bottom and two side surfaces of the supporting bone were fixed. The 1st principal, 2nd principal,

3rd principal, dilatational, and von-Mises stress in the root, PDL and alveolar bone were then calculated.

The sensitivity analysis using Cotter's method was done to test the effect of the fibers in the PDL and Poisson's ratio of cortical and cancellous bone to stress. Previous studies showed that the Poisson's ratio of cancellous bone and cortical bone can be lower than 0.3, even close to 0 [78, 79]. As for PDL, only few of FE studies included fibers in the PDL. A FE model was randomly chosen for the sensitivity test. The loading condition was kept the same. The design of the experiment using Cotter's method included 1) selection of 0.3 for the Poisson's ratio of the cortical and cancellous bone as well as inclusion of the PDL fibers as the upper level and 2) selection of 0.01 for the Poisson's ratios and exclusion of fibers as the lower level. The maximum 1st principal, 3rd principal, and von-Mises stress in root, PDL, cortical bone, and cancellous bone were recorded.

2.5 CRes Quick Assessment Method

As shown in Figure 2.7, the outer layer of the root was considered as the contact surface that estimated by eroding the root with one voxel. The location of CCS was then computed with the formula (1). Program written in Matlab was used to calculate CCS.

As shown in Figure 2.8, the root surface was projected to MD and BL plane. The projection could be easily obtained in MIMICS, which was composed by a layer of voxels. CPCSs in corresponding directions were computed with the formula (2, 3) with the same program. The results were compared with FEM for validation.

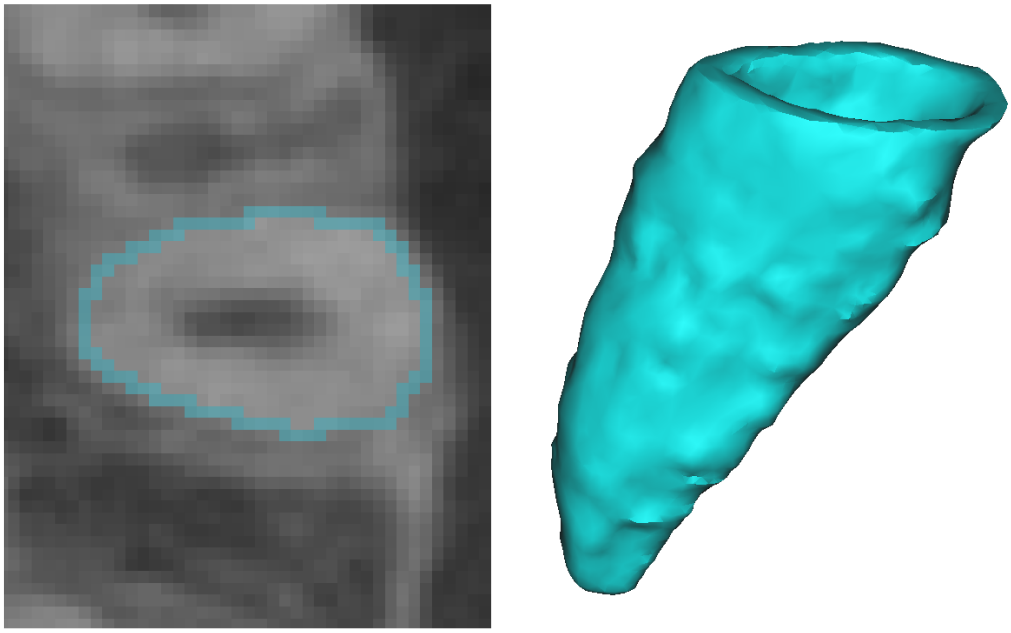

(a) (b)

Figure 2.7: Root's surface segmentation (a) and 3D surface layer (b).

$$CCS(x,y,z) = \frac{\sum voxel(x,y,z)}{number\ of\ voxels} \quad (1)$$

$$CP_{MD}(y,z) = \frac{\sum voxel(y,z)}{number\ of\ voxels} \quad (2)$$

$$CP_{BL}(x,z) = \frac{\sum voxel(x,z)}{number\ of\ voxels} \quad (3)$$

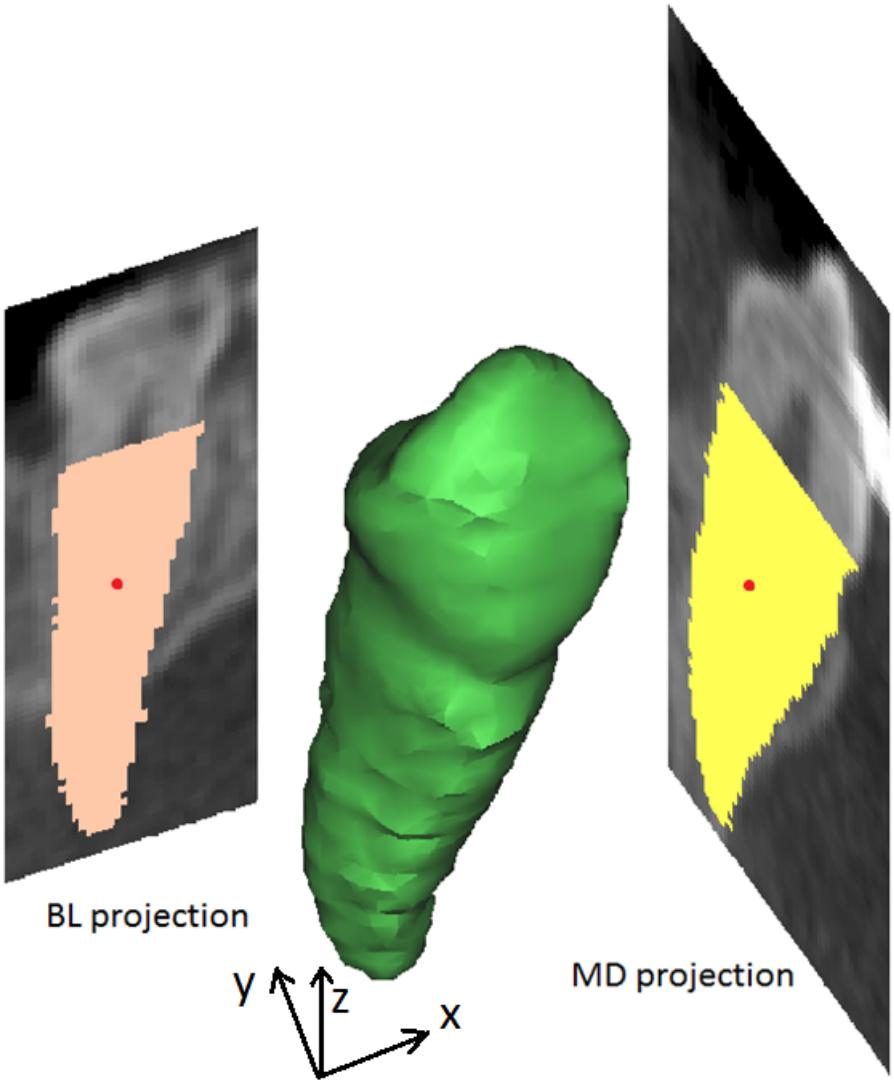

Figure 2.8: CPCS calculation for MD and BL direction.

2.6 Load Measuring System

The load measuring system was designed to measure the orthodontic load at the canine bracket (See Figure 2.12). Two load cells (Multiaxis force/torque Nano17; ATI Industrial Automation, Apex, NC) were used to measure the force and moment components applied at the canine brackets of the acrylic cast. The force range of each load cell was 0 to 20 N, with a 0.025-N resolution, and the moment range was 0 to 100 N-mm with a 0.003 N-mm resolution. An adapter was designed to hold the load cells and

the dental cast. The positions of the load cells can be adjusted to attach to the canines of the cast and be fixed.

2.7 T-loop Design

The calculation of the M/F can be illustrated using Figure 2.9. For a particular direction, the tooth translates when applying a force *F* at the CRes (Figure 2.9a, red). However, the force can only be applied at the bracket (Figure 2.8a, blue), which produces a moment ($F \cdot a$) at the CRes, tipping the tooth. Thus, an anti-tipping moment ($M=-F \cdot a$) needs to be applied at the bracket to prevent tipping and translate the tooth. Then, the M/F ratio is

$$\frac{M}{F} = \frac{F \cdot a}{F} = a$$

which equals to the vertical distance between the bracket and the CRes.

The method was used to determine M/F ratio in different directions. There are 1st order and 2nd order M/F. The former is to prevent the tooth rotation about the long axis of the tooth and the 2nd order is to prevent tipping in the mesial-distal direction. The determination of the 2nd order and the 1st order M/F were illustrated in Figure 2.9. Similarly, the M/F ratio in the 1st order is equal to *b* to prevent the rotation about vertical axis.

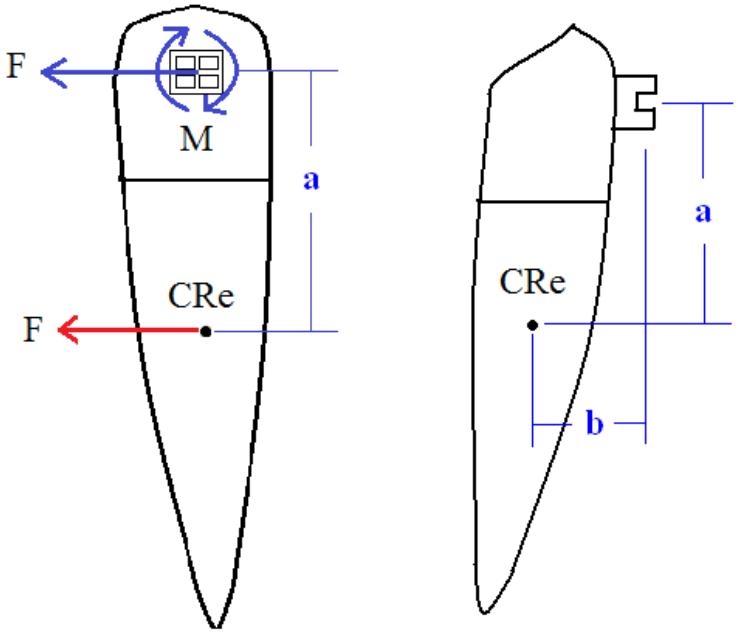

(a) Front view of canine (b) Side view of canine
a and *b* are the vertical and horizontal distance between the center of bracket and CRes

Figure 2.9: Customized M/F design based on the individual CRes.

The customized T-loop is designed in the following steps after the M/Fs for tipping and translation were calculated.

For each patient, the right and left canines were randomly assigned to receive controlled tipping (CT) or translation (TR) orthodontic tooth movements. To accomplish CT or TR, two segmental T-loops, made of 0.017”×0.025” TMA wire (Ormco, Glendora, CA), were designed and fabricated to deliver different M/F to retract canines. The T-loops on both sides were designed to deliver 124 cN of retraction force [16]. The desired M/F ratios for CT and TR were calculated using finite element (FE) models of the patients, constructed based on CBCT described previously.

The IBD was defined as the distance from the mesial aspect of the auxiliary tube of the 1st molar bracket to the distal aspect of the canine bracket. This IBD was expected to decrease during canine retraction and, with it, there would be more decrease in force

then moment, resulting in an M/F increase. For this reason, measures for initial M/F adjustment needed to be conducted. The M/F increase in the retraction plane per 1 mm IBD reduction was estimated using the LOOP (Kifissia, Hellas, Greece) simulation software. An approximate 50% M/F increase was estimated per 1 mm IBD reduction from this analysis. In this study, each treatment period was defined as when a canine was retracted more than 1 mm, which was measured during each office visit. The IBD changes were expected to vary significantly because of variation in treatment time period due to scheduling related issues. Thus, the total M/F increase could only be estimated, which was set at 70%. To be consistent, the calculated M/F for translation was decreased by approximately 35% (half of the estimated total M/F increase) to ensure that the average M/F during the treatment period was close to the ideal value. The M/F for tipping was further discounted to enhance tipping effects. In addition, in order to prevent mesial-out rotation caused by the retraction force, the desired anti-rotation moment for translating the tooth was also calculated using the same FE model. To ensure the average M_z/F_y ratio (See Figure 2.10 for coordinates definition) to be close to the desired value, the implemented initial M_z/F_y was reduced by approximately 35% on both canines to compensate the effects of IBD reduction. However, the target M_z/F_y was difficult to achieve because it was primarily realized by adjusting the 1^{st} order gable angles. Large gable angles were required in many cases, which caused the T-loop to interfere with the cheek or gum. To avoid interference, only smaller gable angles could be introduced, which caused M_z to be lower than the target value. The main focus of this study was on translation and tipping. The control of M_y was considered secondary and thus was allowed to be compromised in some cases. Other load components were kept minimal when the T-loops were produced.

According to the desired load system, the T-loops were bent to express desired force and moment components. These components were calibrated experimentally on the corresponding dental casts. The casts were prepared using the following protocol. Over the period of canine retraction, patients were seen every 5-6 weeks. A decision was made on whether a treatment interval was completed. A treatment interval was defined when

one canine moved more than 1 mm. Thus, multiple intervals might occur for each patient because all patients in this study had more than 3 mm space between the canine and the 2nd premolar. However, the number of intervals various among the patients due to the difference in tooth movement rate and duration between office visits. When an interval was completed, an impression was made, the T-loop was retrieved, and a new T-loop was designed and applied. Then the next treatment interval began. The casts were made before and after each interval. At the beginning of each treatment interval, each T-loop was adjusted on the corresponding duplicate acrylic model attached to a custom-made orthodontic force tester (OFT) [42] to ensure delivering accurate loads. Impression of upper dental arch was made by injecting light and medium-body polyvinylsiloxane (PVS) material (Examix NDS, GC Corporation, Tokyo, Japan) over the brackets, followed by alginate impression. Duplicate canine and first molar brackets with tubes (Burstone TM, Ormco, Glendora, CA) were placed in the PVS and autopolymerizing acrylics (Repair Material, Dentsply, York, PA) were packed into the impression and allowed to cure. The acrylic model was attached to the OFT with two screws. The target teeth (canines) were attached to the load cells with epoxy adhesive (Loctite E-120HP Hysol Epoxy Adhesive, Henkel, Rocky Hill, CT) and then were completely separated from the acrylic model, thus maintaining their original positions and orientations (Figure 2.10).

After measuring the initial IBDs between the canine and molar tubes of the acrylic model, a T-loop was made with the geometry shown in Figure 2.11, The size, shape, leg length, and dimensions of T-loops were determined considering their effects on the load system [80], as well as avoiding interference with the cheek and gum. The first and second order gable bends were added symmetrically to the T-loops to bring the load components to the targets, Figure 2.12. The loop bending and adjustment process was iterated until the desired force and moments were accurately expressed. The horizontal leg was bent on each end of the T-loop to allow easy insertion into the tube, which also ensured that the IBD was identical when transferred the OFT validated T-loop to the patient, Figure 1.3. The validation was performed on the OFT. T-loops were installed on the duplicate acrylic model attached to the OFT for testing force and

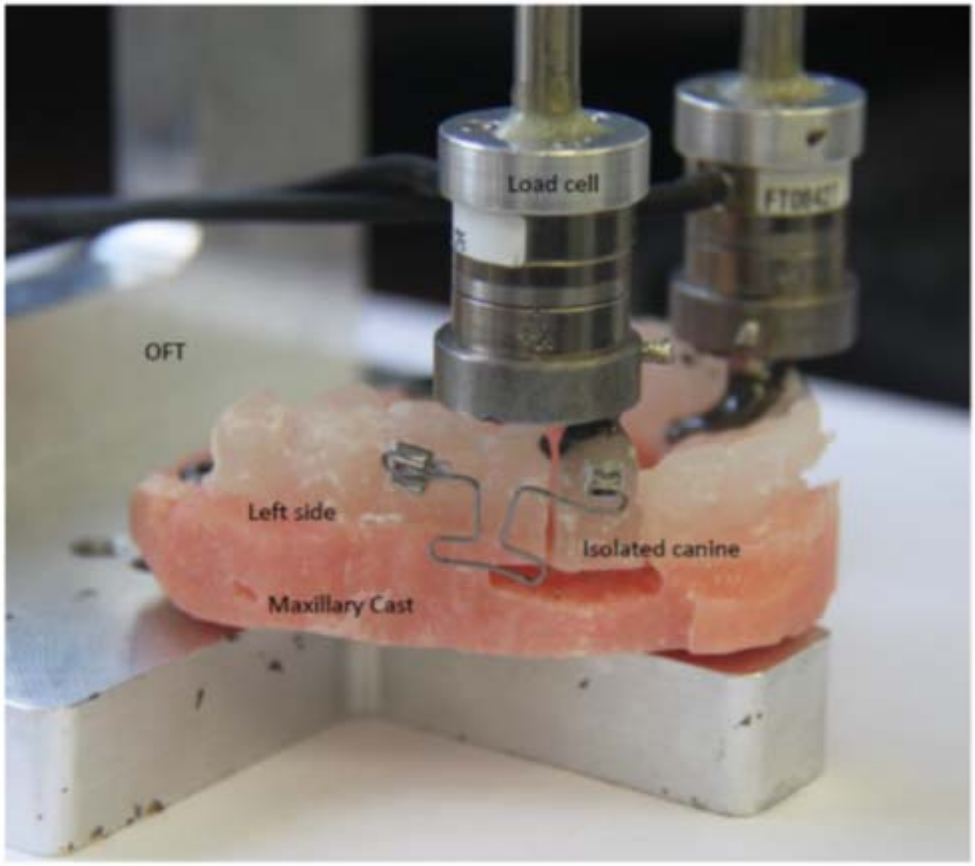

(a)

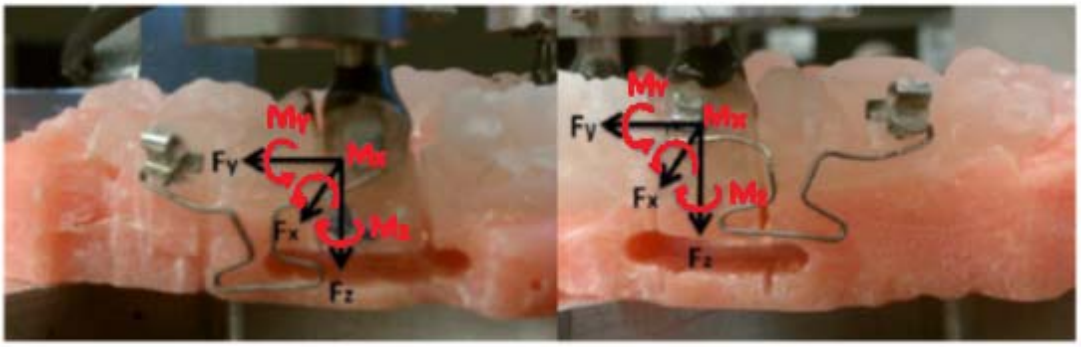

(b) (c)

(a) The laboratory setting for measuring orthodontic load system on the canines. The setting includes an orthodontic force tester, a dental cast with brackets, and the T-loops. The coordinate systems on the left-side (b) and right-side (c) were defined at the centers of the canine brackets.

Figure 2.10: Force measuring system.

moment components. The OFT was designed to measure the orthodontic load system at the canine's bracket (Figure 2.10). Two load cells (Multiaxis force/torque Nano17, ATI Industrial Automation, Apex, NC) were used to measure the six force and moment components applied at the canine brackets. The force range of each load cell is 0-20 N with a 0.025 N resolution and the moment range is 0-100 N-mm with a 0.003 N-mm resolution. A local coordinate system was established on each left canine with the retraction direction aligned with the load cell's positive y axis, the buccal direction with the positive x axis, and the gingival direction with the positive z axis (Figure 2.10). The local coordinate system on the right canine was different from the left canine (Figure 2.10). In this study, the clinically expressed load systems were of interest and the side was not a controlled parameter because tipping or translation was randomly assigned to each side. Thus, the clinically used coordinate system on the left side was used to describe the results.

For each treatment interval, an acrylic model was fabricated after each treatment period and a new T-loop was bent for each canine and adjusted using the OFT. The post-treatment IBDs were also recorded. The T-loops used in the previous treatment were retrieved and installed on the post-treatment acrylic model to measure the residual load system using the OFT. The T-loops retrieved were examined visually for signs of permanent deformation or other damages due to removal. The damaged T-loops were excluded from this study. Consequently, both initial and residual load systems were recorded.

To assess the errors due to wire installation and instrument, a cast and a T-loop were used for a repeatability test. The same T-loop was installed on the same cast ten times. The resulting load system corresponding to each installation was measured. The mean and standard deviation were calculated.

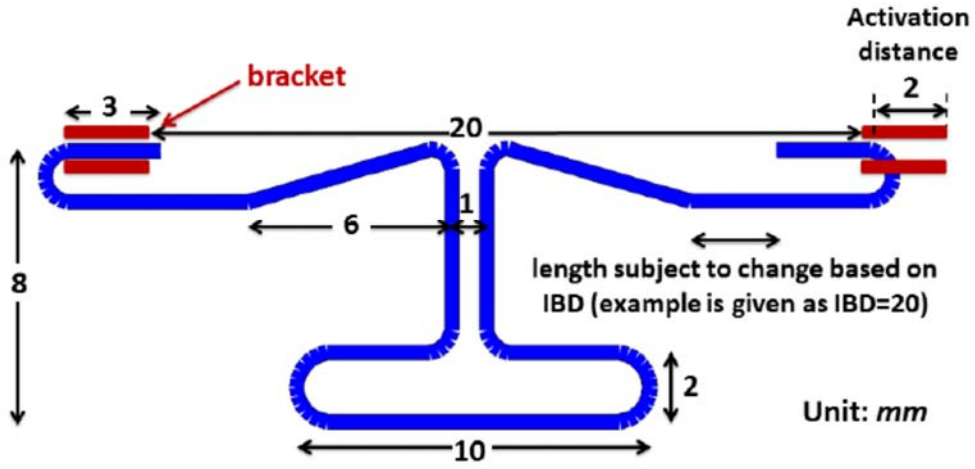

Figure 2.11: The geometry and dimensions of the loop before the 1st and 2nd order bends were added.

Figure 2.12: Calibrated T-loop.

2.8 Root Resorption

After segmentation, the canine length could be easily measured by using the 3D length measuring function in MIMICS. (See Figure 2.13 a) The tooth length was defined as the distance between crown tip and root tip. The length difference could be obtained.

During scanning, the metal bracket caused reflection blur in the images, which leaded to unreliable volume measurement. Unfortunately, removing the brackets just for the CBCT scan was not applicable as the patients may receive further orthodontic treatments after this study. Therefore, the crown portion had to be removed while calculating the root volume. To make a consistent cut for all teeth, a sphere with 10 mm diameter and centered at the crown tip was created, and then the sphere part including the entire crown was cut from the tooth. The volume of the remaining part of the tooth was considered as the root volume. (See Figure 2.13 b)

Paired t-test is applied to test the significance of length and volume change on the CT and TR sides. Besides, tooth length change more than 0.5 mm was considered as evidence for apical root resorption because the voxel size of the CBCT image was 0.25 mm. This is acceptable because the clinical detectable root shortening currently is larger than 0.5 mm.

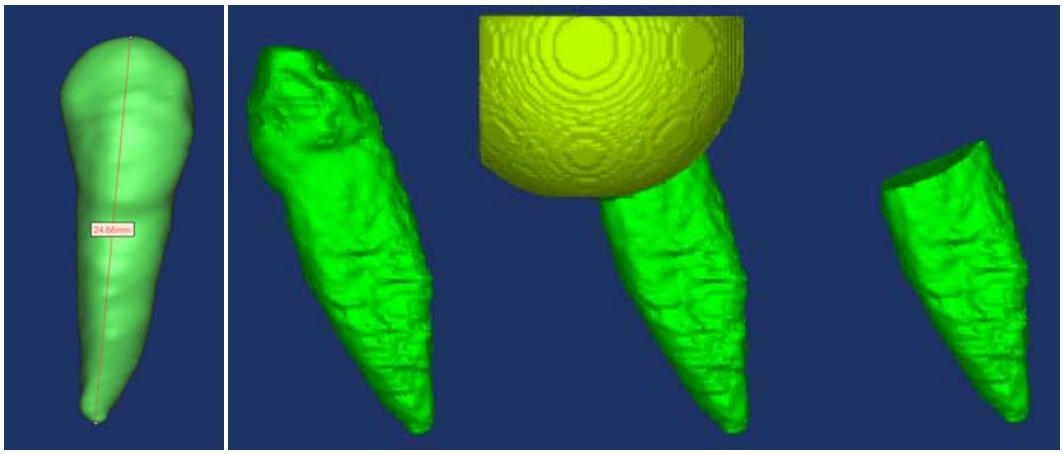

(a) (b)

(a) Tooth length measurement by using MIMICS (b) Root volume was measured by the tooth volume minus the crown volume

Figure 2.13: Tooth length and root volume measurement.

2.9 Mineral Density Study

The HU was related to the tissue mineral density [17, 53, 58-60]. The high the density the higher the HU will be. HU was used to represent the relative BMD change in this study.

To determine the HU change in root and surrounding alveolar bone, the corresponding volume need to be isolated. Inclusion of more alveolar bone would reduce sensitivity. Having the layer too shin might lose cortical bone. In a pilot study, the effect of the bone shell thickness was tested. Larger noise was detected while using 0.25 mm as the thickness, and lower HU change was detected while using 0.75 mm as it was not close to the PDL. Then 0.5 mm was chosen to effectively represent the HU change. The layer was created in following steps. The root was segmented first. The PDL was recognized as one voxel (0.25 mm) of radiolucency surrounding the root. The surrounding alveolar bone within two radiopaque voxels (0.5 mm) to the PDL was formed into a bone shell. A root surface shell was then defined by eroding the PDL with two voxels. (Figure 2.14)

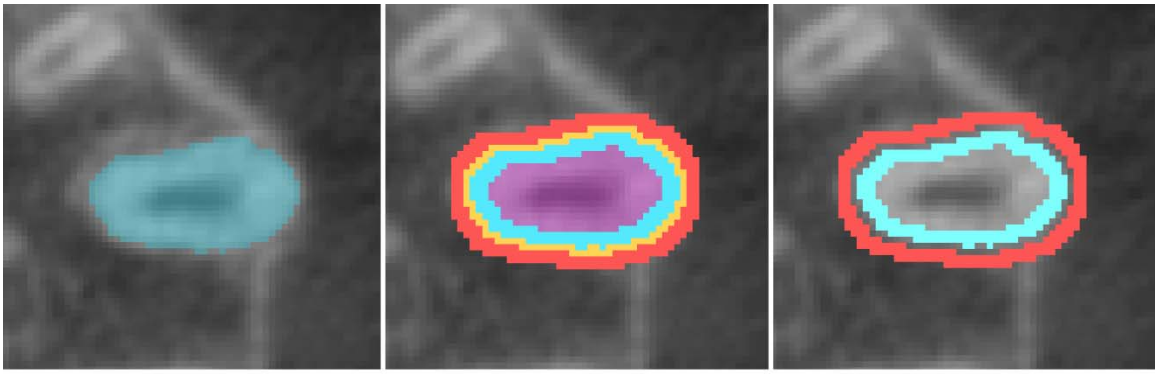

(a) Segmentation of the root. (b) The boundaries of interested areas, root surface and surrounding alveolar bone, were determined by dilating or eroding the root. (c) Root surface layer and surrounding alveolar bone layer were obtained by Boolean operations.

Figure 2.14: Segmentation of root surface and surrounding alveolar bone.

The root surface and alveolar bone shells were divided into 3 by 36 divisions. In the vertical direction, the serial axial slices from the root apex to cervical enamel junction were equally divided into three levels, the apical, middle, and coronal levels. In the occlusal plane, the shells were divided into 36 divisions circumferentially (D1 to D36). Looking in the occlusal direction, the divisions were labeled counterclockwise for the left canine and clockwise for the right canine with the division in the direction of movement (compression side) being labeled as D1. (Figure 2.15) The divisions D19 were opposite to the direction of movement, subjected to tension. While D1 is approximately in the distal direction, the divisions D2-D18 were located on the buccal side, whereas D20-D36 on the lingual side. The average value of HU of each division in each level was computed from both pre- and post-treatment CBCT scans. The changes in HU defined by the subtraction of pre-treatment HU from the post-treatment at each division was computed and plotted.

Mixed-model ANOVA was used to evaluate the effects of treatment strategy, direction of tooth movement, and divisions with different thirds on HU changes. Random effects were included for subject, subject-by-treatment, subject-by-direction, and subject-by-divisions. Means, standard errors, and 95% confidence intervals for the means were estimated using the ANOVA.

To assess reliability of the HU measurement obtained from CBCT images, a custom designed phantom (Computerized Imaging Reference Systems, Inc, Virginia) had been scanned five times using the identical CBCT settings. The phantom has 16 BMD rods distributed on the dental arches with BMD ranging between 100 to 700 mg/cc. The intra-class correlation coefficient (ICC) was calculated to assess the variation and reliability of CBCT. ICC is between 0 and 1. A high ICC value proves the high correlation between the true BMD and the HU shown in CBCT. While the BMD rods distribute on the entire dental arches, it also assess the positon effect to the CBCT scan.

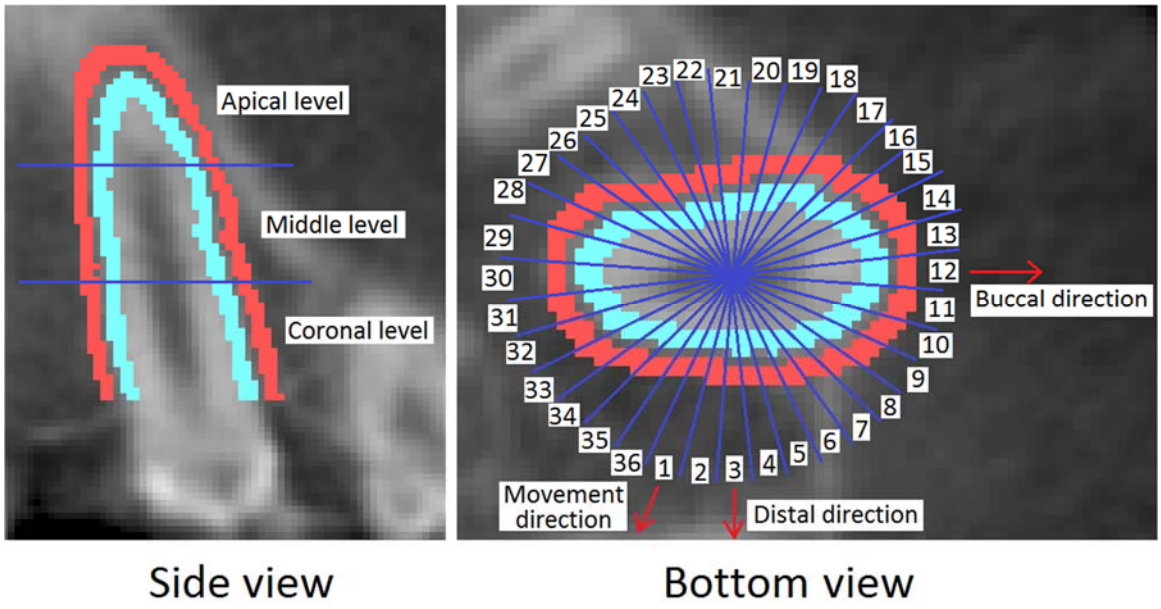

The movement direction was approximately in the distal direction.
It might slightly point to the buccal or lingual direction.

Figure 2.15: Formation of the root surface and alveolar bone shell, and division of the 3 by 36 regions for the left side canine.

The errors due to the segmentation process had also been assessed. As the segmentation process requires some manual clearing of tissue boundary, the reliability of manual operation need to be tested. Thus, the process for segmenting the root surface and surrounding alveolar bone from a single CBCT scan was repeated five times. The average standard deviations of the HU of all directions were computed at the root surface and surrounding alveolar bone to estimate the segmentation errors and variations.

2.10 Relationship Determination

The correlation between tooth movement direction and BMD change in terms of HU would be shown while D1 was aligned with the tooth movement direction. The HU in different divisions were analyzed with mixed model ANOVA. Whether the HU in the divisions of tooth movement direction was different to the other divisions can be shown.

The correlation between BMD change and stress was tested with statistical analysis. By using the same dividing method as shown in section 2.9 (See Figure 2.15), the average nodal stresses in root, PDL, and surrounding alveolar bone were also expressed in the same 3 by 36 divisions, which enable meaningful comparisons between the stress and BMD in terms of HU changes. Mixed model ANOVA was applied to test the correlation between stress and HU change. Correlation coefficient, μ, was used to represent the correlations between stress and HU change distribution. In this study, the correlation coefficients and interpretations are defined as shown in Table 2.2.

Table 2.2: Interpretations of correlation coefficients.

Correlation coefficient range	
$\|\mu\| < 0.5$	Weak correlation
$0.5<\|\mu\| < 0.8$	Moderate correlation
$\|\mu\| > 0.8$	Strong correlation

CHAPTER 3. RESULTS

3.1 Reliability Test of CBCT Scans, Segmentation Operation, and Repeatability Test of Loading the T-loop

The CBCT scan has acceptable variation. The ICC was determined to be 0.94, which represents high correlation among CBCT scans. The segmentation process resulted in an average error of 3.1 HU for root surface and 3.3 HU for surrounding alveolar bone, which is less than 1% of the average HU value.

The variation of the orthodontic load due to installation was assessed. Table 3.1 shows the results as well as the means and standard deviations from loading the same T-loop on the loading measuring device for 10 times. The retraction load is the distal force and the anti-tipping moment is the buccal moment. The variation is about 0.9% for the target force and 1.5% for the target moment, meaning the method meets the accuracy requirement of this project.

3.2 Root Resorption

Table 3.2 and Table 3.3 show the root length and volume changes of the canine on the TR and CT sides. The P-values for comparing the pre- and post- treatment length and volume were calculated by using paired t-test. The tooth length increase was marked blue, and the reduction more than 0.5 mm was marked red.

Table 3.1: Repeatability test of loading the T-loop.

	Force (N)			Moment (N·mm)		
	Buccal	Distal	Apical	Buccal	Distal	Apical
1	-0.28	1.16	0.21	-6.95	-3.32	-5.10
2	-0.29	1.18	0.23	-6.93	-3.29	-4.88
3	-0.29	1.19	0.25	-6.81	-3.22	-4.77
4	-0.30	1.17	0.26	-6.70	-3.54	-4.63
5	-0.29	1.17	0.25	-6.80	-3.49	-4.67
6	-0.30	1.14	0.23	-6.92	-3.56	-4.64
7	-0.28	1.17	0.23	-6.86	-3.23	-4.90
8	-0.28	1.17	0.25	-6.70	-3.47	-4.70
9	-0.29	1.15	0.25	-6.78	-3.47	-4.71
10	-0.28	1.17	0.26	-6.66	-3.41	-4.74
Mean	-0.29	1.17	0.24	-6.81	-3.4	-4.77
STD	0.01	0.01	0.02	0.10	0.12	0.15

Table 3.2: Geometrical change of the canine of translation side.

TR	Tooth length Pre- (mm)	Tooth length Post- (mm)	Difference (mm)	(%)	Root volume Pre- (mm^3)	Root volume Post- (mm^3)	Difference (mm^3)	(%)
P01	25.0	24.4	-0.6	-2.4	281	264	-17	-6.0
P02	31.6	31.4	-0.2	-0.6	367	393	26	7.1
P03	24.8	25.1	0.3	1.2	329	323	-6	-1.8
P04	27.5	26.8	-0.7	-2.5	367	344	-23	-6.3
P05	27.2	26.5	-0.7	-2.6	403	388	-15	-3.7
P06	27.5	27.6	0.1	0.4	390	389	-1	-0.3
P07	26.2	25.7	-0.5	-1.9	284	281	-3	-1.1
P08	24.6	24.7	0.1	0.4	241	251	10	4.1
P09	28.4	28.8	0.4	1.4	415	391	-24	-5.8
P10	24.5	24.2	-0.3	-1.2	337	360	23	6.8
P11	22.8	22.6	-0.2	-0.9	203	201	-2	-1.0
P12	31.1	30.6	-0.5	-1.6	423	400	-23	-5.4
P13	25.2	25.6	0.4	1.6	236	242	6	2.5
P14	26.4	26.1	-0.3	-1.1	375	373	-2	-0.5
P15	24.8	22.7	-2.1	-8.5	302	290	-12	-4.0
P16	29.6	29.6	0	0.0	472	526	54	11.4
P17	27.4	27.4	0	0.0	385	400	15	3.9
P18	25.2	25.5	0.3	1.2	242	254	12	5.0
Average	26.7	26.4	-0.3	-1.0	336.2	337.2	1.0	0.3
STD	2.4	2.5	0.6	2.3	75.9	80.3	20.2	5.2
P-value			0.09				0.84	

Table 3.3: Geometrical change of the canine of tipping side.

CT	Tooth length Pre- (mm)	Tooth length Post- (mm)	Difference (mm)	(%)	Root volume Pre- (mm^3)	Root volume Post- (mm^3)	Difference (mm^3)	(%)
P01	24.6	23.7	-0.9	-3.7	281	230	-51	-18.1
P02	29.1	29	-0.1	-0.3	382	385	3	0.8
P03	25.0	24.7	-0.3	-1.2	305	294	-11	-3.6
P04	27.7	27.2	-0.5	-1.8	356	345	-11	-3.1
P05	25.5	25.2	-0.3	-1.2	376	351	-25	-6.6
P06	27.8	28.1	0.3	1.1	401	406	5	1.2
P07	24.7	25.0	0.3	1.2	293	298	5	1.7
P08	25.0	24.7	-0.3	-1.2	263	275	12	4.6
P09	29.0	29.1	0.1	0.3	397	385	-12	-3.0
P10	25.6	25.4	-0.2	-0.8	360	387	27	7.5
P11	22.8	22.5	-0.3	-1.3	205	188	-17	-8.3
P12	30.1	29.8	-0.3	-1.0	439	438	-1	-0.2
P13	24.4	24.7	0.3	1.2	213	218	5	2.3
P14	28.0	27.9	-0.1	-0.4	413	422	9	2.2
P15	26.6	24.6	-2	-7.5	343	285	-58	-16.9
P16	27.8	27.6	-0.2	-0.7	427	482	55	12.9
P17	27.0	27.1	0.1	0.4	366	370	4	1.1
P18	25.1	25.3	0.2	0.8	258	267	9	3.5
Average	26.4	26.2	-0.2	-0.9	337.7	334.8	-2.9	-1.2
STD	2.0	2.1	0.5	2.1	71.9	82.0	25.8	7.7
P-value			0.084				0.64	

3.3 HU Change

3.3.1 HU Change at Root Surface Using the Data from the Two Strategies

The average HU changes on the root surface due to the canine retraction are shown in Figure 3.1. In general, The HU on the root surface decreased due to the treatment. Apparently, the HU reduction varies among the three levels. The division average HU reduced by 1.7% (±11.2%), 2.0% (±10.1%), and 2.9% (±11.3%) at the Apical, Middle, and Coronal level, respectively. Looking at the HU reduction in different directions, the maximum average reductions occurred in D11 and D27, which were approximately perpendicular to the direction of movement. The maximum changes were

4.3% (±11.6%) in D12 and 4.3% (±11.2%) in D27. The most severe reduction was at the coronal level primarily.

Without considering the level effect, the average division HU values in different color frames were significantly different ($p<0.05$), see in Figure 3.1. The HU reduced more in divisions, D10-D13 and D25-D28, than in D31-D4 and D18-D21. Within the specific canine displacement directions, the level of reduction varied among the levels. The reductions among the three levels in the directions of D11-D13 and D19-D28 were significantly different ($p<0.05$). However, comparing the average HU values among the three levels, there were no significant differences ($p=0.3$) observed.

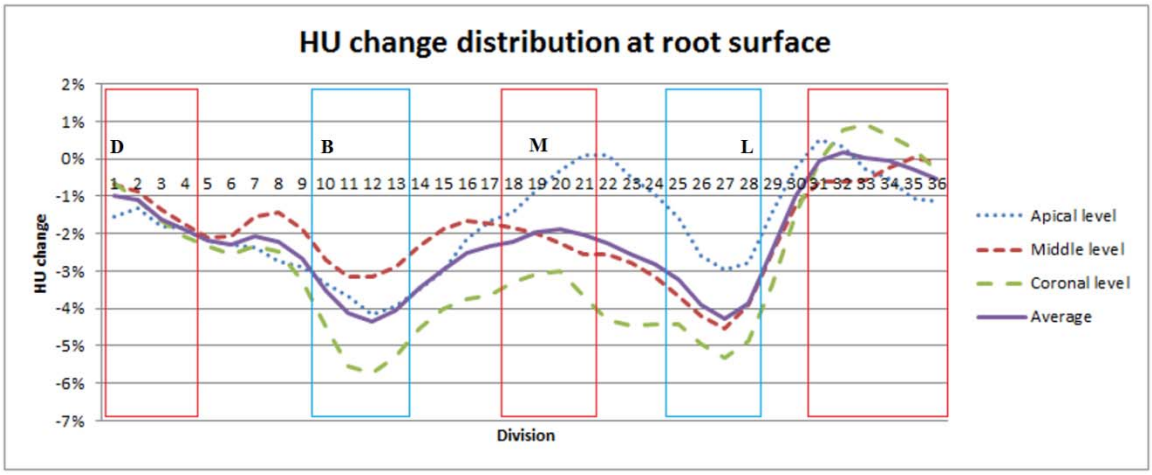

Figure 3.1: Average HU change distribution at root surface.

3.3.2 Comparing HU Change in Root Surface between the Two Strategies

Both strategies resulted in reduction of HU in root surface. Two treatment strategies resulted in similar HU change patterns. No divisions showed statistically significant difference between TR and CT strategies. (See in Figure 3.2) There was no significant difference between the overall HU changes as well ($p=0.32$). At each level, the HU reductions also had no significant differences between the two strategies ($p=0.61$

for Apical level, p=0.29 for Middle level, and p=0.29 for Coronal level). Considering the effects of levels on the HU within each strategy, there were no significant differences among the levels for CT (p=0.47) or TR (p=0.24).

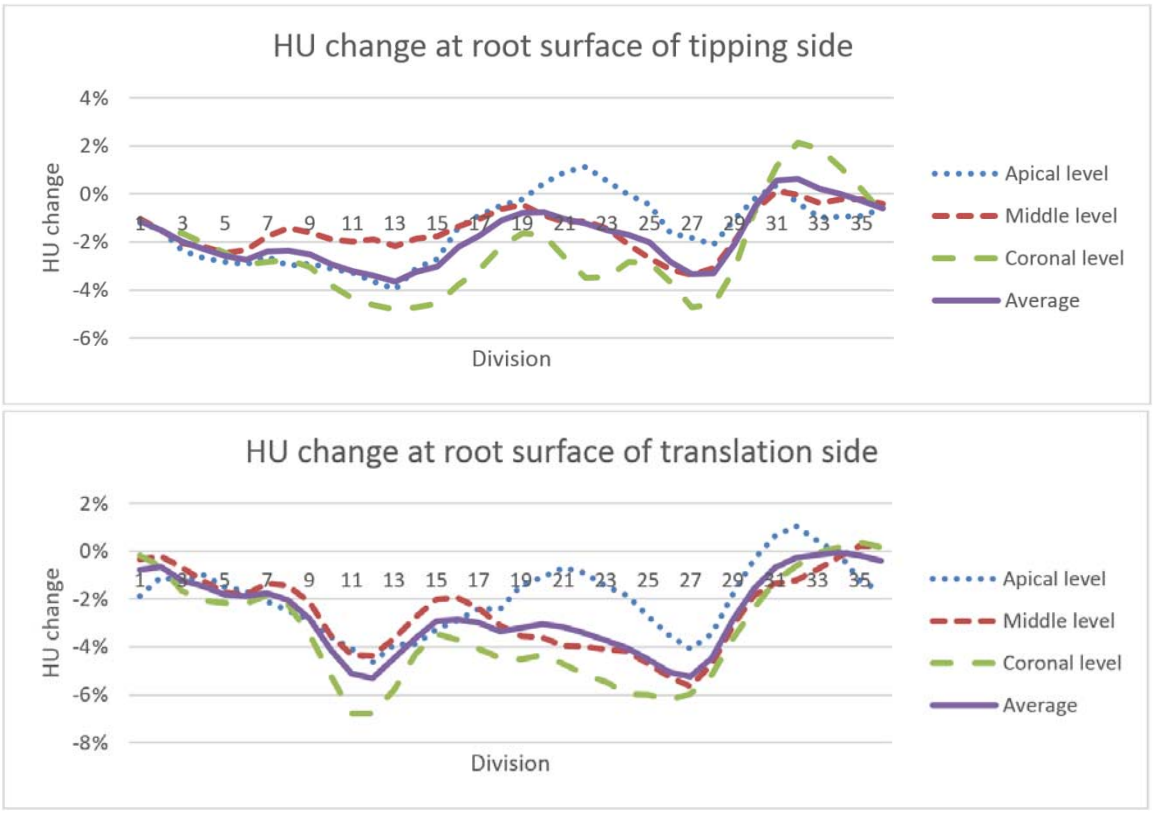

Figure 3.2: Comparison of average HU change in root boundary with treatment strategy.

3.3.3 HU Change in Surrounding Alveolar Bone Using the Data from the Two Strategies

The average HU changes in the three levels in the surrounding alveolar bone due to the canine retractions are shown in Figure 3.3. The HU on the surrounding alveolar bone decreased in most directions. The average division HUs reduced by 4.2% (±26.3%), 3.0% (±27.7%), and 11.0% (±28.5%) at the Apical, Middle, and Coronal levels, respectively. At each level, the maximum reductions occurred in D6 and D20,

which was closely aligned to the tooth's movement direction. The maximum changes were 12.7% (±28.6%) in D6 and 12.0% (±33.7%) in D20. The maximum average increases occurred in D12 and D27, which were approximately perpendicular to the direction of movement. The increases were about 8.1% (±27.4%) in D12 and 3.1% (±25.4%) in D27.

Without considering the level effect, the average division HU values in different color frames were significantly different ($p<0.05$). The HU reduced the most in D17-D22 and D35-D8 while increased in D10-D14 and D26-D28 divisions. Without considering the division effect, there were significant differences among the levels. Coronal level obtained more reduction than Apical level ($p=0.04$) and Middle level ($p=0.01$). Considering the effect of the levels on the specific divisions, the HU reduction in the directions of D27-D3 (distal and distal-lingual region) were significantly different ($p<0.05$).

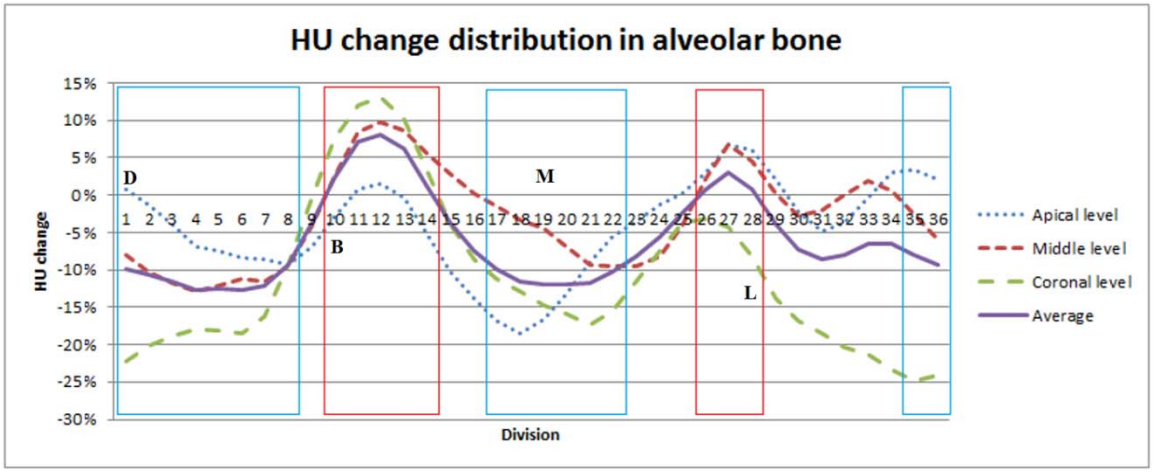

Figure 3.3: Average HU change distribution in alveolar bone.

3.3.4 Comparing HU Change in Alveolar Bone between the Two Strategies

Two treatment strategies resulted in similar HU change patterns. No divisions showed statistically significant difference between TR and CT strategies. (See Figure 3.4) There was no significant difference between the overall HU changes as well ($p=0.62$). At each level, the HU changes had no significant differences between the two strategies ($p=0.91$ for Apical level, $p=0.83$ for Middle level, and $p=0.32$ for Coronal level).

However, the two sides showed some difference in comparison of the level difference individually. Considering individual treatment strategy, there was no significant differences among the levels for TR in general ($p=0.38$) while there was significant differences among the levels for CT in general ($p<0.05$). For CT, HU reduction at the Coronal level was larger than Apical level ($p=0.03$) and Middle level ($p=0.01$). The general significant level difference for CT was primarily introduced by D27-D3 ($p<0.05$, distal and distal-lingual region), with the highest reduction occurred at the Coronal level.

3.4 Location of CRes, CCS, and CPCSs

The root length, locations of CRes in the MD and BL directions, and the difference between the calculated CRes in both directions using the FE method were shown in Table 3.4. The average root length was 16.5 ± 1.7 mm. The average location of CRes was 60.2% ± 2.6% in MD direction, and 58.4% ± 3.2% in BL direction. The average difference was 1.8% ± 2.8%. The difference of CRes in MD and BL directions was statistically significant ($p=0.012$) from the paired T-test. The FEA results were used as the reference locations of CRes.

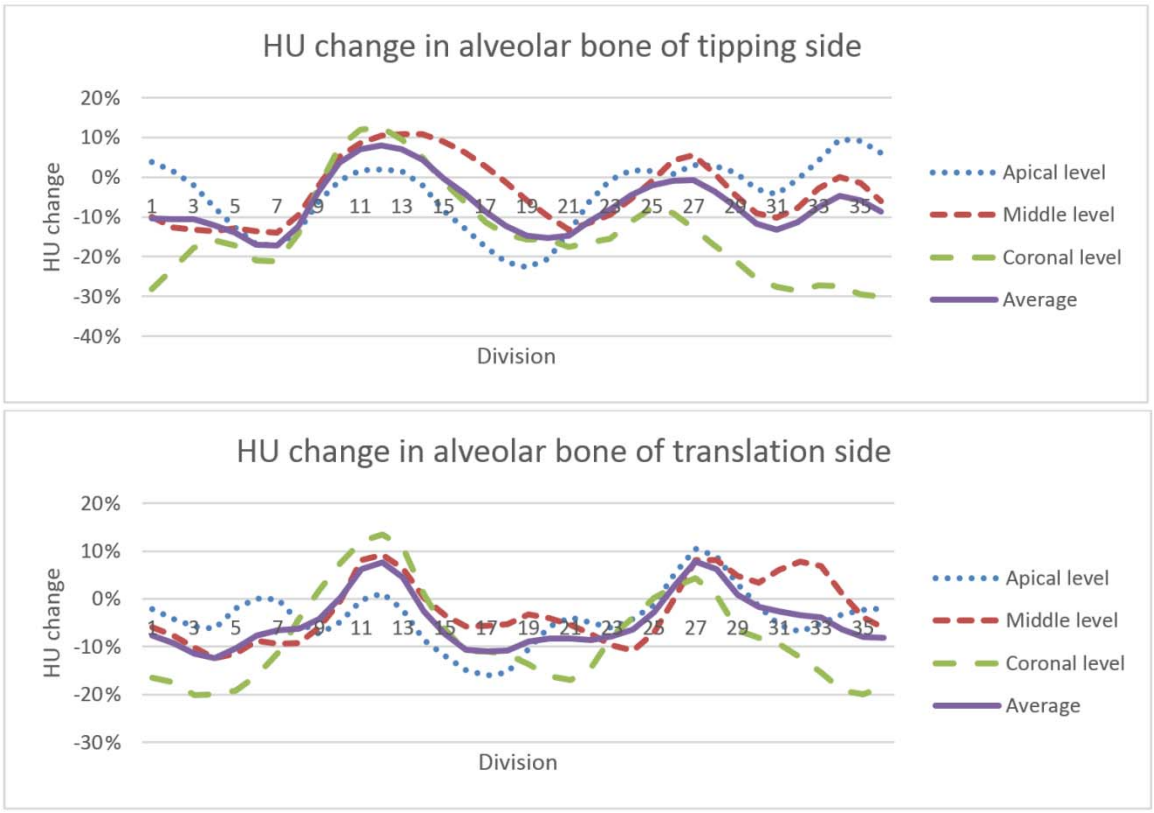

Figure 3.4: Comparison of average HU change in alveolar bone with treatment strategy.

The locations of CCS, and its difference with the CRes in both MD and BL directions are shown in Table 3.5. The location of CCS was 60.9% ± 2.6%. The difference to the reference CRes was 0.7% ± 1.0% occlusally in the MD direction, and 2.5% ± 2.4% occlusally in the BL direction. The variation of difference of CRes in the BL direction was also larger. The largest variation was 7.4% in the BL direction, comparing with 2.9% in the MD direction.

The locations of CPCS in the MD and BL directions, and their differences with the reference CRes in corresponding directions are shown in Table 3.6. The location of CPCS in MD direction was 60.2% ± 2.3%, which resulted in a 0.1% ± 0.8% apically to the reference CRes. The location of CP in BL direction was 59.1% ± 1.7%, which resulted in a 0.8% ± 2.4% occlusally to the reference CRes. CPCS in MD direction was

close to the reference CRes in MD direction than in the BL direction. However, the variation was similar to that from using the CCS method.

Table 3.4: Root length and CRes from FE method (Measured from root tip of root length).

Patient NO.	Root length (mm)	FE_MD (%)	FE_BL (%)	Difference: FE_BL minus FE_MD (%)
1	19.5	56.9	57.5	0.6
2	15.6	60.0	56.4	-3.6
3	17.2	64.9	56.9	-8.0
4	16.3	61.0	54.3	-6.7
5	18.1	60.3	62.7	2.4
6	18.8	61.7	64.1	2.3
7	14.1	59.6	58.8	-0.8
8	15.9	61.4	60.0	-1.4
9	15.4	61.4	59.3	-2.1
10	18	58.5	60.9	2.4
11	15.8	52.1	49.6	-2.5
12	13.5	61.6	60.8	-0.8
13	19.1	61.1	59.2	-1.9
14	15.4	60.7	56.6	-4.1
15	15.7	59.7	58.4	-1.2
16	15.8	61.7	58.3	-3.4
17	17.9	62.2	59.3	-2.9
18	15.3	59.1	57.1	-2.0
Average	16.5	60.2	58.4	-1.8
STD	1.7	2.6	3.2	2.8

Table 3.5: CCS and difference to CRes in MD and BL directions (Measured from root tip of root length).

Patient NO.	CCS (%)	Difference: CCS minus FE_MD (%)	Difference: CCS minus FE_BL (%)
1	56.9	0.0	-0.6
2	61.4	1.4	5.0
3	64.3	-0.6	7.4
4	60.3	-0.7	6.0
5	61.5	1.2	-1.2
6	62.3	0.6	-1.7
7	61.2	1.6	2.4
8	62.7	1.4	2.7
9	61.4	0.0	2.1
10	61.5	2.9	0.6
11	52.1	0.0	2.5
12	62.4	0.8	1.6
13	61.1	0.0	1.9
14	61.4	0.7	4.7
15	61.0	1.4	2.6
16	61.7	0.0	3.4
17	61.8	-0.5	2.5
18	60.7	1.6	3.6
Average	60.9	0.7	2.5
STD	2.6	1.0	2.4

Table 3.6: CPCS in MD and BL directions and the difference to CRes in corresponding directions (Measured from root tip of root length).

Patient NO.	CPCS_MD (%)	Difference: CPCS_MD minus FE_MD (%)	CPCS_BL (%)	Difference: CPCS_BL minus FE_BL (%)
1	57.5	0.6	55.7	-1.8
2	60.7	0.7	60.0	3.6
3	63.7	-1.2	60.6	3.7
4	60.3	-0.7	57.0	2.7
5	59.7	-0.6	60.3	-2.4
6	61.2	-0.6	61.2	-2.9
7	60.4	0.8	58.0	-0.8
8	61.4	0.0	60.7	0.7
9	60.7	-0.7	60.0	0.7
10	59.7	1.2	59.1	-1.8
11	52.1	0.0	56.3	6.7
12	60.8	-0.8	61.6	0.8
13	60.5	-0.5	59.7	0.5
14	60.7	0.0	58.2	1.6
15	60.3	0.7	60.1	1.7
16	61.0	-0.7	58.8	0.5
17	61.7	-0.5	58.5	-0.8
18	60.3	1.2	58.1	1.0
Average	60.2	-0.1	59.1	0.8
STD	2.3	0.8	1.7	2.4

3.5 Stress in Root, PDL, and Bone

3.5.1 Convergence Test

The finite element model was meshed with different element size and applied with same loading conditions. As shown in Figure 3.5, while the element size reaches 0.4 mm, the stress becomes stable. The element sizes at the critical locations have been far smaller than this, meaning that our models passed the convergence test.

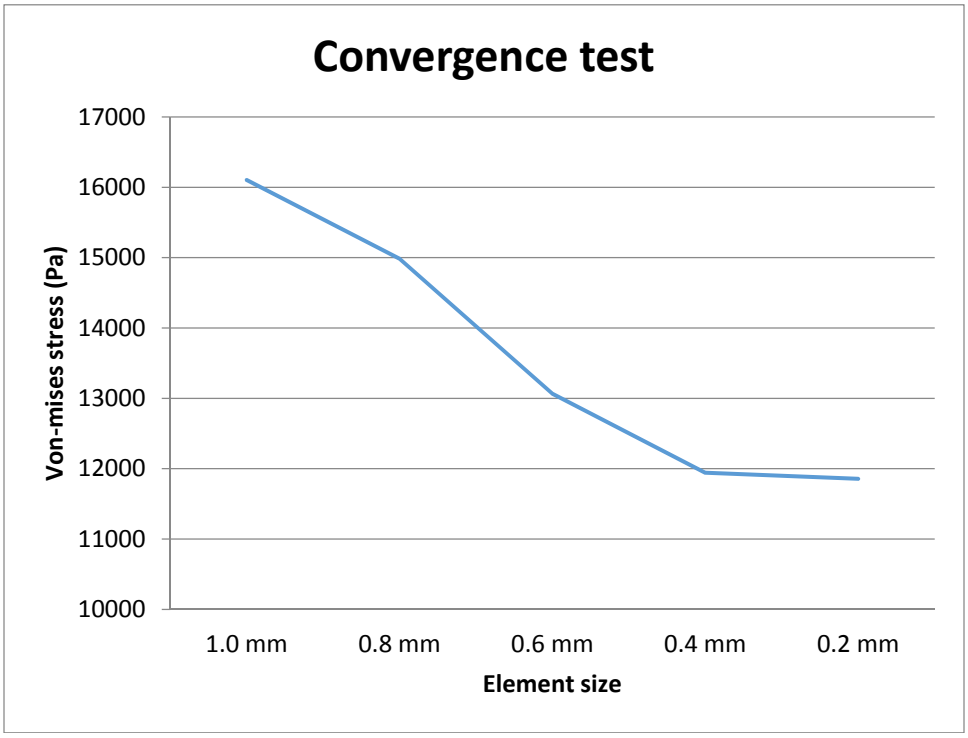

Figure 3.5: Convergence test of element size.

3.5.2 Results of Stress

Stress distribution shows the locations of the high and low stresses. Figure 3.6 shows the dilatational stress distribution in alveolar bone, PDL, and root surface. The

stresses in root are much higher than in the alveolar bone and PDL and are uneven. The stress patterns in the PDL and alveolar bone are significantly different.

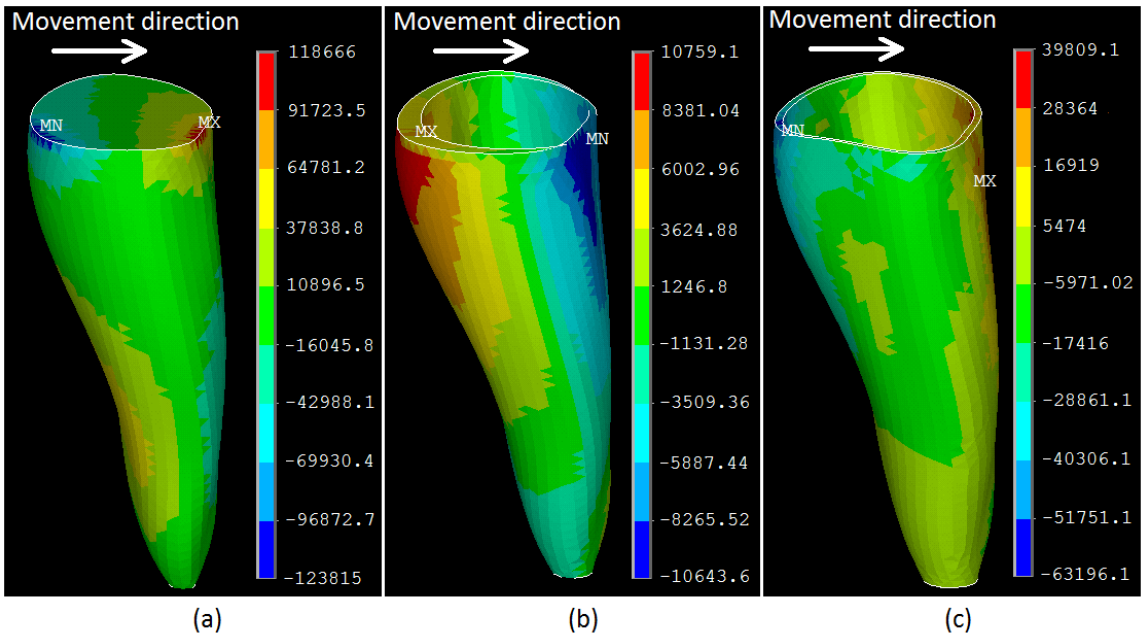

(a) Dilatational stress in root; (b) Dilatational stress in PDL;

(c) Dilatational stress in alveolar bone

Figure 3.6: Example of dilatational stress distribution in root, PDL, and alveolar bone.

The stress distributions of the 5 types of stress invariants in the 3 by 36 root surface divisions are shown in Figure 3.7 to 3.11. Division 1 was in the moving direction, which was close to the distal direction; division 19 was in the opposite direction. The stress distribution was clearly affected by the initial M/F. The major difference occurred at the coronal level. The magnitude of the stress was also very sensitive to the M/F. The M/F close to that for translation resulted in more even stress distribution, with lower stress magnitude and less shear effect characterized by lower von-Mises stress. The stress difference between CT and TR side in root was statistically significant.

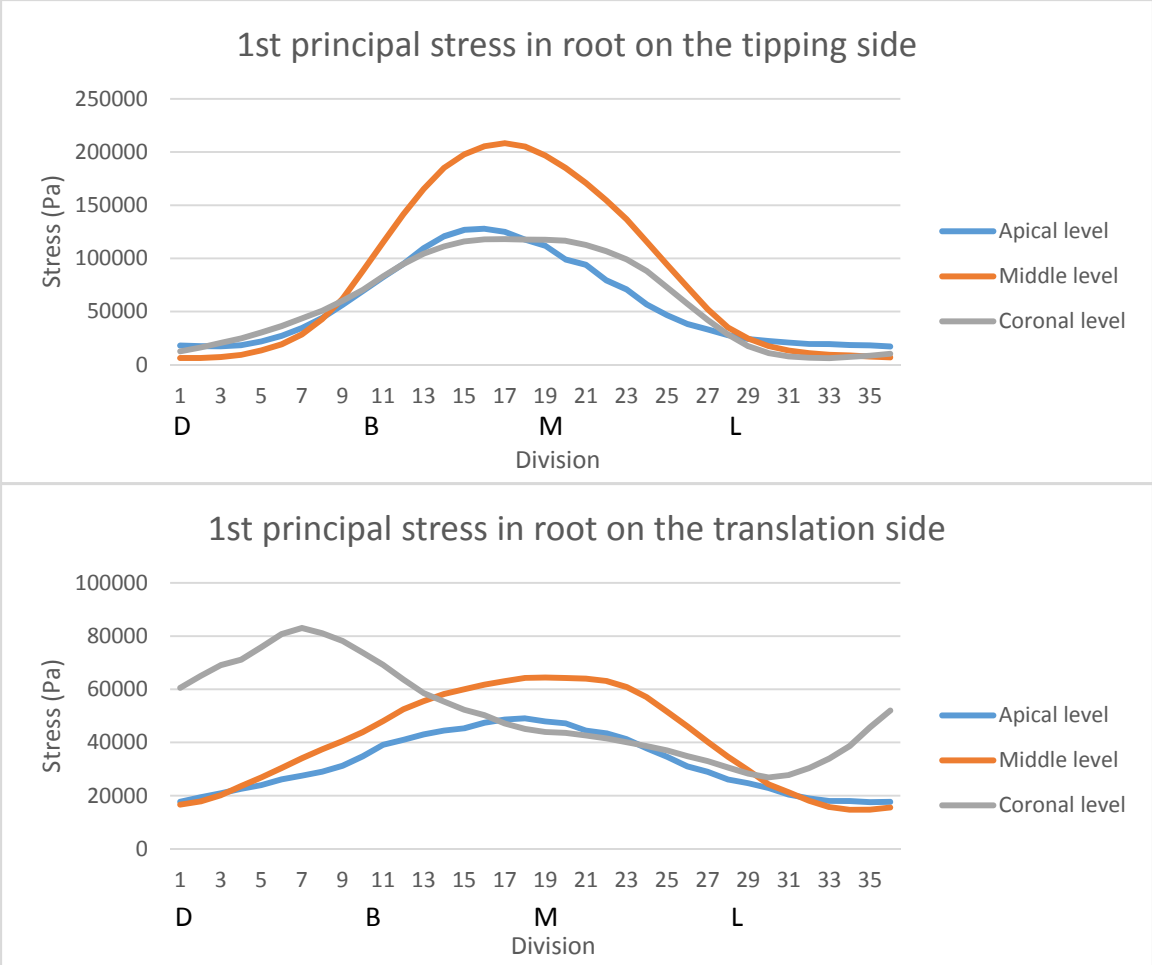

Figure 3.7: 1st principal stress distribution at root surface.

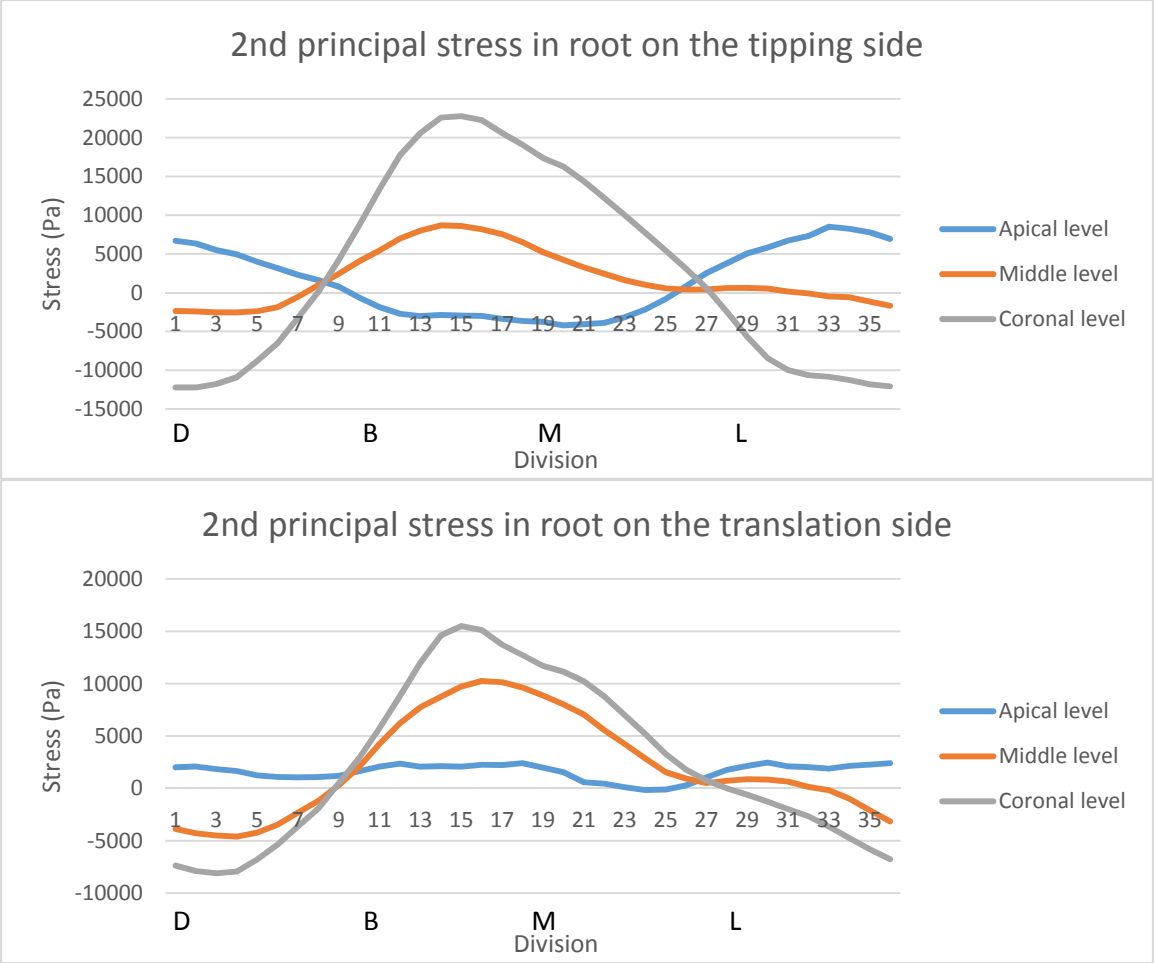

Figure 3.8: 2nd principal stress distribution at root surface.

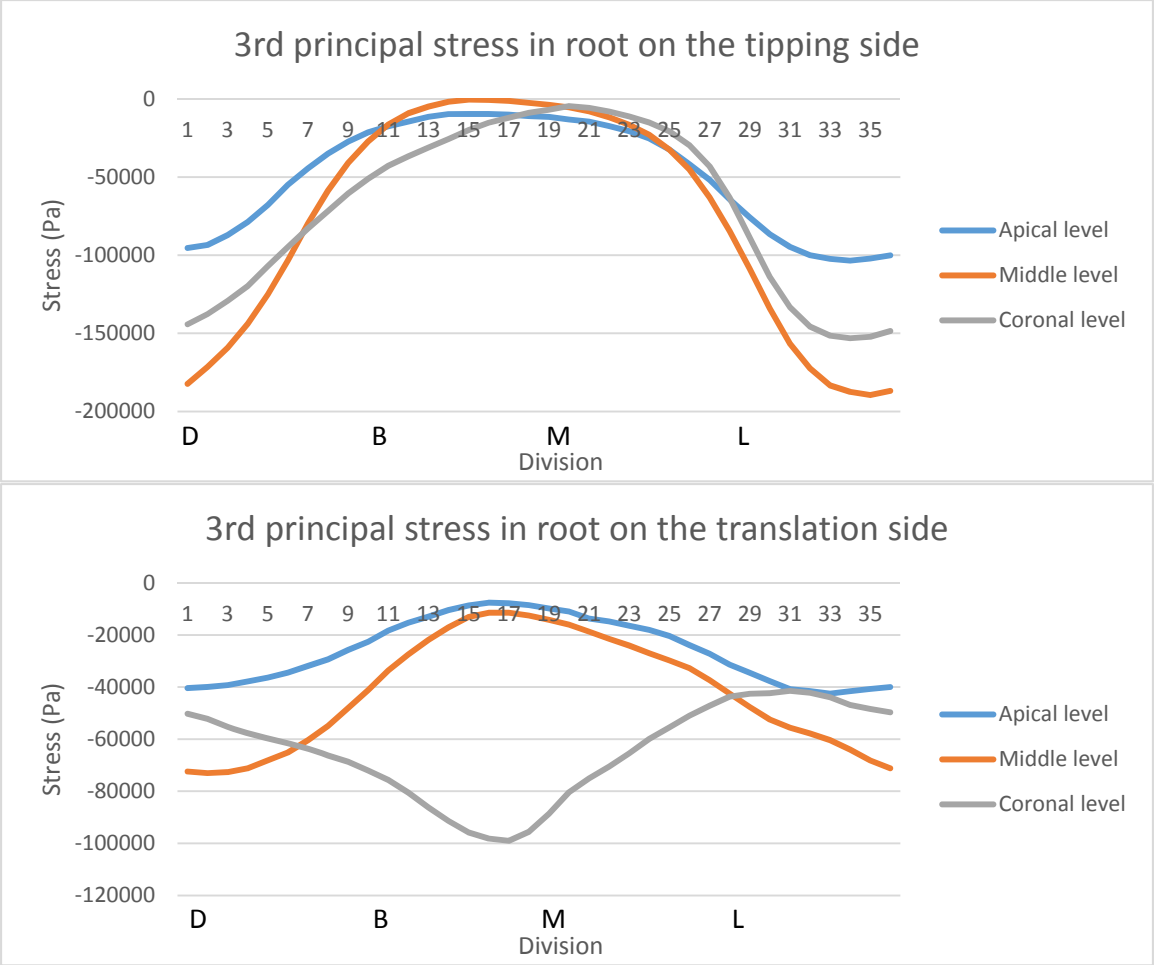

Figure 3.9: 3rd principal stress distribution at root surface.

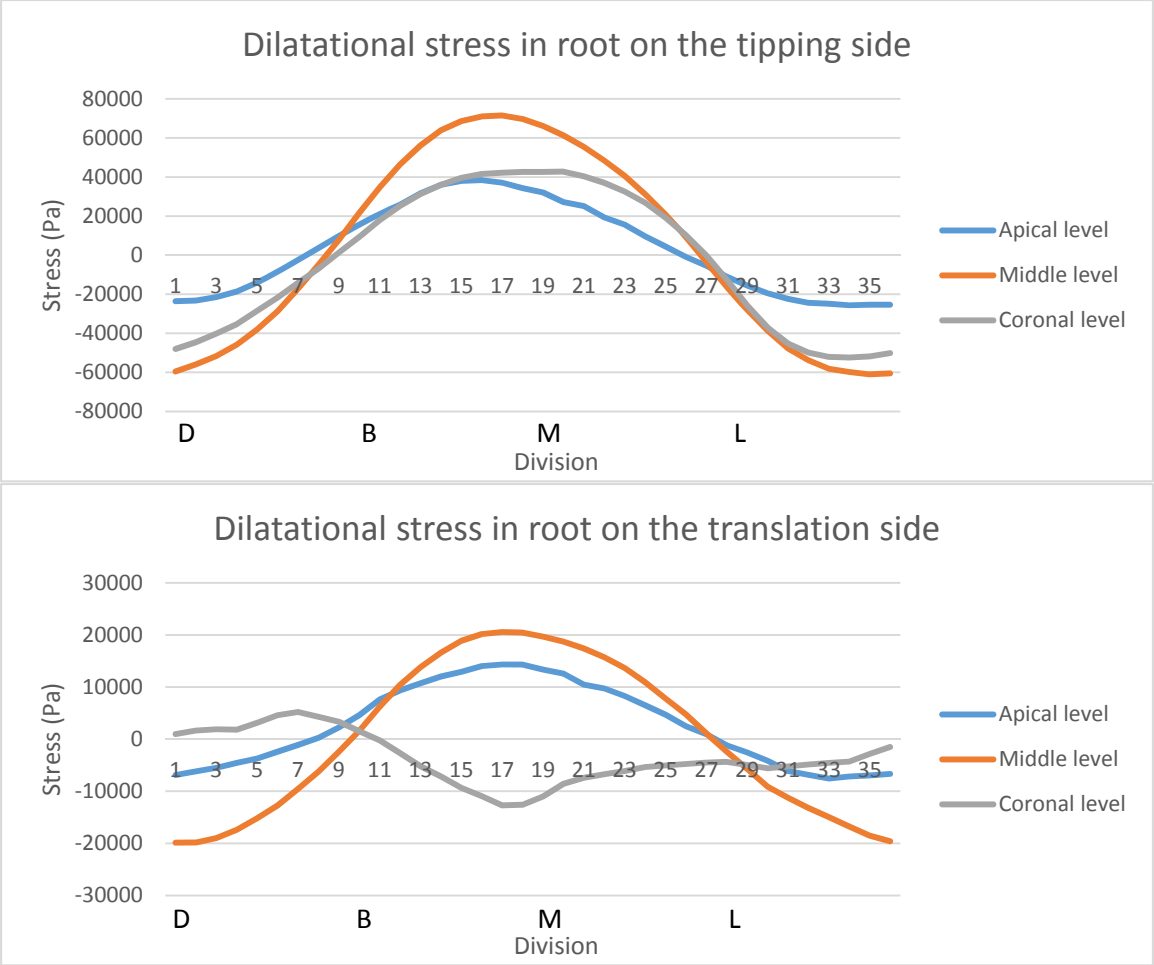

Figure 3.10: Dilatational stress distribution at root surface.

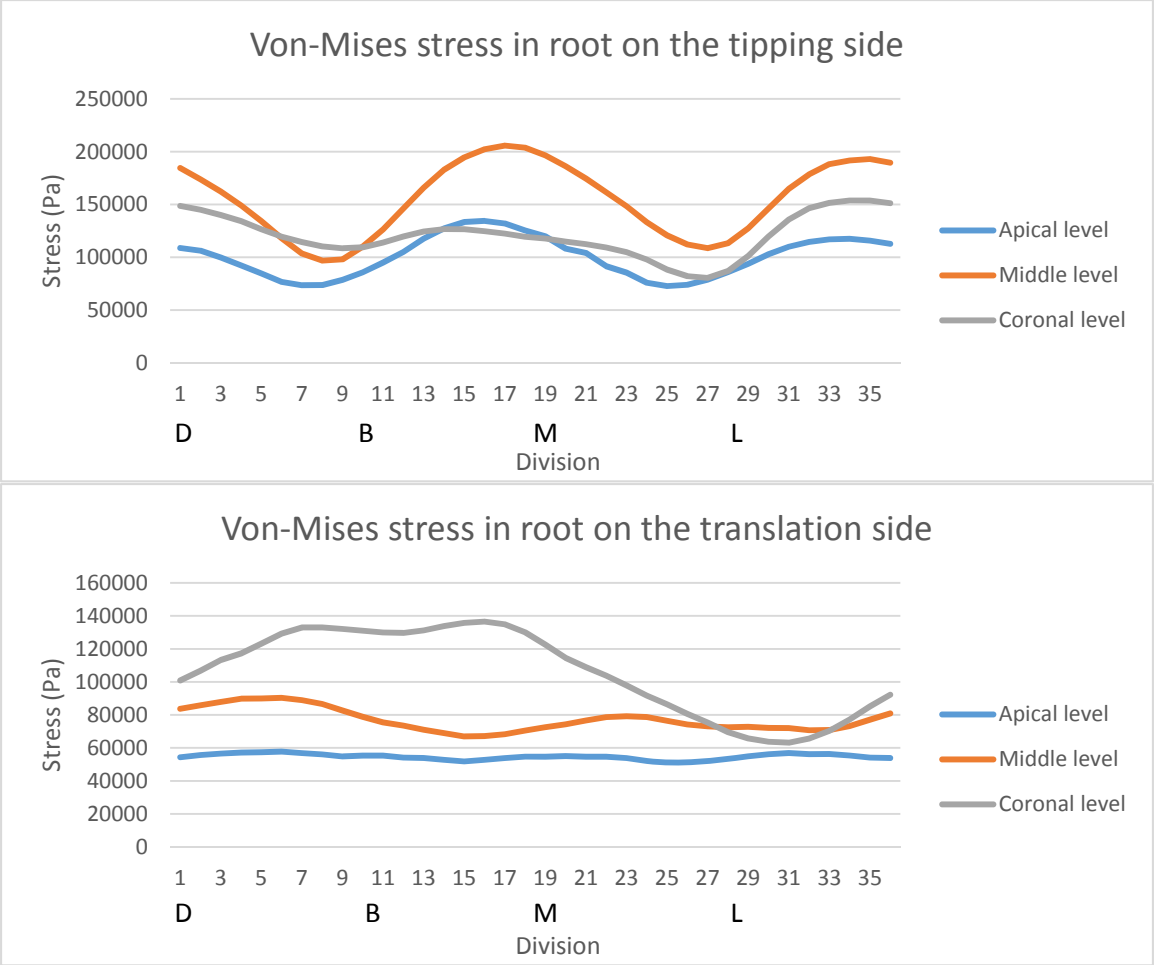

Figure 3.11: Von-Mises stress distribution at root surface.

The stress distributions of the 5 types of stresses in the PDL divisions are shown in Figure 3.12 to 3.16. The stress distributions in PDL corresponding to the tipping and translation strategies were similar, meaning they were less affected by the initial M/F. The stress distributions of the 1st, 2nd, 3rd principal stress, and the dilatational stress were similar, meaning that close to hydrostatic pressure were experienced. The magnitudes were much lower due to PDL's low Young's Modulus. The stresses were more compressive in the tooth moving direction and tension in the opposite direction. The stress difference between CT and TR side in PDL was not statistically significant overall, but was statistically significant in the moving direction and the opposite direction.

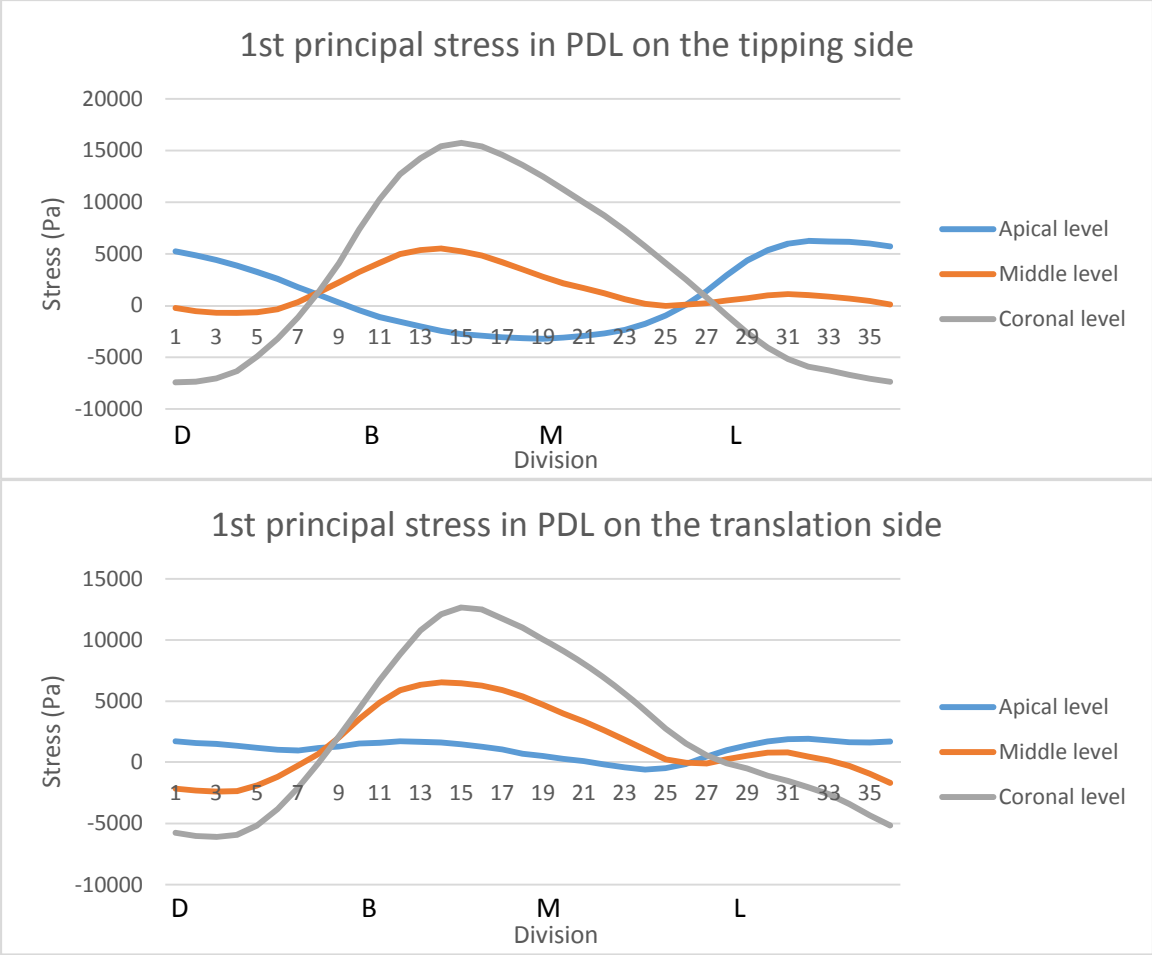

Figure 3.12: 1st principal stress distribution in PDL.

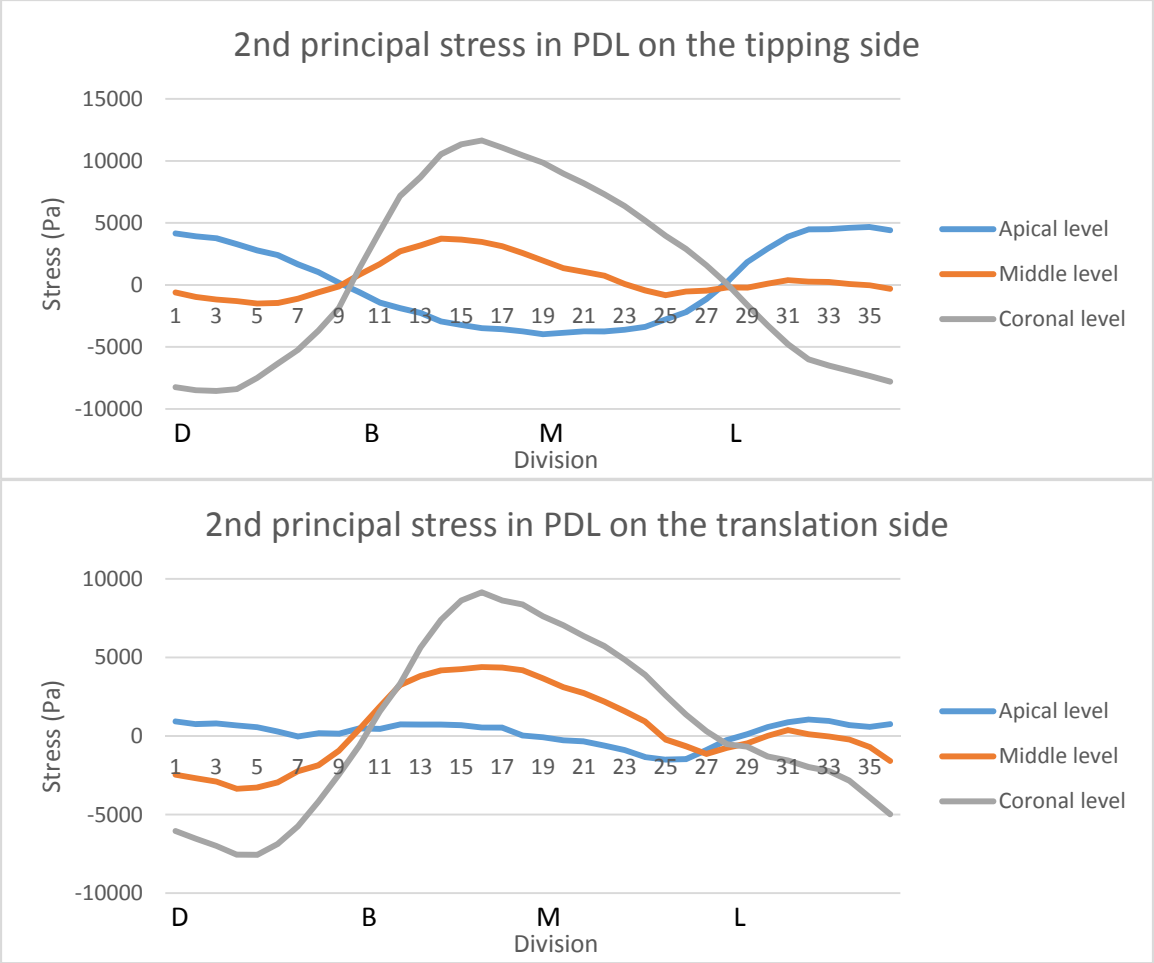

Figure 3.13: 2nd principal stress distribution in PDL.

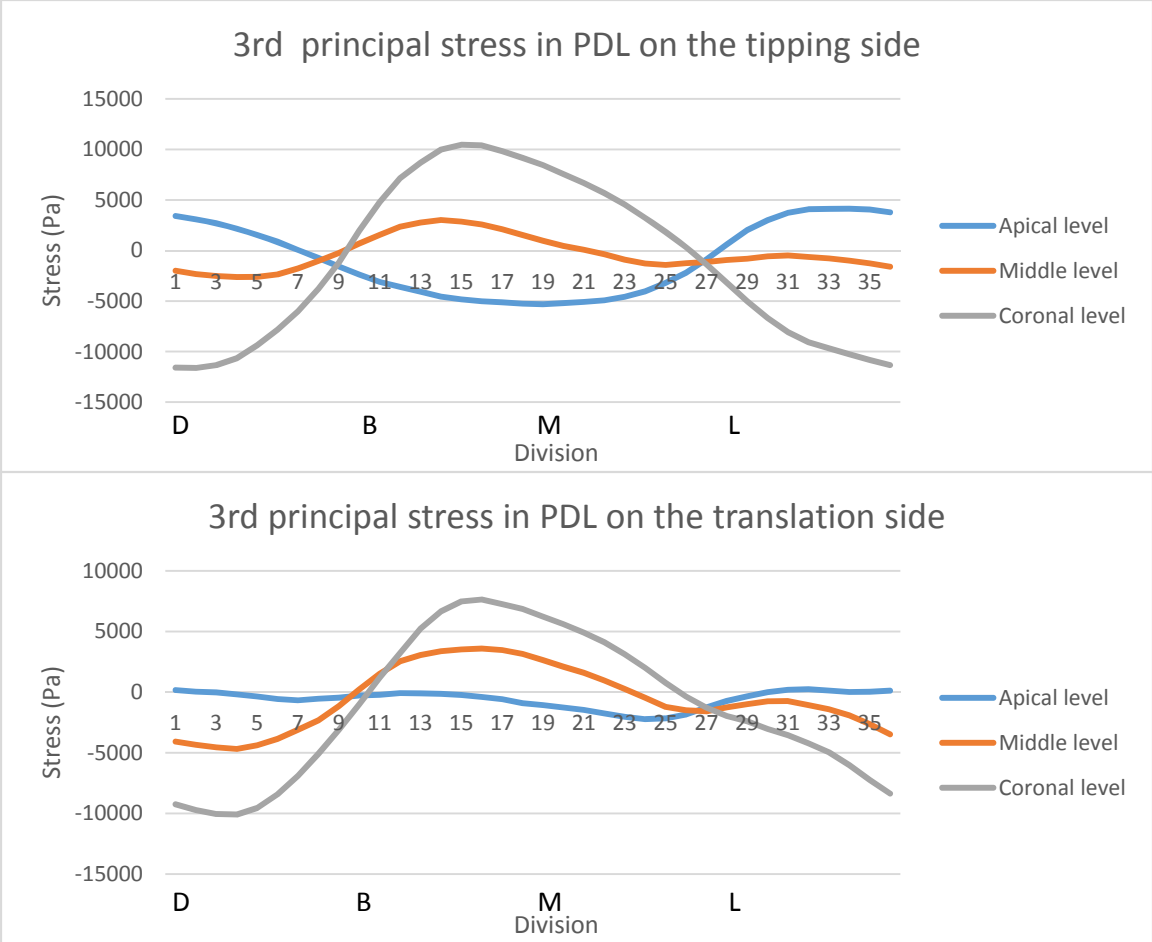

Figure 3.14: 3rd principal stress distribution in PDL.

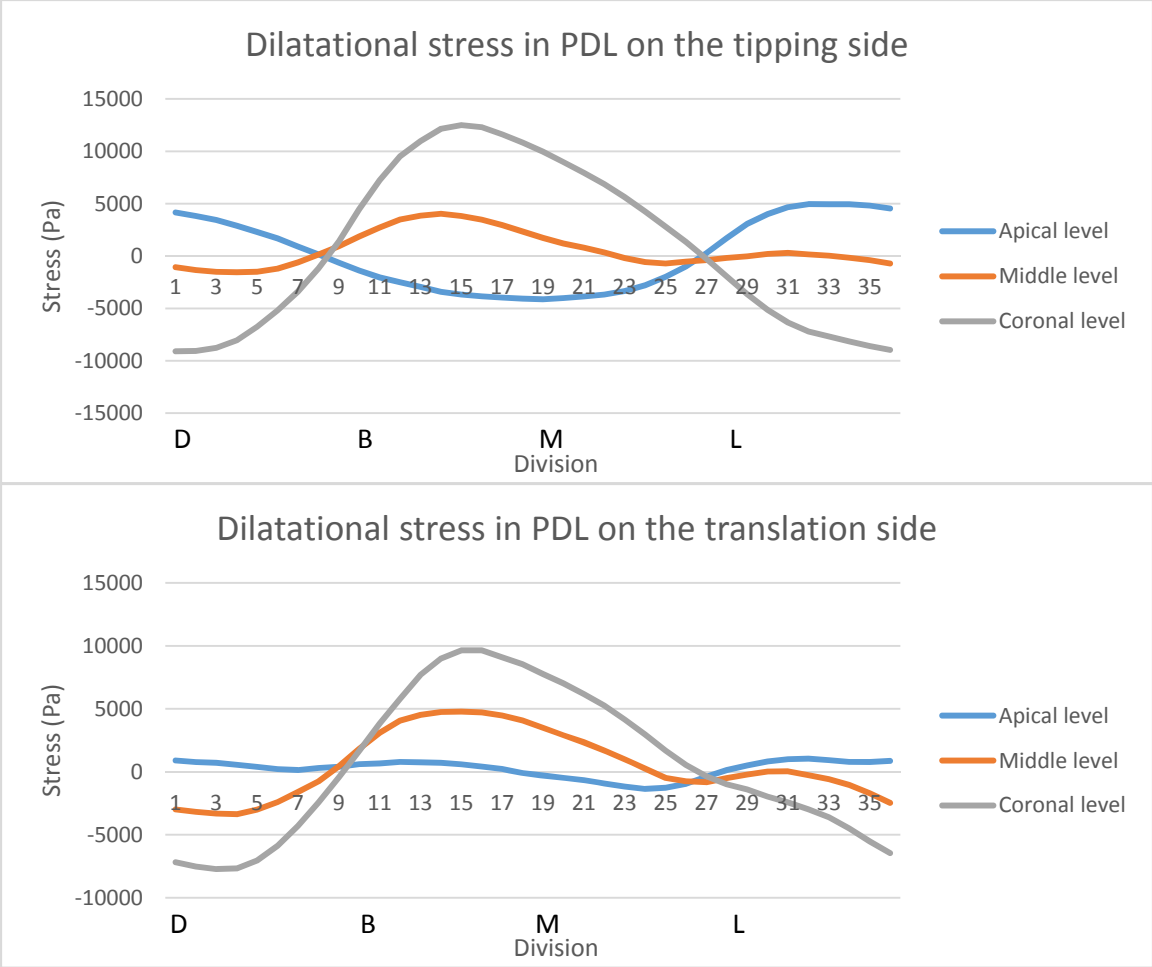

Figure 3.15: Dilatational stress distribution in PDL.

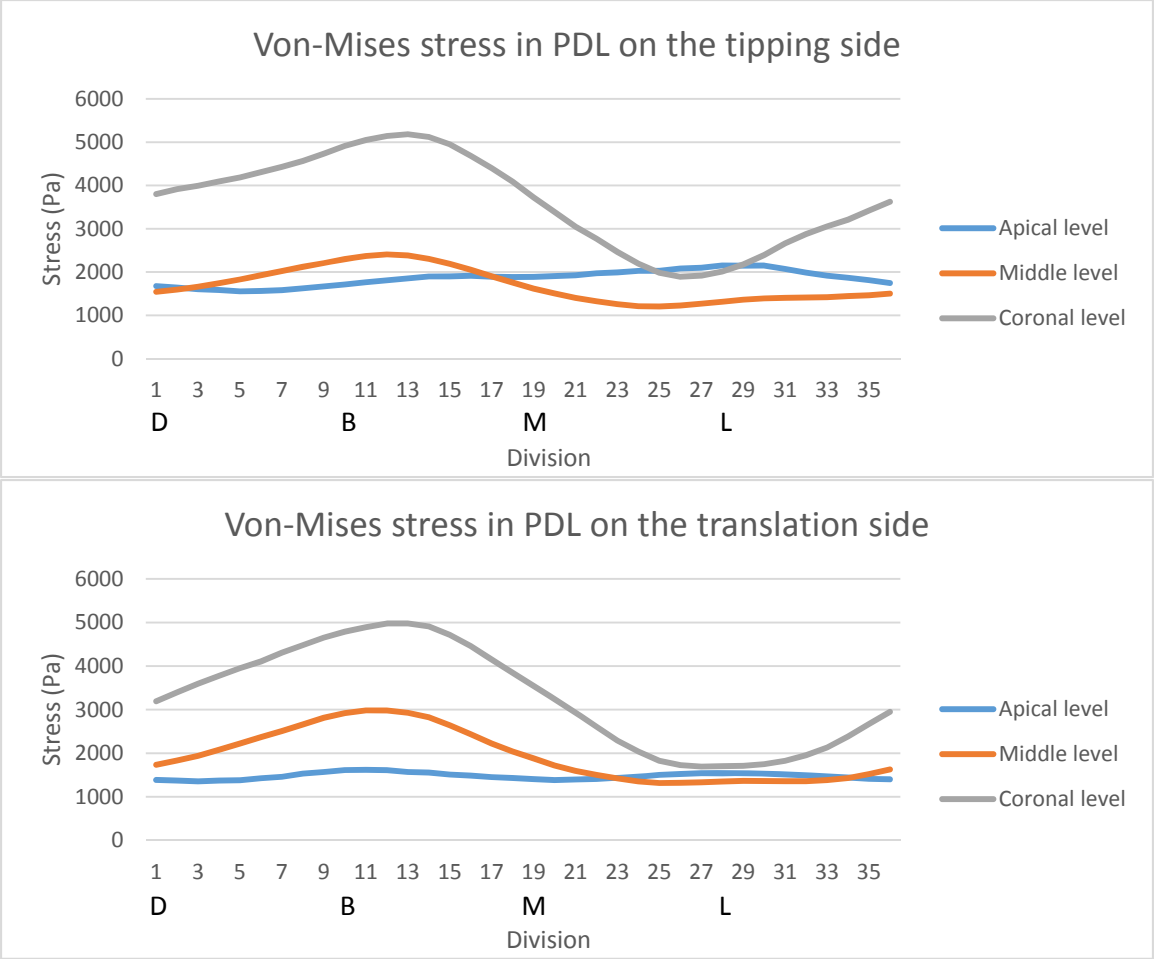

Figure 3.16: Von-Mises stress distribution in PDL.

The stress distribution of the 5 types of stresses in the alveolar bone divisions are shown in Figures 3.17 to 3.21. The stress distributions and magnitudes were similar corresponding to the two treatment strategies, meaning less affected by the M/F. However, the stresses in the alveolar bone showed opposite pattern comparing with these in PDL. The stresses were more tensile on the PDL's compression side, and were more compressive in PDL's tension side. The stresses difference between CT and TR side in alveolar bone was not statistically significant.

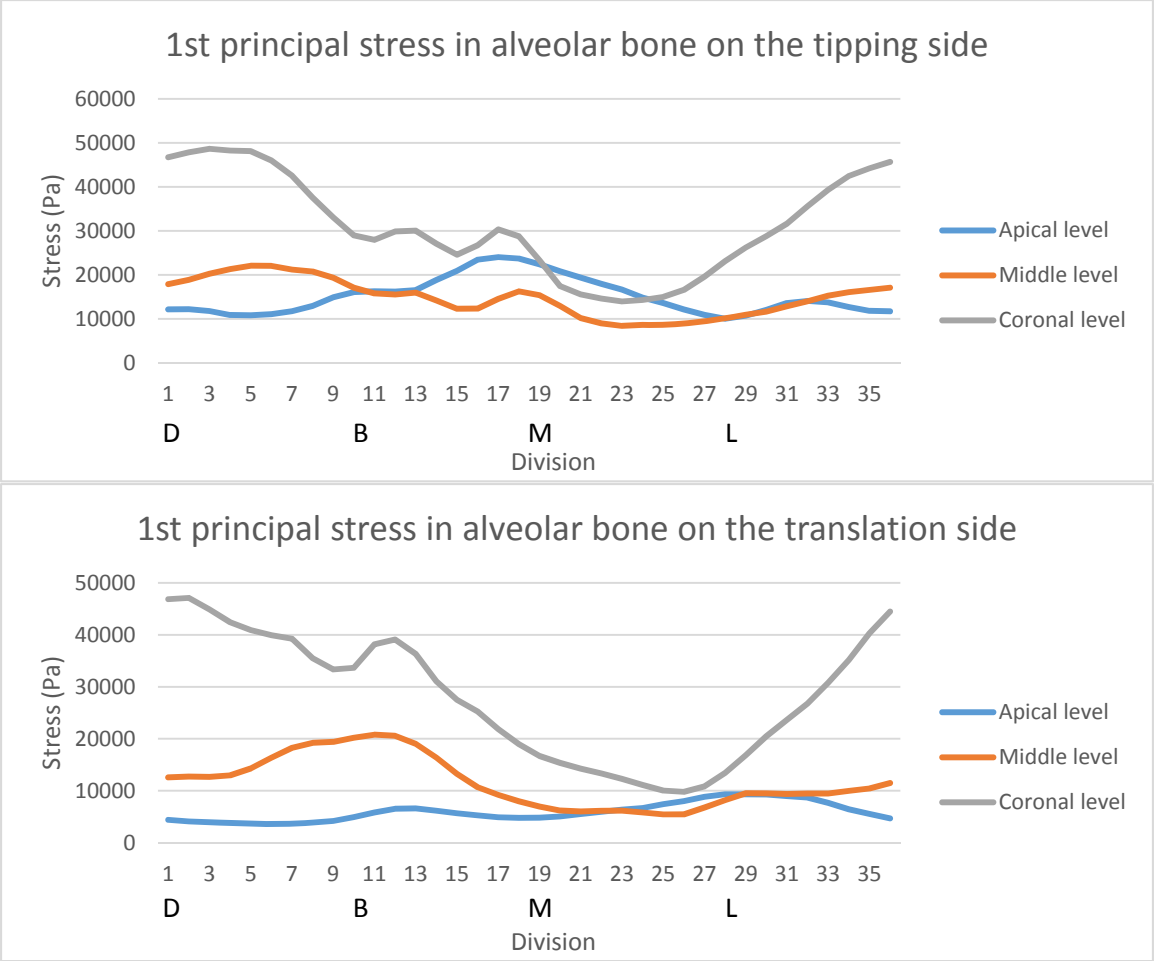

Figure 3.17: 1st principal stress distribution in alveolar bone.

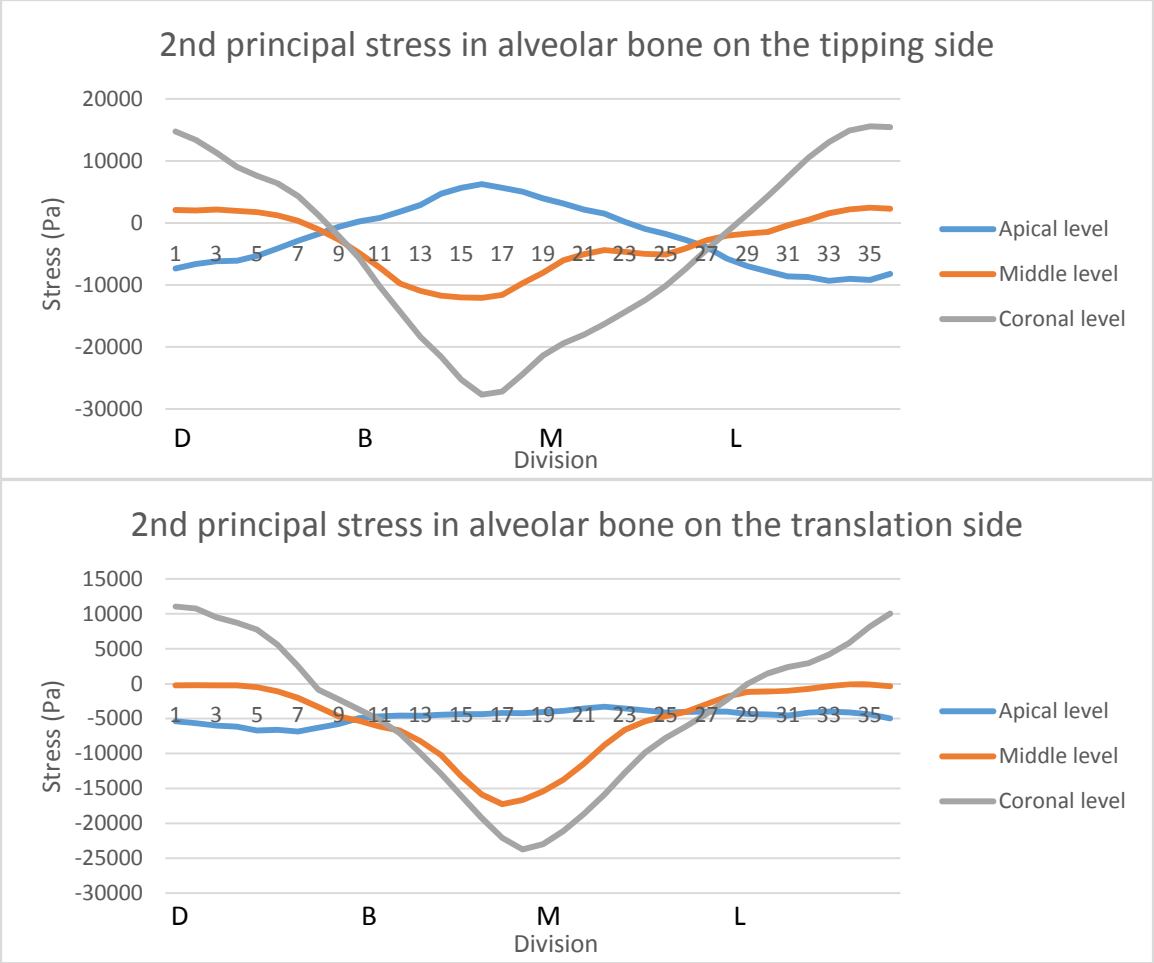

Figure 3.18: 2nd principal stress distribution in alveolar bone.

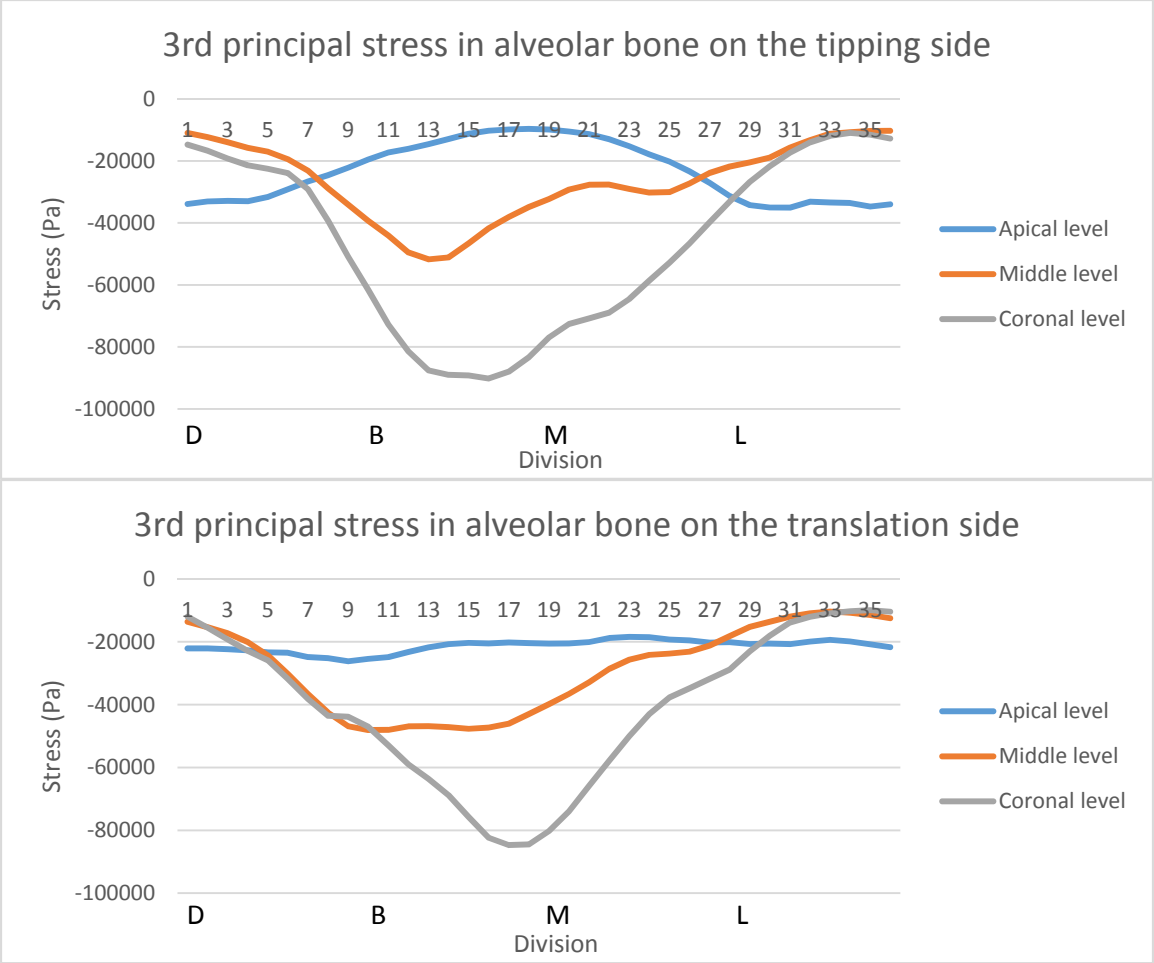

Figure 3.19: 3rd principal stress distribution in alveolar bone.

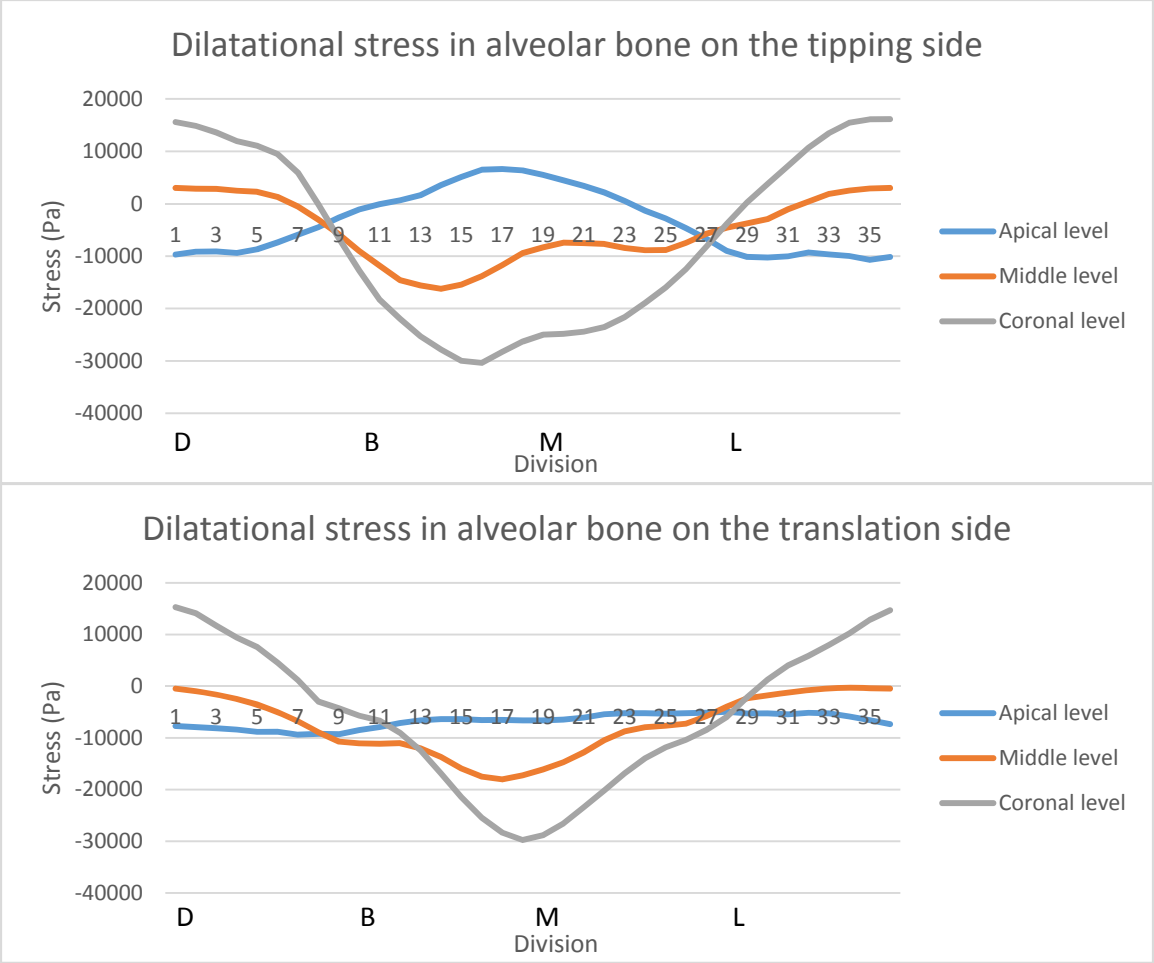

Figure 3.20: Dilatational stress distribution in alveolar bone.

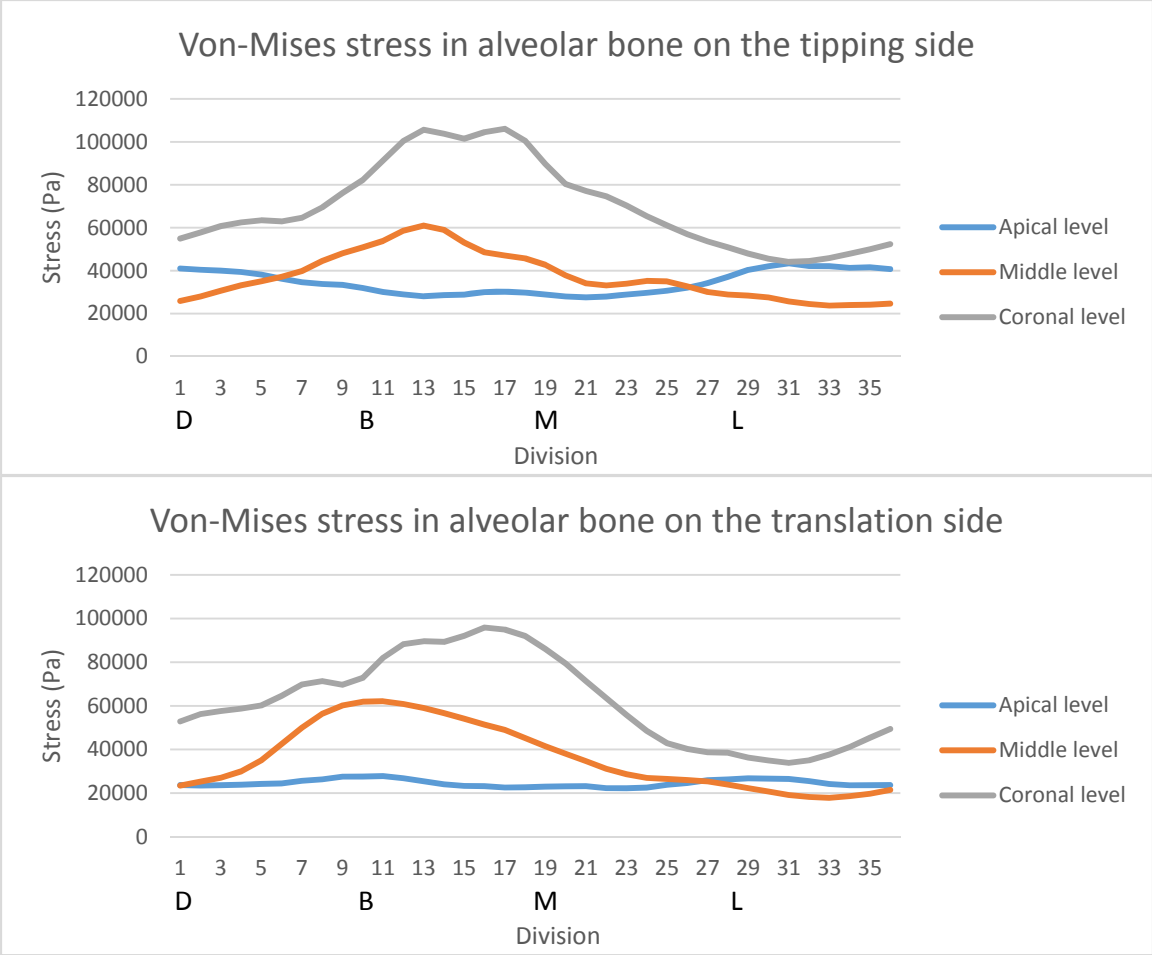

Figure 3.21: Von-Mises stress distribution in alveolar bone.

3.5.3 Sensitivity Test

Table 3.7 shows the sensitivity indices for Cotter's method. The three factors are fiber existence, Poisson's ratio of cortical and cancellous bone. The stress distribution patterns did not significantly change with the factors. With the existence of the PDL fibers, changing the Poisson's ratio caused only less than 10% stress variations.

Table 3.7: Sensitivity indices for Cotter's method.

	Fiber existence	Poisson's ratio of cortical bone	Poisson's ratio of cancellous bone
1st principal stress in root	0.989	0.002	0.009
3rd principal stress in root	0.985	0.005	0.010
Von-Mises stress in root	0.991	0.003	0.006
1st principal stress in PDL	0.989	0.001	0.010
3rd principal stress in PDL	0.989	0.005	0.006
Von-Mises stress in PDL	0.994	0.001	0.005
1st principal stress in cortical bone	0.593	0.126	0.281
3rd principal stress in cortical bone	0.710	0.127	0.163
Von-Mises stress in cortical bone	0.703	0.148	0.149
1st principal stress in cancellous bone	0.767	0.148	0.085
3rd principal stress in cancellous bone	0.794	0.031	0.175
Von-Mises stress in cancellous bone	0.843	0.020	0.137

3.6 Relationship Determination

The overall correlations of the stresses with HU changes are generally weak. When data from all directions are combined, none of the correlations were > |0.5|. For specific directions, Division 35-3 for CT side showed moderate correlations (μ=0.51 to 0.61) between four stress invariants (1st principal/2nd principal/3rd principal/dilatational stress).

CHAPTER 4. DISCUSSION

4.1 Reliability Test of Loading the T-loop (OBJ 1 - Develop a Method to Quantify the 3D Load Systems on the Canine.)

Quantification of the orthodontic load can only be done in-vitro. Accurate measurement of the orthodontic load system requires the identical boundary conditions in vitro and in vivo. The dental cast is reliable as a traditionally used dental geometry recording method. Load cells is also reliable for its high resolution (1/80 N and 1/16 N·mm). The most possible error would come from removing the T-loop from the load measuring device and reloading it in the patient's mouth. The T-loop might deform while removed. Therefore, the repeatability of the load system measurement after removing and reloading the T-loop need to be tested.

As shown in Table 3.1, the reliability test shows that the error of removing and reloading the T-loop is acceptable. The error of force and moment are less than 0.02 N and 0.15 N·mm. The method meets the accuracy requirement of this project.

4.2 Root Resorption (OBJ 2 - Determine the Root Resorption Due to Canine Retraction and Treatment Strategies.)

In this study, "tooth length" was used instead of "root length" to determine apical root resorption. The tooth length is the sum of crown length and root length. It is generally assumed that crown length does not change during orthodontics. Then tooth length can also represent apical root resorption.

The apical root resorption was detected using the CBCT images. The length detection resolution depends on the CBCT scan quality. The resolution should be two times of the voxel size, which was 0.5 mm. This number had been used as a threshold to identify tooth length change for each patient. For tooth length change, due to the resolution, any length changes that were less than 0.5 mm were not considered as a definite change, which was acceptable because only root shortening greater than 0.5 mm was considered as apical root resorption clinically.

All patients had received the same orthodontic loads on the TR or CT side. If the load system is the only dominate factor for root resorption, then all patients would have consistent clinical outcomes. In our study, there were 6 out of 18 patients showed definite apical root resorption on the TR side and 3 on the CT side, indicating the orthodontic load may not be the only dominate factor causing apical root resorption. Three patients had root resorptions on both sides, which indicated that biological factors may also strongly contribute to apical root resorption.

Although the root length change less than 0.5 mm was not considered as definite, the measurements could still be used to see the trends statistically. None of the root showed definite root lengthening, indicating root shortening is dominate during canine retraction. The levels of root shortening on both sides were not statistically significant. However, the p-values were close to 0.05. TR side had more definite root shortenings and higher average root shortening than the CT side. It implied that TR causes more apical root resorption. TR side had higher M/F than CT side, which may be one of the causes.

Theoretically, root resorption may be characterized by the root shortening and surface cavities. Both of them result in volume reduction. The volume change was also calculated and shown in Table 3.2 and 3.3. The change due to canine retraction was not significant with the current resolution, which is closely related to the voxel size. Because the layer of the root surface with one voxel thickness was 73 ± 11 mm^3, only the volume

change larger than that can be determined as definite change. High quality and smaller voxel size will provide more accurate evaluation.

4.3 HU Change Distribution (OBJ 3 - Determine the BMD Change Distribution at Root Surface and Surrounding Alveolar Bone Represented by HU; OBJ 4 - Determine the Relationship between BMD Change and Movement Direction.)

4.3.1 Reliability Test

Although using HU from the CBCT is not a reliable way to quantify BMD, it is still the best method to monitor changes of BMD in terms of HU in this study. The primary purpose of this study was to investigate HU changes, thus only relative HU was of interest. The variation of the segmentation has been proven to be small (<1% of the maximum value) and the multiple scans of the same phantom produced consistent results (ICC = 0.94), proving that same machine and scan setting produces consistent results, and the high correlation between the HU and BMD exists. The correlation was not affected by the locations of the BMD rods. High ICC would not be obtained if BMD was sensitive to position under the setting used in this study. In this study, the canines moved within a small region only, thus the results are still comparable. In this study, we have chosen the best resolution that allows us to maximize the image quality and minimize the scanning time without motion blur. In order to obtain the best reliable results, we used the same CBCT scanning setting and standardized imaging process without alternating original images using any cosmetic processing. In addition, we only used the commonly used imaging processing techniques, such as thresholding, for segmentation and original grey scale for estimating HU.

The results showed that the method can reveal HU change difference within root surface and surrounding alveolar bone. The HU change is related to the moving direction.

Part of the results matched and supported literatures, and others showed new information, which are described below.

The study focused on HU changes in the alveolar bone and root surface as the canines move due to the two treatment strategies, TR and CT. The HU changes were expressed relative to the clinical tooth movement direction for the purpose of this study. The orthodontic load systems on the canines were well-controlled, with a higher moment/force on the TR side than the CT side [71]. However, the resulting canine displacements varied and did not fully agree with the intended displacement pattern. Therefore, the CT and TR sides used in this study refer to the T-loop design rather than resulting clinical displacement patterns.

4.3.2 HU Change Distribution in Root

HU at the surface layer of the canine roots decreased in all divisions, indicating remodeling activities happened in the root. Relatively larger reductions occurred at the divisions located closely perpendicular to the moving direction, indicating that high stress in PDL might not be the only factor triggering the remodeling. When the canine moves, the root experiences high compressive stress in the moving direction and tensile stress on the back. The stresses in the perpendicular directions are less affected. The observation contradicts the theory that remodeling occurs at high stress areas in bone. However, the root may respond differently from bone which needs to be further investigated.

Higher HU reduction at the Coronal level in the direction perpendicular to the movement direction indicates higher remodeling activities resulting in relatively less dense root surface. The area is less affected by the orthodontic load comparing to the direction of tooth movement, but experiences less resistance to tooth movement. The HU at the apical level was reduced significantly in certain divisions (D10-D13 and D25-D28). The apex has small surface area. When its density decreases, it becomes vulnerable for surface lose, which may result in root shortening. Consistent surface density loss at a

longer period of time may be the cause of root resorption, which has been observed clinically [54].

4.3.3 HU Change Distribution in Alveolar Bone

HU in the surrounding alveolar bone had mixed changes, decreasing along and increasing perpendicular to the direction of tooth movement. Contrary to the root, the maximum HU reduction occurred in the direction of tooth movement (D33-D6). The bone on the tension side also experienced significant HU reduction. The results confirmed the general finding report by Cheng et al. [17] that the BMD reduces in the direction of tooth movement, but our results show less level of reduction. The average HU reduction (4.2% to 11.0% among levels) in alveolar bone in this study was less than the 24% reported by Chang and Hsu [17, 53]. On the other hand, HU increased in D10-14 and D26-28, which were approximately perpendicular to the moving direction. Only 2 teeth out of 144 showed increased bone density around the teeth in a previous study [17, 53]. The inconsistency could be due to the difference in treatment and analysis. In their studies, the treatment period was longer (7 month) than ours (4.9 month); the tooth displacement was shorter (non-extraction orthodontic treatments) than ours (space closure treatment). Furthermore, their studies divided the surrounding alveolar bone into three layers and only four directions, and the region studied did not cover all the surrounding alveolar bone. Generally, our results agree with the common believe that the alveolar bone remodels as the canine moves into the area in front of it and models at behind, which result in formation of less mineralized bone.

The modeling and remodeling occurred with different intensity at different levels. In the moving direction (D33-D6), HU reduction at the Coronal level was more severe than at Apical and Middle levels. Considering the larger bony areas are being affected at the Coronal level, the relatively less dense bone may be needed for the intended tooth movement. Contrary to root surface, the high modeling and remodeling areas in the alveolar bone are experiencing higher stresses/strains due to the orthodontic movement.

Considering the effects of treatment strategy on the HU reductions, only the CT side showed significant HU reduction among the three levels in certain directions. The load on the CT side has a relatively lower M/F, which results in a relatively higher compressive force at the Coronal level. As shown in Figure 3.4, the Coronal level showed statistically significant higher HU reduction than at the Apical level on the CT side, especially in the moving direction (D33-D3), which may be due to the higher compressive stress.

Treatment strategy difference did not lead to overall significant difference in the HU change distribution in the root surface or surrounding alveolar bone. Significant differences were determined only in few divisions. The results may explain the conclusion from a previous study, which showed that apical root resorption was not related to translation or tipping of the root [81].

4.4 CRes Variation and Projection Method Verification (OBJ 5 - Determine the Location, Variation of CRes between Patients; OBJ 6 - Establish a Reliable and Quick Assessment Method of CRes Determination.)

The locations of the CRes in MD and BL directions were significantly different although the average difference was small (0.3 mm on average). If this amount is considered insignificant clinically, the location of CRes calculated in one direction may be used for the other direction. However, the clinicians may keep in mind that the difference may be large for some patients, like patients #3 and #4, due to the shape of the root, see Table 3.4.

Our study has narrowed the location of CRes in MD direction down to 60.2% ± 2.6%. The variation (52.1% to 64.9%) also provide a useful reference for clinical treatment. Compared to previous studies, the result of our study was close to previous

studies with 3D analysis of single root teeth (60% [20], 60% [82], 63% to 65.6% [22], 57.2% [34], 61.7% [25]).

Average CRes in BL direction located coronally than some of the previous studies (43.5% [34], 53.8% [25]), close to one study (58% [83]), and lower than another (66% [23]). The potential explanations of the difference could be attributed to the sample size, reference point, and tooth difference. Our study had a moderate sample size of 18, and the location of CRes in BL direction varied from 49.6% to 64.1%. The result from single object may fall on any point within the range. Our study used the average height of alveolar crest as the reference while other studies used highest point of the alveolar crest [23, 34]. Furthermore, some of the results were from incisors, which may contribute to the difference.

Our study has shown that the locations of the CRes can be estimated using the CCS. The CCS is a point in the space that is not necessarily on the long axis of the tooth. Only it's projection on the long axis is of interest. The difference of the CCS to the CRes in MD direction was small (0.7% ± 1.0% or 0.12 ± 0.17 mm). The difference to the CRes in BL direction was larger (2.5% ± 2.4% or 0.41 ± 0.40 mm). The average estimated locations in both directions are occlusal.

CPCS method showed better estimates of CRes than the CCS method. The difference to the reference CRes (0.1% ± 0.8% or 0.02 ± 0.13 mm apically in MD direction, and 0.8% ± 2.4% or 0.13 ± 0.40 mm occlusally in BL direction) was smaller than these with CCS method.

Our study showed that the CRes can be reliably estimated by using the CPCS method. Our study had larger sample size than the previous study (18 vs. 3 [34]), thus allowed us to study the averages CRes locations and variations. There were discrepancies existed with the previously published results. These may be due to the difference in reference point (average vs. highest point of alveolar crest [34]), modeling technics, and

tooth difference (canine vs. incisor [34]). The CRes location would be affected if the definition of the tooth length was different. For modeling, effort was made to create reliable FE models. In this study, the same CBCT scanning setting for all the scans and standardized imaging process without alternating original images using any cosmetic processing was used. The FE model was composed of crown, root, PDL, cortical bone, and cancellous bone. PDL was modeled as fiber-reinforce structure. The models were different from these reported previously [34].

This study provides a foundation for a simple, and reliable method to predict the locations of the CRes in both MD and BL directions clinically. In this study, the root length was measured in 3D. The projections are on the planes perpendicular to the occlusal plane, and the location of CPCS was represented using the percentage of root length. The projection of the root and the centroid can be easily found from the CBCT images. To be consistent, the occlusal plane is used as the reference plane. It is also possible to apply the method to X-ray images, which is more commonly used clinically. The projection of the root in the BL directions is available from the X-ray images. However, the feasibility need to be further investigated due to the following reason. The root length measured on X-ray image may not be the true length in 3D. Tilting the tooth affects the root length and distorts the projected images, which may affect the results. The CPCS in the MD direction from X-ray image is not available, but the CRes location may be estimated based on the data from this study.

4.5 Stress in Root, PDL, and Bone (OBJ 7 - Determine the Stress in Root, PDL, and Bone, and Test the Relationship between Stress and BMD Change to Determine the Relationship between Force and Biological Response.)

The stress distribution is related to the canine structure. How well the finite element model represents the geometry would affect the accuracy of FEM. Coarse mesh may cause artificial stress concentration, and too fine mesh is over time consuming. The

convergence test results shown in Figure 3.5 demonstrated that the stress came to a stable stage while the element size reduced to 0.4 mm under the same loading condition. Therefore, 0.4 mm of element size was selected for good accuracy and less time consuming.

As shown in Table 3.7, the fibers in PDL affected the stress the most. The Poisson's ratio of the cortical bone and cancellous bone had limited and similar levels of effects. With existence of the fibers, changing the Poisson's ratio to 0.01 only introduced less than 10% difference to the stress in any region.

Only the initial M/Fs were well-controlled. The M/F of a segmental T-loop increased significantly as the canines moved distally so that none of the CT or TR side experienced a constant M/F for translation [71]. Therefore, the CT or TR referred here corresponded to the treatment intentions only. Reduction of the M/F increases tipping. Thus, the M/F for CT was lower than TR. Theoretically, an evenly distributed stress occurs if the M/F for translation is applied; as the M/F decreases, the canine tips more distally, which results in uneven stress distributions.

Five stress invariants, 1st principal stress, 2nd principal stress, 3rd principal stress, dilatational stress, and von-Mises stress were reported due to their distinct physical characteristics. Mathematically, the 1st principal stress represents the algebraically maximum tensile stress at a point or element [84]. It can be negative, then the element is physically compressed. Similarly, the 3rd principal stress shows the algebraically maximum compressive stress mathematically at a point or element in the perpendicular direction to the 1st principal stress. The 2nd principal stress is in the perpendicular direction to both 1st and 3rd principal stress. The dilatational stress characterizes volume change with expansion if positive or "squeezing" if negative. Thus, change of this invariant will force the fluid in the element to flow either in or out. The von-Mises stress represents element distortion with no volumetric change. The invariant characterizes shear effect, but will not cause fluid to flow. These are the stress invariants that are

unique to the point or element, thus are the preferred parameters for our study. The physical effect may need to be analyzed based on multiple invariants. A high 1st principal stress and low 3rd principal stress in an element result in more severe stretching than the case where both 1st and 3rd stresses are at the similar level. However, the dilatational stress and von-Mises represent volume change and distortion respectively, which can be used to evaluate their impact on cells directly. Viecilli had discussed the tension and compression in different directions and the coexisting of both in the same element with an ideal FE model [85]. In this study, compression and tension was distinguished by the dilatational stress. It was generally considered to be compression while the dilatational stress in negative.

Our results showed that the stresses in the root were affected the most from the differential M/F, not in the alveolar bone. The load on the bracket is transmitted to the alveolar bone through the root and PDL. At the root surface, CT and TR strategies created distinct stress magnitude and distribution patterns, Figures 3.7 to 3.11. The PDL is much softer than the root and the bone. When it was loaded, the dilatational stress was affected the most, Figure 3.15, squeezing the element on the compression side and expanding the element on the tension side. The stresses then were transmitted to the alveolar bone in a form of more evenly distributed and relatively lower pressure, which resulted in lower stresses in the bone, Figures 3.7 to 3.21. Because of the PDL's buffering effect, the effects of CT and TR strategies diminished, resulting in a similar stress distribution in the alveolar bone, Figures 3.17 to 3.21.

While the PDL was compressed in front of the moving tooth, the pressure on the cortical shell stretched the bone tangentially. On the other hand, the alveolar bone in the opposite direction was pulled by the PDL fibers, causing the bone to be compressed in the circumferential direction. Consequently, 1st principal/dilatational/3rd principal stress in PDL and alveolar bone showed reversed patterns. Traditionally, a tooth movement has been described as having a compression and a tension sides. The statement will need to be more specific because it is true only in PDL, not in alveolar bone. Viecilli had detected

the similar phenomenon with the ideal FE model [85]. This study provides more information based on clinical treatments.

Investigation of the ME change and how the cells are affected helps understanding the mechanism of mechanotransduction. It is commonly accepted that the bone modeling and remodeling is initially triggered by mechanical load through a mechanotransduction path although the path has not been fully agreed. The level of bone modeling and remodeling can be characterized by the change of BMD. Strong bone turnover results in a lower BMD. Thus, it is helpful to see whether the initial ME change in terms of each of the stress invariants is related to the BMD reduction, which may indicate whether certain ME change triggers the bone remodeling process. In this discussion, the BMD were expressed in terms of HU as was reported previously [17, 86, 87].

The five stress invariants changes in the root and alveolar bone were compared with the HU changes. The overall correlations of the stresses with HU changes are generally weak. When data from all directions are combined, none of the correlations were > |0.5|. For specific directions, Division 35-3 for CT side showed moderate correlations (μ=0.51 to 0.61) between four stress invariants (1^{st} principal/2^{nd} principal/3^{rd} principal/dilatational stress) and HU change in the alveolar bone, meaning the two parameters were modest correlated if the comparisons were along the direction of tooth movement. The stresses in other directions were less changed and were weakly correlated to the HU changes. The level of correlation indicates that the initial stress may not be the only stimulus that determines the HU changes. Patient specific biological responses may also be major factors.

To better understand the relationship, the dilatational stress at the coronal level was compared with the corresponding BMD changes, Figure 4.1. The results showed that the high dilatational stress area in the bone in the direction of tooth movement had high HU reduction, indicating high remodeling. The stress indicates volume expansion,

meaning less pressure on the osteocytes. The area corresponds to bone resorption, thus the pressure reduction may be related to osteoclast recruitment. The low dilatational stress in the bone in the opposite direction also had high HU reduction, indicating high remodeling. The stress indicate volume reduction, meaning squeezing the cells. The area corresponds to bone deposition, thus increasing pressure on the cells may be related to osteoblast recruitment. This explanation is in agreement with the traditional orthopedic view that bone is generated under compression and resorbed under tension [88-90].

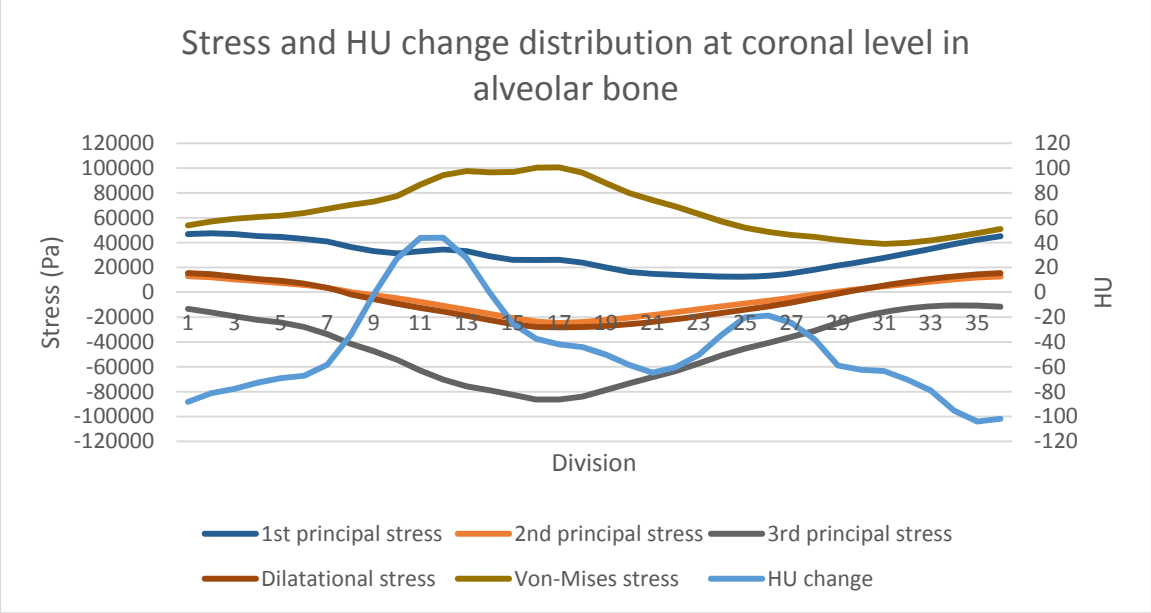

Figure 4.1: Coronal level stress and HU change distribution in alveolar bone.

In this study, the dilatational and 2nd principal stress distributions had similar trend. The dilatational stress had a slightly higher correlation to the HU change in bone in the moving direction divisions. Roberts et al. [91] had done an animal study with long bone, and obtained the highest correlation between the 2nd principal stress and new bone apposition. The difference of species and treatment could be the reason to cause the discrepancy, which needs to be further investigated.

Studies [6, 9-11] showed that the osteocyte senses the mechanical stimuli and releases signaling molecules to regulate osteoblasts and osteoclasts. The potential mechanisms are due to unloading of osteocyte for producing more osteoclasts [92] and loading or increasing strain-driven fluid flow for producing more osteoblasts [93]. The osteocyte is embedded within the calcified bone matrix. As the tooth is loaded, the bone deforms, which affects the osteocytes. Our study has estimated the level of bone deformation, stress changes, and locations of the maximum changes, which are the key information for understanding their biological effects.

How osteocytes sense the load as the mechanosensing cells had been studied. Substrate strain, fluid shear stress, and the loading-induced hydraulic pressure are the potential mechanical stimulus for osteocytes [8].One popular theory is that the osteocytes sense local strains amplified by the extracellular fluid flow. Experimental evidence had been obtained to support the idea that interstitial fluid flow is driven by the deformations of the bone [94-96]. Osteocytes also possibly respond to matrix strains directly [8]. This study has provided evidence that the area that has high volumetric change has more HU reduction, meaning more modeling/remodeling activities. The change affects both strain and extracellular fluid flow, which provides the needed stimuli.

It had been discussed previously that no significant difference of BMD change patterns had been detected in the surrounding alveolar bone under the two treatment strategies. This is in agreement with our stress analysis. Due to the buffering effect, the stress in bone was minimally affected by the M/F, which may be the reason that BMD change was not related to M/F as well.

4.6 Limitations

The CBCT has lower resolution than other types of CT. The voxel size used in this study was 0.25 mm, and the scanning time was 29 seconds. Reducing the voxel size would have increased the scanning time and it may have caused unacceptable motion

blur. Due to the 0.25 voxel size, tooth length changes smaller than 0.5 mm and root volume changes smaller than 73 mm^3 could not be reliably detected, thus the use of the 0.5 mm and 73 mm^3 thresholds. Higher CBCT quality and resolution will increase the ability to detect smaller root resorptions. The voxel size is larger than the PDL thickness at most of sites, which made the PDL images not reliable. The uniform thickness PDL in the finite element models was grown from the root.

The segmental T-loop cannot provide constant force and moment as the tooth displaces and the study shows that the moment-to-force ratio is very sensitive to those displacements. This made it difficult to control treatment, so a more reliable appliance is needed for further studies of treatment strategies.

Morphological change during the treatment was undetectable. Due to the radiation dose issue, CBCT scan can be taken only before and after the entire canine retraction. The BMD changes during treatment could not be assessed. This pieces of information may help to better explain the biological response and further improve tooth movement control.

The sample size in this study was 18 patients. A much larger sample size will be needed to determine the correlation between clinical outcomes and age, genotype, or apical root resorption in canine retraction. The number of patients who took part in our research was less than expected. Besides, four patients were dropped from this study due to failed CBCT scans, unfitted T-loops, and personal reasons.

CHAPTER 5. CONCLUSIONS

The overall apical root resorption is not statistically significant for canine retraction with the current CBCT resolution. Translation had a higher chance than tipping to lead to definite apical root resorption. ME change may not be the determining factor causing apical root resorption. Other biological factors may also be important.

HU distribution changed significantly in both root and alveolar bone. The maximum BMD reduction was on the coronal level in the direction perpendicular to the direction of movement in root. The maximum BMD reduction was on the coronal level in the direction of the direction of movement in bone.

The locations of the CRes in the MD and BL directions are significantly different. The locations of the CRes of a human canine in MD and BL directions can be estimated by finding the CPCSs in the two directions.

The stress invariants can be used to characterize how the osteocytes feel when ME changes. The stress invariants' distributions in bone, PDL, and root are significantly different, meaning the cells in the tissues experience different stimuli. The stress invariants in the alveolar bone are not significantly affected by different M/F. The higher bone modeling/remodeling activities along the direction of tooth movement may be related to the initial volumetric increase and decrease in the alveolar bone.

LIST OF REFERENCES

LIST OF REFERENCES

1. Wise, G.E. and King, G.J., *Mechanisms of tooth eruption and orthodontic tooth movement.* J Dent Res, 2008. **87**(5): p. 414-34.
2. Roberts-Harry, D. and Sandy, J., *Orthodontics. Part 11: orthodontic tooth movement.* British Dental Journal, 2004. **196**(7): p. 391-4; quiz 426.
3. Rody, W.J., Jr., King, G.J., and Gu, G., *Osteoclast recruitment to sites of compression in orthodontic tooth movement.* Am J Orthod Dentofacial Orthop, 2001. **120**(5): p. 477-89.
4. Onal, M., et al., *Receptor activator of nuclear factor kappaB ligand (RANKL) protein expression by B lymphocytes contributes to ovariectomy-induced bone loss.* J Biol Chem, 2012. **287**(35): p. 29851-60.
5. Vezeridis, P.S., et al., *Osteocytes subjected to pulsating fluid flow regulate osteoblast proliferation and differentiation.* Biochem Biophys Res Commun, 2006. **348**(3): p. 1082-8.
6. You, L., et al., *Osteocytes as mechanosensors in the inhibition of bone resorption due to mechanical loading.* Bone, 2008. **42**(1): p. 172-9.
7. Bonewald, L.F., *The amazing osteocyte.* J Bone Miner Res, 2011. **26**(2): p. 229-38.
8. Klein-Nulend, J., Bacabac, R.G., and Bakker, A.D., *Mechanical loading and how it affects bone cells: the role of the osteocyte cytoskeleton in maintaining our skeleton.* Eur Cell Mater, 2012. **24**: p. 278-91.
9. Robling, A.G., Bellido, T., and Turner, C.H., *Mechanical stimulation in vivo reduces osteocyte expression of sclerostin.* J Musculoskelet Neuronal Interact, 2006. **6**(4): p. 354.
10. Santos, A., et al., *Pulsating fluid flow modulates gene expression of proteins involved in Wnt signaling pathways in osteocytes.* J Orthop Res, 2009. **27**(10): p. 1280-7.
11. Tan, S.D., et al., *Osteocytes subjected to fluid flow inhibit osteoclast formation and bone resorption.* Bone, 2007. **41**(5): p. 745-51.
12. Barbagallo, L.J., et al., *Physical properties of root cementum: Part 10. Comparison of the effects of invisible removable thermoplastic appliances with light and heavy orthodontic forces on premolar cementum. A microcomputed-tomography study.* Am J Orthod Dentofacial Orthop, 2008. **133**(2): p. 218-27.

13. Chan, E. and Darendeliler, M.A., *Physical properties of root cementum: part 7. Extent of root resorption under areas of compression and tension.* Am J Orthod Dentofacial Orthop, 2006. **129**(4): p. 504-10.

14. Chan, E.K. and Darendeliler, M.A., *Exploring the third dimension in root resorption.* Orthod Craniofac Res, 2004. **7**(2): p. 64-70.

15. Harris, D.A., Jones, A.S., and Darendeliler, M.A., *Physical properties of root cementum: part 8. Volumetric analysis of root resorption craters after application of controlled intrusive light and heavy orthodontic forces: a microcomputed tomography scan study.* Am J Orthod Dentofacial Orthop, 2006. **130**(5): p. 639-47.

16. Viecilli, R.F., et al., *Orthodontic mechanotransduction and the role of the P2X7 receptor.* Am J Orthod Dentofacial Orthop, 2009. **135**(6): p. 694 e1-16; discussion 694-5.

17. Chang, H.W., et al., *Effects of orthodontic tooth movement on alveolar bone density.* Clin Oral Investig, 2012. **16**(3): p. 679-88.

18. Viecilli, R.F., Budiman, A., and Burstone, C.J., *Axes of resistance for tooth movement: does the center of resistance exist in 3-dimensional space?* American Journal of Orthodontics & Dentofacial Orthopedics, 2013. **143**(2): p. 163-72.

19. Smith, R.J. and Burstone, C.J., *Mechanics of tooth movement.* American Journal of Orthodontics, 1984. **85**(4): p. 294-307.

20. Bourauel, C., et al., *Computer-aided analysis of the biomechanics of tooth movements.* Int J Comput Dent, 2007. **10**(1): p. 25-40.

21. Choy, K., et al., *Effect of root and bone morphology on the stress distribution in the periodontal ligament.* Am J Orthod Dentofacial Orthop, 2000. **117**(1): p. 98-105.

22. Provatidis, C.G., *A comparative FEM-study of tooth mobility using isotropic and anisotropic models of the periodontal ligament.* Medical Engineering & Physics, 2000. **22**(5): p. 359-370.

23. Yoshida, N., et al., *Experimental evaluation of initial tooth displacement, center of resistance, and center of rotation under the influence of an orthodontic force.* Am J Orthod Dentofacial Orthop, 2001. **120**(2): p. 190-7.

24. Nagerl, H., et al., *Centers of rotation with transverse forces: an experimental study.* Am J Orthod Dentofacial Orthop, 1991. **99**(4): p. 337-45.

25. Meyer, B.N., Chen, J., and Katona, T.R., *Does the center of resistance depend on the direction of tooth movement?* Am J Orthod Dentofacial Orthop, 2010. **137**(3): p. 354-61.

26. Campos, M.J., et al., *The role of orthodontic tooth movement in bone and root mineral density: a study of patients submitted and not submitted to orthodontic treatment.* Medical Science Monitor, 2012. **18**(12): p. CR752-7.

27. Coimbra, M.E., et al., *Mechanical testing and finite element analysis of orthodontic teardrop loop.* Am J Orthod Dentofacial Orthop, 2008. **133**(2): p. 188 e9-13.

28. Haskell, B.S., Spencer, W.A., and Day, M., *Auxiliary springs in continuous arch treatment: Part 1. An analytical study employing the finite-element method.* Am J Orthod Dentofacial Orthop, 1990. **98**(5): p. 387-97.

29. Martins, R.P., et al., *Optimizing the design of preactivated titanium T-loop springs with Loop software.* Am J Orthod Dentofacial Orthop, 2008. **134**(1): p. 161-6.

30. Wang, H., et al., *Initial stress in the periodontal membrane of maxillary first molar with different alveolar bone height by intrusion: 3-dimensional finite element analysis.* Shanghai Kou Qiang Yi Xue, 2013. **22**(3): p. 247-51.

31. Katona, T.R., et al., *Stress analysis of bone modeling response to rat molar orthodontics.* J Biomech, 1995. **28**(1): p. 27-38.

32. O'Grady, J., Sheriff, M., and Likeman, P., *A finite element analysis of a mandibular canine as a denture abutment.* Eur J Prosthodont Restor Dent, 1996. **4**(3): p. 117-21.

33. Qian, H., Chen, J., and Katona, T.R., *The influence of PDL principal fibers in a 3-dimensional analysis of orthodontic tooth movement.* American Journal of Orthodontics & Dentofacial Orthopedics, 2001. **120**(3): p. 272-9.

34. Geiger, M.E. and Lapatki, B.G., *Locating the center of resistance in individual teeth via two- and three-dimensional radiographic data.* J Orofac Orthop, 2014. **75**(2): p. 96-106.

35. Burstone, C.J. and Koenig, H.A., *Optimizing anterior and canine retraction.* American Journal of Orthodontics, 1976. **70**(1): p. 1-19.

36. Burstone, C.J., *The segmented arch approach to space closure.* American Journal of Orthodontics, 1982. **82**(5): p. 361-78.

37. Techalertpaisarn, P. and Versluis, A., *Mechanical properties of Opus closing loops, L-loops, and T-loops investigated with finite element analysis.* Am J Orthod Dentofacial Orthop, 2013. **143**(5): p. 675-83.

38. Faulkner, M.G., et al., *A parametric study of the force/moment systems produced by T-loop retraction springs.* Journal of Biomechanics, 1989. **22**(6-7): p. 637-47.

39. Proffit, W., *Contemporary Orthodontics*, ed. S. Louis. 2000: Mosby, Inc.

40. Katona, T.R., Le, Y.P., and Chen, J., *The effects of first- and second-order gable bends on forces and moments generated by triangular loops.* Am J Orthod Dentofacial Orthop, 2006. **129**(1): p. 54-9.

41. Gajda, S. and Chen, J., *Comparison of three-dimensional orthodontic load systems of different commercial archwires for space closure.* Angle Orthod, 2012. **82**(2): p. 333-9.

42. Chen, J., Isikbay, S.C., and Brizendine, E.J., *Quantification of three-dimensional orthodontic force systems of T-loop archwires.* Angle Orthodontist, 2010. **80**(4): p. 754-758.

43. Viecilli, R.F., *Self-corrective T-loop design for differential space closure.* Am J Orthod Dentofacial Orthop, 2006. **129**(1): p. 48-53.

44. Halazonetis, D.J., *Design and test orthodontic loops using your computer.* Am J Orthod Dentofacial Orthop, 1997. **111**(3): p. 346-8.

45. Chen, J., Markham, D.L., and Katona, T.R., *Effects of T-loop geometry on its forces and moments.* Angle Orthod, 2000. **70**(1): p. 48-51.

46. Katona, T.R., Isikbay, S.C., and Chen, J., *Effects of first- and second-order gable bends on the orthodontic load systems produced by T-loop archwires.* Angle Orthod, 2014. **84**(2): p. 350-7.

47. Katona, T.R., Isikbay, S.C., and Chen, J., *An analytical approach to 3D orthodontic load systems.* Angle Orthod, 2014. **84**(5): p. 830-8.

48. Kroczek, C., et al., *Comparison of the orthodontic load systems created with elastomeric power chain to close extraction spaces on different rectangular archwires.* Am J Orthod Dentofacial Orthop, 2012. **141**(3): p. 262-8.

49. Bridges, T., King, G., and Mohammed, A., *The effect of age on tooth movement and mineral density in the alveolar tissues of the rat.* American Journal of Orthodontics & Dentofacial Orthopedics, 1988. **93**(3): p. 245-50.

50. Melsen, B., *Biological reaction of alveolar bone to orthodontic tooth movement.* Angle Orthod, 1999. **69**(2): p. 151-8.

51. Verna, C., Dalstra, M., and Melsen, B., *The rate and the type of orthodontic tooth movement is influenced by bone turnover in a rat model.* Eur J Orthod, 2000. **22**(4): p. 343-52.

52. Verna, C., Zaffe, D., and Siciliani, G., *Histomorphometric study of bone reactions during orthodontic tooth movement in rats.* Bone, 1999. **24**(4): p. 371-9.

53. Hsu, J.T., et al., *Bone density changes around teeth during orthodontic treatment.* Clinical Oral Investigations, 2011. **15**(4): p. 511-9.

54. Sameshima, G.T. and Sinclair, P.M., *Predicting and preventing root resorption: Part II. Treatment factors.* American Journal of Orthodontics & Dentofacial Orthopedics, 2001. **119**(5): p. 511-5.

55. Weltman, B., et al., *Root resorption associated with orthodontic tooth movement: a systematic review.* American Journal of Orthodontics & Dentofacial Orthopedics, 2010. **137**(4): p. 462-76; discussion 12A.

56. Schulze, D., et al., *Diagnostic criteria for the detection of mandibular osteomyelitis using cone-beam computed tomography.* Dentomaxillofac Radiol, 2006. **35**(4): p. 232-5.

57. Nomura, Y., et al., *Reliability of voxel values from cone-beam computed tomography for dental use in evaluating bone mineral density.* Clinical Oral Implants Research, 2010. **21**(5): p. 558-62.

58. Georgescu, C.E., et al., *Quantitative and qualitative bone analysis in the maxillary lateral region.* Surg Radiol Anat, 2012.

59. Gonzalez-Garcia, R. and Monje, F., *The reliability of cone-beam computed tomography to assess bone density at dental implant recipient sites: a histomorphometric analysis by micro-CT.* Clinical Oral Implants Research, 2012.

60. Kaya, S., et al., *Measuring bone density in healing periapical lesions by using cone beam computed tomography: a clinical investigation.* J Endod, 2011. **38**(1): p. 28-31.

61. Araki, K. and Okano, T., *The effect of surrounding conditions on pixel value of cone beam computed tomography.* Clinical Oral Implants Research, 2011.

62. Mah, P., Reeves, T.E., and McDavid, W.D., *Deriving Hounsfield units using grey levels in cone beam computed tomography.* Dento-Maxillo-Facial Radiology, 2010. **39**(6): p. 323-35.

63. Nomura, Y., et al., *Stability of voxel values from cone-beam computed tomography for dental use in evaluating bone mineral content.* Clinical Oral Implants Research, 2012.

64. Norton, M.R. and Gamble, C., *Bone classification: an objective scale of bone density using the computerized tomography scan.* Clinical Oral Implants Research, 2001. **12**(1): p. 79-84.

65. Baswaraj, et al., *An experimental study of arch perimeter and arch width increase with mandibular expansion: a finite element method.* J Contemp Dent Pract, 2013. **14**(1): p. 104-10.

66. Chen, S., et al., *Individualized three-dimensional finite element model of facial soft tissue and preliminary application in orthodontics.* Zhonghua Kou Qiang Yi Xue Za Zhi, 2012. **47**(12): p. 730-4.

67. Szucs, A., et al., *Finite element analysis of the human mandible to assess the effect of removing an impacted third molar.* J Can Dent Assoc, 2010. **76**: p. a72.

68. Jiang, F. and Chen, J., *Hounsfield Units Shown in CBCT is Affected by Surrounding Tissue.* J Dent Res 91(Spec Iss A): 918 (www.dentalresearch.org). 2012.

69. Miles, D.A., *A clinician's guide to understanding cone beam volumetric imaging (CBVI).* www.ineedce.com, 2007.

70. Li, S., et al., *Three-dimensional Canine Displacement Patterns in Response to Translation and Controlled Tipping Retraction Strategies.* The Angle Orthodontists, 2015. **85**(1): p. 18-25.

71. Xia, Z., et al., *Load system of segmental T-loops for canine retraction.* American Journal of Orthodontics & Dentofacial Orthopedics, 2013. **144**(4): p. 548-56.

72. Bath-Balogh, M., *Illustrated Dental Embryology, Histology, and Anatomy*. 2011: Elsevier, 176.

73. Auyeung, L., Bouwsma, O.J., and Polson, A.M., *Periodontal fiber attachment and apical root resorption.* Endod Dent Traumatol, 1988. **4**(5): p. 219-25.

74. Kurihara, S. and Enlow, D.H., *An electron microscopic study of attachments between periodontal fibers and bone during alveolar remodeling.* Am J Orthod, 1980. **77**(5): p. 516-31.

75. Bernick, S., *The organization of the periodontal membrane fibres of the developing molars of rats.* Arch Oral Biol, 1960. **2**: p. 57-63.

76. Cawson, R.A., *Cawson's essentials of oral pathology and oral medicine*. 2008: USA: Elsevier Limited

77. Natali, A.N., Pavan, P.G., and Scarpa, C., *Numerical analysis of tooth mobility: formulation of a non-linear constitutive law for the periodontal ligament.* Dental Materials, 2004. **20**(7): p. 623-9.

78. Shahar, R., et al., *Anisotropic Poisson's ratio and compression modulus of cortical bone determined by speckle interferometry.* J Biomech, 2007. **40**(2): p. 252-64.

79. Dickerson, D.A., Sander, E.A., and Nauman, E.A., *Modeling the mechanical consequences of vibratory loading in the vertebral body: microscale effects.* Biomech Model Mechanobiol, 2008. **7**(3): p. 191-202.

80. Burstone, C. and Koenig, H., *Optimizing anterior and canine retraction.* Am J Orthod, 1976. **70**: p. 1-19.

81. Simplicio, H., et al., *External apical root resorption in retracted incisors.* Orthodontics (Chic.), 2012. **13**(1): p. 86-93.

82. Vollmer, D., et al., *Determination of the centre of resistance in an upper human canine and idealized tooth model.* Eur J Orthod, 1999. **21**(6): p. 633-48.

83. Geramy, A., *Alveolar bone resorption and the center of resistance modification (3-D analysis by means of the finite element method).* Am J Orthod Dentofacial Orthop, 2000. **117**(4): p. 399-405.

84. Ugural, A.C., *Advanced Strength and Applied Elasticity*. 4th ed. 2003: Prentice Hall PTR.

85. Viecilli, R.F., et al., *Three-dimensional mechanical environment of orthodontic tooth movement and root resorption.* Am J Orthod Dentofacial Orthop, 2008. **133**(6): p. 791 e11-26.

86. Jiang, F. and Chen, J., *Bone Mineral Density Loss is Related to Tooth Movement Direction*, in *IADR/LAR General Session and Exhibition*. 2012: Iguaçu Falls, Brazil.

87. Hsu, J.T., et al., *Bone density changes around teeth during orthodontic treatment.* Clin Oral Investig, 2011. **15**(4): p. 511-9.

88. Currey, J., *The Mechanical Adaptations of Bones*. 1984, Princeton: Princeton University Press.

89. Martin, R.B., Burr, D.B., *Structure, Function, and Adaptation of Compact Bone*. Vol. Ch.6. 1989, New York: Raven Press.

90. Jansen, M., *On Bone Formation: Its Relation to Tension and Pressure.* Longmans, London., 1920.

91. Roberts, M.D., Santner, T.J., and Hart, R.T., *Local bone formation due to combined mechanical loading and intermittent hPTH-(1-34) treatment and its correlation to mechanical signal distributions.* J Biomech, 2009. **42**(15): p. 2431-8.

92. Tatsumi, S., et al., *Targeted ablation of osteocytes induces osteoporosis with defective mechanotransduction.* Cell Metab, 2007. **5**(6): p. 464-75.

93. Robinson, J.A., et al., *Wnt/beta-catenin signaling is a normal physiological response to mechanical loading in bone.* J Biol Chem, 2006. **281**(42): p. 31720-8.

94. Knothe T.M., Niederer, P., and Knothe, U., *In vivo tracer transport through the lacunocanalicular system of rat bone in an environment devoid of mechanical loading.* Bone, 1998. **22**(2): p. 107-17.

95. Knothe T.M., et al., *In vivo demonstration of load-induced fluid flow in the rat tibia and its potential implications for processes associated with functional adaptation.* J Exp Biol, 2000. **203**(Pt 18): p. 2737-45.

96. Price, C., et al., *Real-time measurement of solute transport within the lacunar-canalicular system of mechanically loaded bone: direct evidence for load-induced fluid flow.* J Bone Miner Res, 2011. **26**(2): p. 277-85.

APPENDIX

APPENDIX

IRB approval:

INDIANA UNIVERSITY INSTITUTIONAL REVIEW BOARD (IRB)

RENEWAL

CLOSED TO ENROLLMENT

Reviewing IRB (please choose one):
Biomedical: ☒ IRB-02 ☐ IRB-03 ☐ IRB-04 ☐ IRB-05
Behavioral: ☐ IRB-01 ☐ IUB IRB

IRB STUDY NUMBER: 1011003026
Date Submitted: June 25, 2014

Please type only in the gray boxes. To mark a box as checked, double-click the box, select "checked", and click "OK". Please see the Renewal/Closeout Form Instructions for more information.

SECTION I: INVESTIGATOR INFORMATION

Principal Investigator:
Name *(Last, First, Middle Initial)*: **Chen, Jie**
Department: Mechanical Engineering Phone: 317-274-5918 E-Mail: jchen3@iupui.edu

Additional Study Contact:
Name: Sue Kelly Phone: 4-3954 E-Mail: sakelly@iupui.edu

Project Title: **Evaluation of Canine Retraction Strategies**
Sponsor/Funding Agency: NIDCRSponsor Number: 1R01DE018668-01A2

Sponsor Type: ☒ Federal ☐ Federal Pass-Through ☐ State ☐ Industry ☐ Not-for-Profit ☐ Unfunded ☐ Internally Funded
Funding Status: ☐ Pending ☒ Funded ☐ N/A

SECTION II: CURRENT STUDY STATUS

☒ **ONGOING – CLOSED TO ENROLLMENT**
Date study was initiated: April 2009
Projected date of completion: Dec. 2014

☐ **Re-consenting/re-authorizing**

☒ **NOT re-consenting/re-authorizing**

(Select one)
☒ Participants are still receiving research-related intervention or interaction.
☐ Participants have completed research-related interventions; however, long-term follow-up continues. Long term follow-up includes research interactions that involve no more than minimal risk to subjects, or collection of follow-up data from procedures or interventions that would be done as part of routine clinical care. Research interventions which would not be performed for clinical purposes are considered research-related intervention are not considered follow-up.
☐ Participants have completed all research-related intervention or interaction and long-term follow-up has been completed. The remaining research activities are limited only to data analysis that may require access to records and/or specimens.

☐ **Please check here if the study is currently suspended (temporarily) and indicate the reason(s) for the suspension:**

SECTION III: SUBJECT SUMMARY

☐ Check here if your study utilizes records or specimens only, i.e. there is no interaction with human subjects. When the form asks for the number of subjects, document the number of subjects for which data/specimens have been collected.

☐ Check here if the IRB has approved a waiver of consent for your study. When the form asks for the number of subjects consented, document the number of records that have been reviewed or the number of individuals enrolled.

1. **Subject Summary Table**

		On-Site
Since last IRB review	Total number of subjects **CONSENTED**	**1**
	Total number of subjects who **FAILED SCREENING** (e.g. found ineligible to participate)	**0**
	Total number of subjects who have **WITHDRAWN** from the study	**0**
Since beginning of study	Total number of subjects **CONSENTED**	**30**
	Total number of subjects who **FAILED SCREENING** (e.g. found ineligible to participate)	**0**
	Total number of subjects who have **WITHDRAWN** from the study	**6**
Number of **ACTIVE** subjects		**1**
Number of subjects who have **COMPLETED** the study		**23**

If necessary, please provide further explanation regarding the subject summary: na

2. **Withdrawal.** Have any subjects withdrawn from the study since the last IRB review?
   - ☐ No
   - ☒ Yes, state the reasons for withdrawal: Stopped showing with no explanations

3. **Vulnerable Populations.** Are any of the subjects who have consented or enrolled in the study members of a vulnerable population?
   - ☐ No.
   - ☒ Yes. Has the IRB previously approved enrollment of these subjects?
     - ☒ Yes. Continue to Question 5.
     - ☐ No. **You must submit an amendment to the IRB to request the inclusion of these subjects.** Subjects in the following vulnerable populations were enrolled without IRB approval.
       - ☐ Children
       - ☐ Prisoners
       - ☐ Cognitively Impaired
       - ☐ Pregnant Women and Human Fetuses
       - ☐ Economically/Educationally Disadvantaged
       - ☐ Students

5. **Short Form Consent.** Were any subjects consented using the short form written consent document?
   - ☒ No.
   - ☐ Yes. Please describe the circumstances of each subject enrolled, including language in which the consent process was conducted: _____
     - ☐ Is there a reasonable possibility that additional subjects who speak this language could be enrolled?
       - ☐ No.
       - ☐ Yes. Please submit a translated version of the IRB-approved consent document for review and approval by the IRB.

4. **For studies employing waivers of assent**:
   a. State the number of assent waivers that were employed since the last IRB review: _____
   b. Explain the circumstances surrounding each assent waiver employed: _____

SECTION IV: ETHNIC/RACIAL REPORTING REQUIRED FOR FEDERALLY-SPONSORED AND VA STUDIES

SUBJECT ACCRUAL				
Ethnic Category	**Sex/Gender**			**Total**
	Females	**Males**	**Unknown or Not Reported**	
Hispanic or Latino	4	0	0	4
Not Hispanic or Latino	15	11	0	26
Unknown (Individuals Not Reporting Ethnicity)	0	0	0	0
Ethnic Category Total of All Subjects*	19	11	0	30
Racial Categories				
American Indian/Alaska Native	0	0	0	0

Asian	0	0	0	0
Native Hawaiian or Other Pacific Islander	0	0	0	0
Black or African American	8	1	0	9
White	6	9	0	15
More Than One Race	1	1	0	2
Unknown or Not Reported	4	0	0	4
Racial Categories Total of All Subjects*	**19**	**11**	**0**	**30**

If ETHNIC and RACIAL category totals are not equal, please explain: _____

1. Have there been any unexpected difficulties accruing subjects in a particular category (including children and women)?
   ☒ No.
   ☐ Yes. Please explain: _____

2. **Is this study conducted at, funded by, or recruiting from the VA?**
   ☒ No.
   ☐ Yes. In the table below, please indicate the total number of VA subjects enrolled in the study and indicate in which categories those subjects fall and how many represent each category indicated.

   Total number of VA subjects: _____

☐	Children:	_____
☐	Cognitively Impaired:	_____
☐	Economically/Educationally Disadvantaged:	_____
☐	Pregnant Women and Fetuses:	_____
☐	Prisoners:	_____
☐	Students:	_____

SECTION V: SUMMARY OF EVENTS

1. **Since the last IRB review**, did any unanticipated problems, including adverse events, protocol deviations, or subject complaints, or noncompliance occur that required prompt reporting to the IRB?
   ☒ No.
   ☐ Yes. Were these events reported previously to the IRB and VA, if applicable?
      ☐ No. Please explain why these events were not previously reported: _____
      ☐ Yes. Provide a **summary** of these events: _____
         ☐ Check here if the **summary** is attached.

2. **Since the last IRB review**, did any related problems, including adverse events, protocol deviations, or subject complaints occur involving an IU IRB-approved performance site that did **not** require prompt reporting to the IRB?
   ☒ No.
   ☐ Yes. Provide a **summary** of these events: _____
      ☐ Check here if the **summary** is attached.

3. Is there a data safety monitoring plan for this study?
   ☐ No. This study is minimal risk (exempt or expedited).
   ☒ Yes. Does the plan include a data safety monitoring board?
      ☒ No.
      ☐ Yes. Please provide the most recent monitoring report if it has not already been provided to the IRB or explain why one cannot be provided: _____

4. Based on the above information, do you feel the validity of the data is affected?
   ☒ No.
   ☐ Yes. Explain: _____

5. Based on the above information, do you feel there is an increase in risk to subjects or others or in the frequency or severity of adverse events, protocol deviations, problems, complaints, etc. since the last IRB review?
   ☒ No.
   ☐ Yes. Explain: _____

SECTION VI: SUMMARY

1. Describe the progress of the research, including any preliminary observations and information about study results or trends: We have completed 23 patients. Only one patient is still under treatment. We are processing the data and prepare publications.

2. Have subjects experienced any **direct** benefit(s) from their participation in the study?
   - ☒ No.
   - ☐ Yes.

   Please explain: _____

3. If any recent literature has been published or presented by you or others since the last IRB review, has it demonstrated a significant impact on the conduct of the study or the well-being of subjects?
   - ☐ N/A. There has not been any recent literature published or presented since the last IRB review.
   - ☒ No.
   - ☐ Yes. Attach a copy or explain:

1. Xia, Z., Chen, J., "Biomechanical Validation of an Artificial Tooth-PDL-Bone Complex for in vitro Orthodontic Measurement" Angle Orthodontists, 2013;83(3):410-7

2. Xia, Z., Jiang, F., and Chen, J. "Estimation of Periodontal Ligament's Equivalent Mechanical Parameters for Finite Element Modeling" American Journal of Orthodontics and Dentofacila Orthopedics, Volume 143, Issue 4, Pages 486-91, 2013

3. Xia, Z., Chen, J., Jiang, F., Li, S., Viecilli, R.F., and Liu, S., "Load System of Segmental T-Loops for Canine Retraction" the American Journal of Orthodontics and Dentofacila Orthopedics, 2013 Oct;144(4):548-56 PMC3829684

4. Li, S., Xia, Z, Liu, S., Eckert, G., and Chen, J., "Three-dimensional Canine Displacement Patterns in Response to Translatio Controlled Tipping Retraction Strategies" the Angle Orthodontists, accepted 4/17/2014

4. Have there been any audits from federal agencies conducted since the last IRB review that identified unanticipated problems involving risks to subjects or others or noncompliance?
   - ☒ No.
   - ☐ Yes. Attach the report(s).

5. Do you believe the risk:benefit ratio has changed based on all of the information provided on this form and any attachments?
   - ☒ No.
   - ☐ Yes. Explain:_____

SECTION VII: CO-INVESTIGATOR UPDATE

☐ This submission does NOT include additions to or removals from the Personnel Tab in KC IRB. *Proceed to section VIII.*

☒ This submission includes additions to or removals from the Personnel Tab in KC IRB.

The following investigators are being added to the Personnel Tab:

The following investigators are being **removed** from the Personnel Tab and will no longer be participating in this research:
Francisco Eraso

SECTION VIII: REQUIRED ATTACHMENTS

All current study documents must be included with your renewal submission. Please check the appropriate boxes as they apply to your study.

- ☐ Clinical Investigator's Brochure, dated: _____
- ☐ Drug or Biological Products Form, dated: _____
- ☒ HIPAA & Recruitment Checklist, dated: _____
- ☐ Medical Device Form, dated: _____
- ☒ Protocol, dated: _____

☒ Request form(s) for vulnerable population(s) (please list and date); **Children**
☐ Surveys, questionnaires (please list and date): _____
☒ Summary Safeguard Statement or HUD Form, dated: _____
☒ Test Articles Supplement, dated: _____
☐ Other (please list and date): _____

If reconsenting/reauthorizing:
☐ Informed Consent, dated: _____
Number of consent documents: _____
☐ Assent, dated: _____
Number of assent documents: _____
☐ Authorization, dated: _____
Number of authorizations: _____

Include the following documents, as applicable:
☐ Publications, if you answered YES to VI.3. above
☐ Audit reports, if you answered YES to VI.4 above
☐ Summaries, if you indicated in Section V that summaries are attached
☐ DSMB report, if the study includes a DSMB and you are submitting the most recent DSMB report
☐ Interim findings, if there are any to report
☐ Multi-center trial reports, if there are any available

NOTES:
- No changes to previously approved study documents are allowed at the time of renewal unless requested by the IRB.
- Incomplete submissions will result in a processing delay, which could result in study expiration.
- **VA Requirements**: For studies conducted at the VA, utilizing VA funding or VA patients, you must provide a copy of the approved renewal form to the VA Research Service office.

SECTION IX: INVESTIGATOR STATEMENT OF COMPLIANCE

By submitting this form, the Principal Investigator assures that all information provided is accurate. He/she assures that procedures performed under this project will be conducted in strict accordance with federal regulations and Indiana University policies and procedures that govern research involving human subjects. He/she acknowledges that he/she has the resources required to conduct research in a way that will protect the rights and welfare of participants, and that he/she will employ sound study design which minimizes risks to subjects. He/she agrees to submit *any* change to the project (e.g. change in principal investigator, research methodology, subject recruitment procedures, etc.) to the Board in the form of an amendment for IRB approval prior to implementation.

SECTION X: IRB APPROVAL

For IU Human Subjects Office Use Only

Type of review: ☒ Full Board
☐ Expedited, Category: _____ Approved for a period of: ☐ one (1) year ☐ two (2) years

STATUS OF STUDY: ONGOING - Closed to Enrollment

This renewal has been reviewed and approved as meeting the criteria for IRB approval as outlined in 45 CFR 46.111(a) by the Indiana University IRB. Based on the criteria for determining the frequency of renewal and the level of risk, this study will expire on: 8.11.15. If the study is not re-approved prior to that date all research activities must cease on that date, including enrollment of new subjects, intervention/interaction with current participants, and analysis of identified data.

Authorized IRB Signature: _____ IRB Approval Date: 8.12.14

Printed Name of IRB Member: Kenneth Fifty

VITA

VITA

Education

- Purdue University
    - Ph.D. in Mechanical Engineering, 2009 – present (Prospective graduation: May/2015)
- Indiana University Purude University Indianapolis
    - Master of Science in Mechanical Engineering, 2007 – 2009
- Tsinghua University (China)
    - Bachelor of Engineering in Department of Precision Instrument and Mechanology, 2001 – 2005

Experience

- Research assistant in Department of Mechanical Engineering of Purdue University, 2009 – present
    - Project: Mechanical Environment Changes and Biological Responses of Canine Retraction Using T-loop
- Teaching assistant in Department of Mechanical Engineering of Purdue University, 2014 – 2015
    - Courses: Thermodynamics, Fundamental of Engineering
- Research assistant in Department of Mechanical Engineering of Indiana University Purdue University Indianapolis, 2007 – 2009
    - Project: Longitudinal Evaluation of Bone Healing on Rats – A Finie Element Study
- Beida Qingniao, inc, Beijing, China, Manager Assistant, 2005 – 2006

LIST OF PUBLICATIONS

LIST OF PUBLICATIONS

- Mechanical environment change in root, periodontal ligament, and alveolar bone in response to two canine retraction treatment strategies, Feifei Jiang, Zeyang Xia, Shuning Li, George Eckert, Jie Chen, Orthodontics & Craniofacial Research, 2015. 18(1): p. 29-38.
- Hounsfield Unit Change in Root and Alveolar Bone during Canine Retraction, Feifei Jiang, Sean Y. Liu, Zeyang Xia, Shuning Li, Jie Chen, Katherine S. Kula, George Eckert, American Journal of Orthodontics & Dentofacial Orthopedics. (Accepted)
- Podcast 6: Three-Dimensional Mapping of the Ipsilateral Olecranon Tip to Determine Autograft Suitability for Unrepairable Coronoid Fractures. Andy Putman, Jie Chen, Feifei Jiang, Aakash Chauhan, Gregory A. Merrell, 69th Annual Meeting of the ASSH, Boston, 09/2014
- Lower Moment-to-force Ratio During Canine Retraction Causes Higher Gingival Inflammation, Z. XIA, J. CHEN, S.S. LIU, M. KOWOLIK, H. GU, and F. JIANG, J Dent Res 92(Spec Iss A): 2429, 2013 (www.dentalresearch.org)
- Estimation of periodontal ligament's equivalent mechanical parameters for finite element modeling. Xia, Z., F. Jiang, and J. Chen, Am J Orthod Dentofacial Orthop, 2013. 143(4): p. 486-91.
- Load system of segmental T-loops for canine retraction. Xia, Z., Chen, J., and Jiang, F., Am J Orthod Dentofacial Orthop, 2013. 144(4): p. 548-56.
- Hounsfield Units Shown in CBCT is Affected by Surrounding Tissue, F. Jiang and J. Chen, J Dent Res 91(Spec Iss A): 918, 2012 (www.dentalresearch.org)
- Change of Loadings Delivered by Segmental T-Loops for Canine Retraction, Z. XIA, J. CHEN, S.S. LIU, F. JIANG, and R. VIECILLI, J Dent Res 91(Spec Iss A): 1036, 2012 (www.dentalresearch.org)
- Comparison of the force systems of 3 appliances on palatally impacted canines. Yadav S, Chen J, Upadhyay M, Jiang F, Roberts WE. Am J Orthod Dentofacial Orthop, 2011. 139(2): p. 206-13.
- HEALING PROGRESS OF FRACTURED BONE - A LONGITUDINAL STUDY, Feifei Jiang, Jie Chen, David E. Komatsu, and Shuning Li, Proc. ASME 2009 Summer Bioengineering Conference (SBC2009-204787), June 17-21, Lake Tahoe, CA, USA